CONTROL OF COLOR, MOLECULAR ORDER AND CHARGE TRANSPORT IN CONJUGATED POLYMERS

By

UNSAL KOLDEMIR

A DISSERTATION PRESENTED TO THE GRADUATE SCHOOL
OF THE UNIVERSITY OF FLORIDA IN PARTIAL FULFILLMENT
OF THE REQUIREMENTS FOR THE DEGREE OF
DOCTOR OF PHILOSOPHY

UNIVERSITY OF FLORIDA

2012

To Dr. Fikret Koc

ACKNOWLEDGMENTS

I would like to first thank my advisor, Prof John R. Reynolds, for his guidance and support in all aspects of my graduate school work during my 5 years at the University of Florida. He has been a role model for me in terms of conducting research, mentoring students, guiding a research team, teaching an undergraduate level course, as well as a good family member. He has been very influential in building my academic career, not only for research purposes, but also in teaching undergraduate level courses. He supported me for a research visit to the Max Planck Institute for Polymer Research in Mainz, Germany, which has advanced my skills through research collaboration important for future work with other groups. Through his deep insights in research, I was exposed to many of the challenges of organic chemistry, polymer chemistry, electrochemistry, physical characterization, as well as transistor device applications.

I would also like to thank the members of my committee, Prof. Kenneth Wagener, Prof. Aaron Aponick, Prof. Yun C. Cao and Prof. Xiangeng Xue, for their valuable discussions and contribution throughout my studies at the University of Florida. I would like to thank Prof. Kenneth Wagener for leading the Butler Polymer Laboratories.

This work would not be possible without the contribution of my research collaborators, Prof. Franky So, Prof. Jiangeng Xue in the Department of Materials Science and Engineering at UF and Klaus Muellen at the Max Planck Institute for Polymer Research. I would like to thank Prof. Franky So for his valuable feedback in solar cell devices over the past 4 years. He offered critical insights into the design of polymers for high impact solar cell devices. Additionally, I really enjoyed the SoRey meetings with the So group members held every month. Dr. Wojtek Pisula and Dr.

Sreenivasa R. Puniredd have contributed significantly to my work through their knowledge of X-ray characterizations and organic field effect transistor devices.

I want to specifically thank to Dr. Chad Amb and Dr. Pengjie Shi. Chad's positive personality helped to create a wonderful team environment for my research for 3 years. His feedback has helped me overcoming many synthetic challenges. Pengjie has been a close friend in and outside of the group, and I enjoyed spending time with him especially for fishing trips.

During my 5 years in the Reynolds group, I had the opportunity to work with many great researchers. Dr. Frank Arroyave was a walking library; Dr. Jianguo Mei was always full of great ideas and new synthetic routes; Dr. Romain Stalder was full of kindness; Dr. Mike Craig was full of laughter and rarely known organic chemistry purification methods; Dr. Stefan Ellinger was full of motivation for research; Dr. Kenneth Graham was full of details. I also owe thanks to Dr. Aubrey Dyer, Dr. Svetlana Vasilyeva and Dr. David Liu for helping me to perform electrochemistry experiments. I also enjoyed working with the younger graduate students in our group, James Deininger and Caroline Grand.

Special thanks should be given to Cheryl Googins and Sara Klossner, who devoted their time in facilitating administrative procedures. I really enjoyed the time when Sara took me for a Christmas show when I had to stay in Gainesville over the winter holidays.

Lastly, I would like to thank my parents, who supported me unconditionally through all my endeavors. Without their support, I would have never made it to this point.

TABLE OF CONTENTS

page

LIST OF TABLES

Table page

LIST OF FIGURES

Figure page

LIST OF ABBREVIATIONS

AFM	Atomic force microscopy
APFO	Alternating polyfluorene
BTD	2,1,3-Benzothiadiazole
CV	Cyclic voltammetry
DOT	3,4-Dioxythiophene
DPV	Differential pulse voltammetry
DTG	Dithienogermole
DTS	Dithienosilole
EC	Electrochromic
ECD	Electrochromic device
ECP	Electrochromic polymer
EtHx	2-Ethylhexyl
Fc/Fc^{+}	Ferrocene/Ferrocenium
FET	Field effect transistor
FF	Fill Factor
GPC	Gel permeation chromatography
GIWAXS	Grazing Incidence Wide angle X-ray Scatterring
HOMO	Highest occupied molecular orbital
ICBA	Indene-C_{60} bisadduct
ITO	Indium tin oxide
IR	Infrared Spectrum
J_{sc}	Short current density
LED	Light emitting diode
LUMO	Lowest occupied molecular orbital

MALDI	Matrix assisted laser desorption/ionization
M_n	Number average molecular weight
M_w	Weight average molecular weight
NMR	Nuclear magnetic resonance
OPVs	Organic photovoltaics
OFET	Organic field effect transistor
OLED	Organic light emitting diode
PCE	Power conversion efficiency
PCBM	[6,6]-Phenyl-C61-butyric acid methyl ester fullerene
PDI	Polydispersity index
ProDOT	Propylenedioxythiophene
PSC	Polymer solar cell
p-TSA	*p*-Toluenesulfonic acid
PV	Photovoltaic
SCE	Saturated calomel electrode
TGA	Thermogravimetric analysis
TLC	Thin layer chromatography
UV	Ultraviolet spectrum
Vis	Visible spectrum
V_{oc}	Open circuit voltage

Abstract of Dissertation Presented to the Graduate School
of the University of Florida in Partial Fulfillment of the
Requirements for the Degree of Doctor of Philosophy

CONTROL OF COLOR, MOLECULAR ORDER AND CHARGE TRANSPORT IN CONJUGATED POLYMERS

By

Unsal Koldemir

December 2012

Chair: John R. Reynolds
Major: Chemistry

Conjugated polymers with a high degree of molecular order were developed and integrated into organic electronic applications, where the mechanical robustness, processibility, and high charge transport properties of these materials were taken advantage of to yield high performance devices. This dissertation examines strategies for improving device performance first through optimizing synthetic protocols for the scalable preparation of photovoltaic materials with aesthetically pleasing color; and also through synthetic manipulation, via heavy atom substitution and end capping, of commonly used polymers to yield improved charge transport in field effect transistor applications.

A dioxythiophene donor-acceptor based polymer, PGreen, was synthesized through oxidative polymerization (later optimized through Stille polymerization) and implemented in photovoltaic devices. The synthesis was both reproducible and scalable. PGreen was chosen because of its aesthetically pleasing green color, achieved via a trough in its absorption profile in the green region of the spectrum. This work is the first to study the scalability of both the synthesis and processing of a polymer other than poly(3-hexylthiophenes) for large area solar cell applications. In

particular, the performance differences between spin coated, small area solar cells, and large scale slot die coated solar cells were investigated to highlight the importance of processing techniques on device performance.

In the second portion of this thesis, a germanium atom was substituted in place of a silicon atom as the bridging atom in fused thiophene aromatic units in six polymers obtained by Stille polycondensation by 1% stoichiometric imbalance. Heavy atom substitution is discussed as a means of increasing the molecular organization of conjugated polymers, leading to higher charge transport properties. Ge atom substitution provided a way to tune both the HOMO and LUMO levels and thereby the absorption profiles of the polymers in the visible spectrum. Furthermore, longer C-Ge bond lengths enhanced Pi stacking with closer intermolecular interactions, as shown by X-ray analyses, resulting in higher charge carrier mobilities.

As an alternative approach, the effects of end groups on the molecular order of the best performing dithienogermole-benzothiadiazole based copolymer were studied and compared with the performance of a non-end capped control polymer. End groups were confirmed by ^{1}H-NMR, 2D NMR and MALDI-MS analyses. The presence of end groups resulted in an increased tendency to stack with closer intermolecular interactions. Independent of the processing conditions, a much higher hole mobility was obtained by end capping.

CHAPTER 1
INTRODUCTION

1.1 Fundamentals of Conjugated Polymers

With the new millennium came a revolution in consumer electronics which would forever change the public view of electronic devices. Through miniaturization and sophistication, products such as ipads and E-readers have been created, which years ago could only be imagined. This has turned the attention of the electronics industry towards alternative high performance semiconducting materials, and the subsequent development of materials that can be easily deposited in nanometer thicknesses even onto flexible surfaces. This is where conjugated polymers entered the arena as a family of new materials that combine the optoelectronic properties associated with inorganic materials with the plastic features of organic materials. Extensive research in this field has led to the realization of real life applications such as SONY organic light emitting diode displays,[1] E-paper,[2] and Konarka solar cell laptop bags.[3]

Synthetic chemistry is an invaluable tool for the development of high performance, optoelectronic materials because it encompasses an infinite number of strategies for the design and preparation of conjugated polymers, allowing them to be custom tailored for specific applications. Moreover, by studying the structure-property relationships of conjugated polymers, the performance of optoelectronic devices can be further enhanced. In Chapter 1, the fundamental properties unique to conjugated polymers are discussed along with important criteria for achieving high performance materials based these polymers. To this end, discussion of the band gap formation of a conjugated polymer is followed by synthetic strategies for controlling the polymer's color, and molecular order. Next, polymerization methods are described that facilitate

the synthesis of high molecular weight, scalable, low dispersity polymers. Lastly, a detailed analysis of processing methods is introduced along with a discussion of selected optoelectronic applications of conjugated polymers.

1.1.1 Band Gap Control

The electronic structure of conjugated polymers relies on a backbone of alternating single and double bonded carbon atoms with delocalized π orbitals along the polymer chain. From the simplest ethylene molecule to an infinite theoretical chain of polyacetylene, molecular orbitals overlap to form continuous energy levels; these are the so called energy bands as shown in Figure 1-1a.[4] In theory, polyacetylene has a fully filled valence band (VB) and an empty conduction band (CB), with a zero energy difference between the two bands. Thus it should yield equivalent resonance structures such as in Figure 1-1b.[5] In reality, there exists an energy difference between the highest occupied molecular orbital (HOMO), and lowest unoccupied molecular orbital (LUMO) in the infinite chain. This difference is defined as the band gap and is denoted as E_g. For example, consider the geometrical difference in structure between the aromatic and quinoid forms of polythiophene as depicted in Figure 1-1c. An energy difference arises as a result of bond length alternation or double bond localization, which results in the formation of non-degenerate HOMO and LUMO levels. In solid state physics, this phenomenon is known as Peierls distortion.[4] Additionally; planarity, substitution, aromaticity and interchain interactions can play a role in determining the band gap of a material, as shown in Figure 1-1d. To broach these factors, E_{BLA} defines the difference of length between the double and single bonds. The higher the bond length alternation, the larger the bandgap.[6] For instance, in the aromatic form of polythiophene, π electrons

are more localized in the ring system than they are in the quinoid form. Thus, the carbon-carbon bond lengths between the thiophene rings exhibit more single bond character.

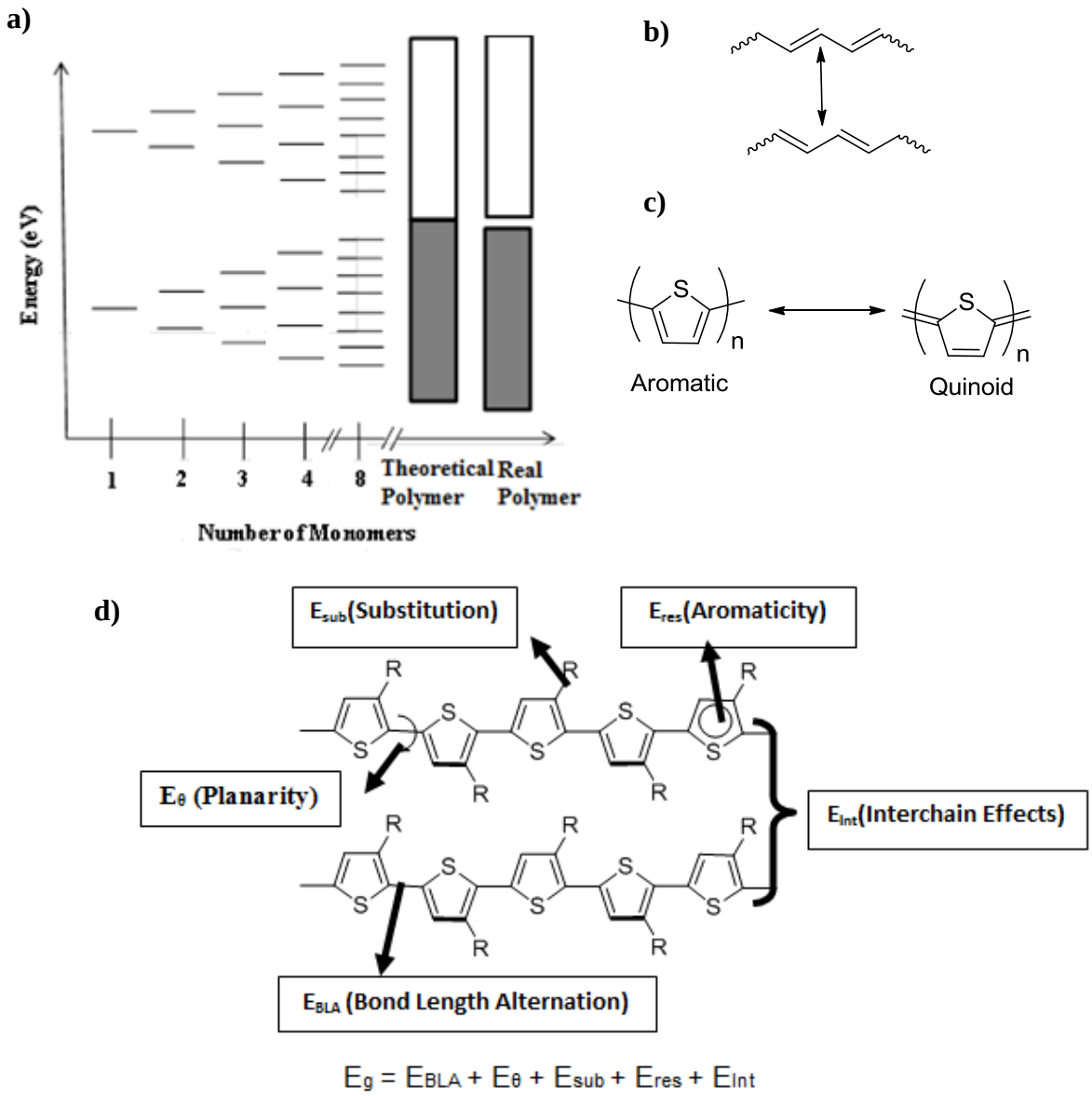

Figure 1-1. The concept of band gap as in conjugated polymers. a) Formation of bands in a conjugated polymer. b) Resonance forms of poly(acetylene). c) Aromatic and quinoid resonance structures for polythiophene. d) The structural factors affecting the energy of the band gap in an alkylated polythiophene. (Adapted and modified with permission from Roncali)

The parameter E_θ describes energy differences that arise due to torsion between two aromatic rings (resulting in a twisting of the polymer described by the angle theta) caused by the steric congestion between the atoms or substituents on the rings.[7] The torsional angle can be decreased by forming more planar geometries, thus favoring a better overlap of the π orbitals. Increased delocalization of the π electrons along the polymer chain reduces the band gap. From a synthetic organic chemistry perspective, placing double or triple bonds in between aromatic rings can be effective in reducing the amount of torsional strain.[8-10] E_{sub} is related to the effect of the substituents on the aromatic rings. These moieties can be of the electron donating kind (e.g. -OR), resulting in increased HOMO energy levels,[11] or can be of the electron withdrawing kind (e.g. -CN), operating in decreased LUMO energy levels.[12, 13] Apart from these, the substituents are mostly bare alkyl chains that induce solubility to the polymer.[14, 15] Strong π–π interactions occurring between polymer chains enable the delocalization of π electrons, thus governing the energy difference due to interchain effects, E_{Int}. Lastly, the energy difference between resonance structures, $E_{res,}$ is related to the degree of aromaticity in the quinoid form, and thus describes energy difference between the aromatic and quinoid forms. This strategy has been applied in realization of the very low band gap conjugated polymers based on isothianaphtene and thienothiophene.[16-18]

The donor-acceptor strategy first introduced by Havinga *et al*., also known as the *push-pull* method, is an effective method to control the band gap.[19] This approach finds its remarkable power through reducing the bond length alternation in a polymer by bringing together electron-rich (donor) units with the electron-poor (acceptor) units. The difference in electronegativity between two units causes polarization of the bond, such

that a resonance structure can be written as (D-A $\leftrightarrow D^+ = A^-$). This enhances the delocalization of π electrons along the polymer chain by reducing the bond length alternation. Figure 1.2 shows this phenomenon schematically. The molecular orbitals of the donor and acceptor moieties are hybridized so that they form new molecular orbitals with a reduced band gap. The effectiveness of this method in reducing the band gap has been realized by Reynolds and coworkers, who report a 0.5 eV band gap copolymer of dithienopyrrole and benzobisthiadiazole.[20]

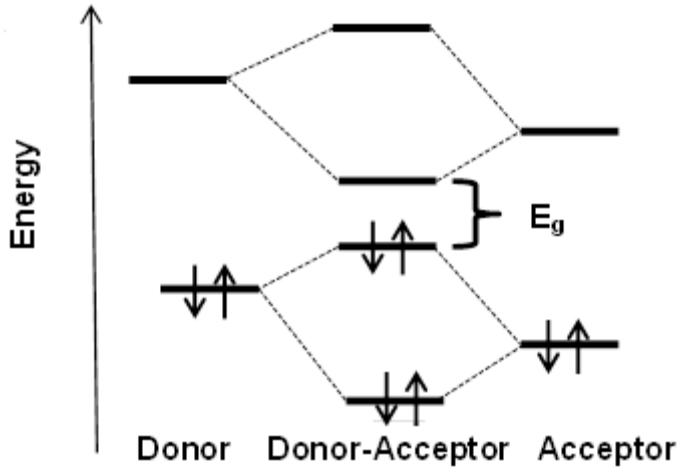

Figure 1-2. Reduction of the band gap in a donor-acceptor copolymer.

There are many possible donor and acceptor moieties that can be selected for creating conjugated polymers for device applications, including integration into OFETs,[21, 22] OPVs,[23-26] electrochromics[27, 28] and OLEDs.[29] Some of the available electron-rich and electron-poor units are depicted in Figure 1-3. The large variety of available units allows polymer properties to be tailored through judicious choices of donor and acceptor combinations. For instance, the Mats Anderson group has reported band gaps between 2.1 to 1.3 eV by varying the electron poor unit in the structure of alternating polyfluorene (APFO) type donor-acceptor polymers.[30]

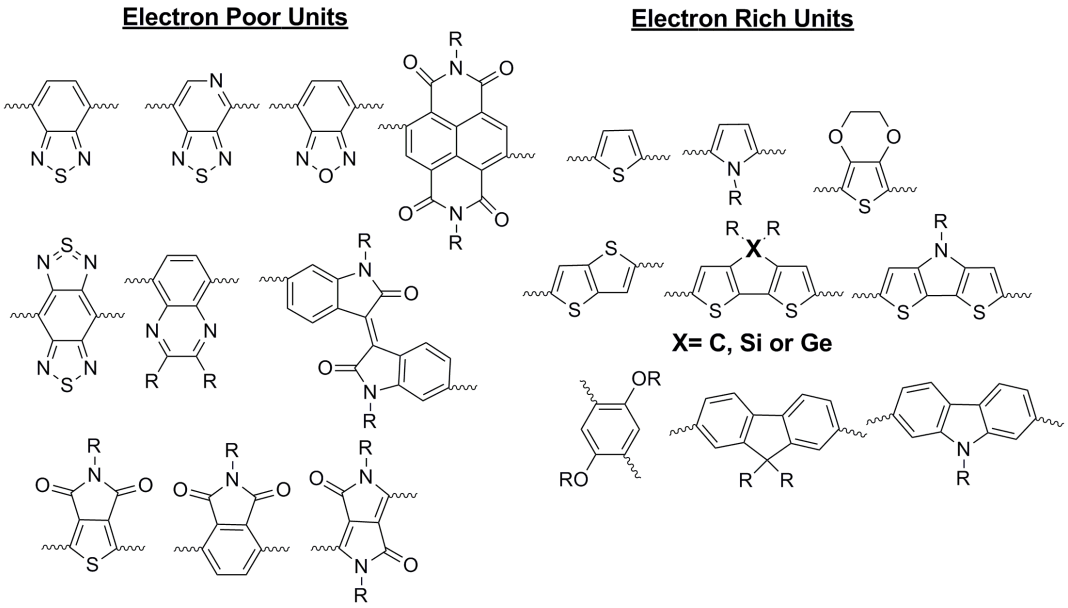

Figure 1-3. Representative electron poor and electron rich units employed in donor-acceptor type polymers.

1.1.2 Color Control

The color of a conjugated polymer depends on its light absorption behavior in the visible region of the spectrum and the relative intensity of its absorption bands. There are multiple reasons for the occurrence of absorption bands, such as the extent of conjugation in the polymer and the energy levels of the HOMO and LUMO of the polymer. Along with the considerations mentioned for band gap control, relative energies of the HOMO-LUMO levels become a challenge to be addressed by synthetic chemistry. This phenomenon has been important in controlling the color of non-emissive electrochromic materials, where a neutral color is switched to a transmisssive color upon redox processes. The design of electrochromic polymers with specific colors has been reviewed by our group recently.[27] Particularly, 3,4-dialkylateddioxythiophenes have been employed in the design of polymers to obtain red, orange, magenta, blue,

cyan, green, yellow and black colors. Figure 1-4 describes the absorption profiles of the desired colors for each specific polymer.[31]

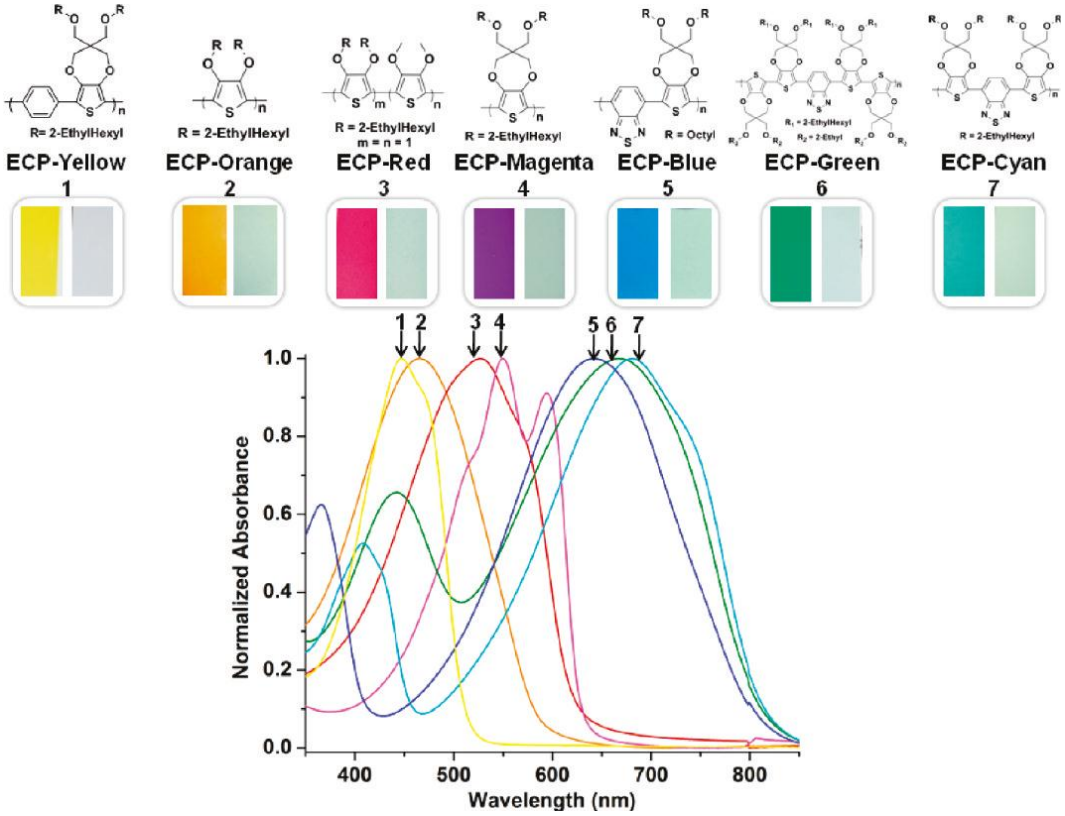

Figure 1-4. Colors obtained from 3,4- dioxythiophene based polymers along with their normalized absorption spectra. (Adapted with permission from Reynolds)

It is worth noting here that previously, electrochromic polymers enjoyed low band gap polymers with high HOMO levels to obtain the colors stated above with the exception of yellow. A neutral yellow colored copolymer was obtained by employing dioxythiophene-benzene moieties.[32] This polymer had a band gap of 2.38 eV with an absorption maximum at 455 nm and an onset of absorption of 520 nm. The absorption profile in the blue region yields a vibrant yellow color. Removing the benzene unit and changing the propylenedioxy bridge to 2-ethylhexyloxy groups on the thiophene shifts the absorption maxima to 490 nm, achieving an orange colored polymer. The same electron rich moiety was randomly copolymerized with 3,4-dimethoxythiophene to yield

a red colored polymer by reduced steric interactions because of the smaller size of the methoxy groups. Additionally, a random copolymer approach has been successfully applied with 3,4-propylenedioxythiophene and benzothiadizole units to control the whole absorption in the visible spectrum in order to obtain neutral black colored polymers.[33]

For organic solar cell polymers, the color has not been the central concern. The highly studied P3HT is orange in color due to minimal absorption above 650 nm. Cylopentadithiophene-benzothiadiazole (PCPDT-BTD) copolymer, also commonly used in solar cell applications, is blue green[34], and dithienosilole-benzothiadiazole (PDTS-BTD)[35] achieves a red shift of absorption leading to its green color. In this regard, the Andersson group has shown a systematic approach to span the visible spectrum using the alternating polyfluorene (APFO) type donor-acceptor polymers.[36] As seen in Figure 1-5, by changing the nature of the acceptor unit, the absorption can be expanded up to 1000 nm by varying the energy of the polymers' LUMO levels.

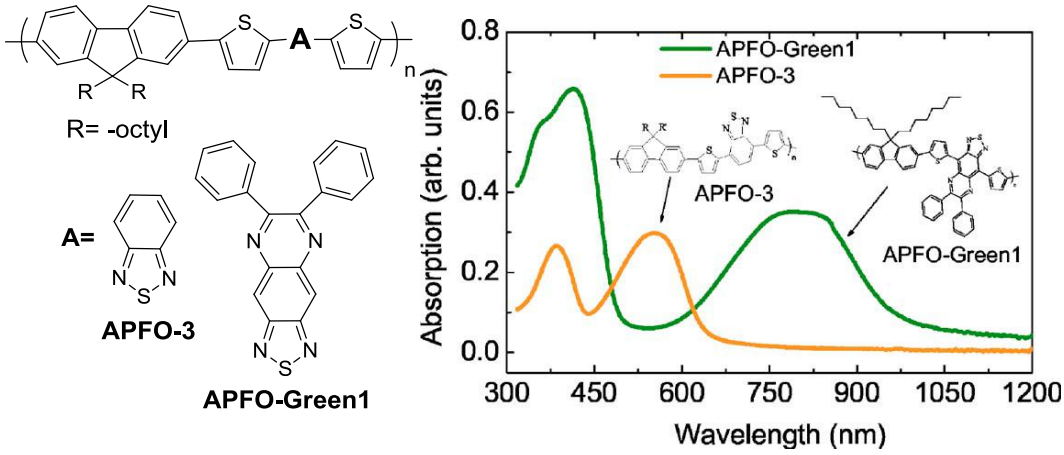

Figure 1-5. Repeat unit structures for the APFO type polymers displaying green and purple color along with their normalized absorption spectra. (Adapted with permission from Andersson

When the acceptor moiety is benzothiadiazole, the polymer is purple in color due to minimal absorption in the blue and red region. By changing the acceptor to

thiadiazoloquinoxaline, the polymer achieves a green color due to absorption in the blue and red region with transmission in the green region, *ca*. 500-550 nm. The absorption bands are due to π- π * transitions. Beaujuge *et al.* have proposed concepts in an attempt to explain the origin of dual band absorption, particularly in the donor-acceptor type polymers.[37] In particular, the concentration of donor and acceptor units has been varied in the repeat unit structure of the polymers based on 3,4-propylenedioxy-thiophene and benzothiadizole. By increasing the electron rich moieties in the polymer backbone, the longer wavelength absorption band is reduced and slightly blue shifted. At the same time, the shorter wavelength absorption band is increased in intensity and red shifted, minimizing the trough between this band and the longer wavelength absorption band. In a simple assumption, the donor-acceptor polymers are treated as consisting of two distinct chromophores. One chromophore involves the donor units and increasing the number of electron rich moieties decreases the band gap of these chromophores and leads to the aforementioned red shifted absorption. A second chromophore results from the donor-acceptor segment, and increasing the electron rich units in the repeat unit causes the dilution of donor-acceptor interactions. Consequently, the high energy band's energy is depleted and slightly blue shifted.

1.1.3 Molecular Order and Charge Transport Control

Many inorganic semiconductors form crystalline solids through the periodic arrangement of their atoms into a three dimensional network bound together with strong ionic and covalent bonds. Organic semiconductors, on the other hand, rely on attractive non-bonded interactions, such as π - π stacking between aromatic units through delocalized π orbitals. The extent of the spatial arrangement of π orbitals, with respect

to each other, determines the stacking ability or so-called *molecular order*. In fact, molecular order/packing determines the transfer integral and reorganization energy of a polymer.[38] The transfer integral is determined by the difference between the HOMO and LUMO energy levels, and is directly related to π overlap between adjacent molecules.[39] The reorganization energy is the energy lost concomitant to the charge transport through a molecule. It is dependent on the extent of conjugation in organic molecules and on the molecular order in their films.[40-43] Lower reorganization energy correlates with higher charge carrier transport, a necessary component for organic molecules in optoelectronic applications. Improved molecular ordering decreases the reorganization energy.[44] Therefore, this section describes important synthetic tools to increase molecular order in small molecules and polymers, in conjunction with their charge transport properties. While this dissertation does not focus on the synthesis of small molecules, it is important to cover these strategies as an *a priori* for understanding the molecular order in polymers. Highly ordered films made of organic molecules can form semicrystalline materials, which, in general, correspond to higher charge carrier mobilities as suggested by Street *et al.*[45] Conjugated molecules/polymers result in films with slightly less order, but can still be treated as distinct from random structures. In the subsequent two sections, examples are presented of strategies to induce order in the solid state. Small molecule conjugated systems are analyzed first, as their physical analysis relatively simple, followed by the more complex macromolecular systems.

1.1.3.1 Molecular Order and Charge Transport in Small Molecules

Alkyl chain substitution is a powerful way to create, not only soluble molecules, but also to control the mesoscopic organization these molecules.[46] This method was

used to prepare two oligomers based on anthracene and thiophene in order to study the effect of side n-hexyl chains, as illustrated in Figure 1-6a.

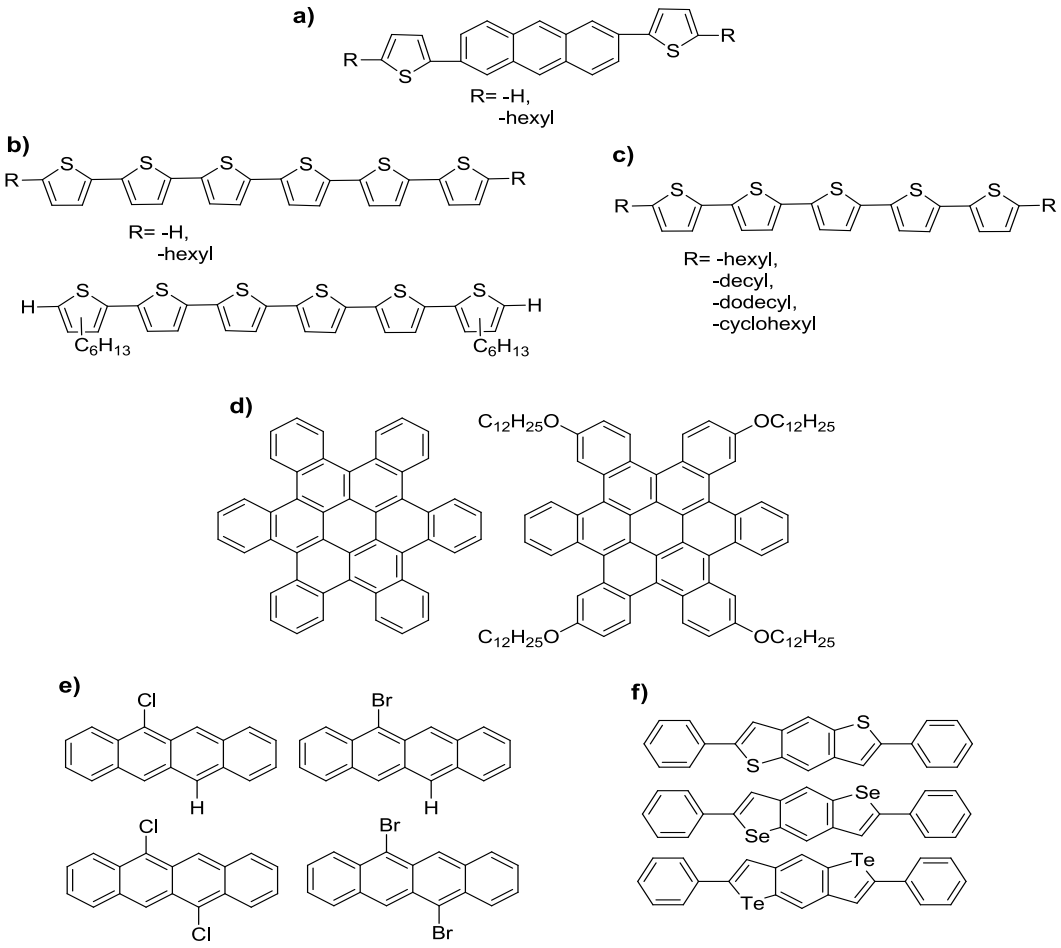

Figure 1-6. Examples of chemical modifications to study the molecular order. a-c) Alkyl chain substitution. d) Alkoxy substitution. e) Halogen atom substitution. f) Heavy atom substitution.

Oligomers were prepared by Suzuki coupling between pinacolatoboronic ester-substituted 2,6-anthracene and the corresponding 2-bromothiophenes.[47] Both oligomers presented with a herringbone-type packing geometry, similar to that of pentacene, while the dihexyl substituted oligomer demonstrated smaller unit cell dimensions in the solid state. The difference in packing structures of these two oligomers revealed distinct charge transport properties when implemented in OFET devices. The dihexyl

substituted oligomer exhibited a hole mobility of 0.5 cm^2/V.s. with an on/off ratio as high as 10^7, whereas the non-substituted oligomer showed a hole mobility value of only 0.063 cm^2/V.s. with an on/off ratio of 10^5. This order of magnitude difference in the charge transport behavior can be attributed to the hexyl chains promoting long range order in the molecule by favoring self-assembly processes during crystallization. This analysis is separately discussed by Garnier *et al.* through the examination of oligomers composed of sexithiophenes. [46] In their work, three sexithiophene oligomers were prepared as shown in Figure 1-6b. β–β' dihexylsexithiophene presented excellent solubility of 400 mg/mL in chloroform, whereas non-substituted and α-α' dihexylsexithiophene showed poor solubility in either dichloromethane or chloroform, *ca*. 1 mg/mL. This observation was attributed to the strong π- π interactions in non-substituted sexithiophene and α-α' dihexylsexithiophene. Additionally, melting temperatures observed for these compounds were, 80 ^oC, 280 ^oC, and 290 ^oC, respectively, for β–β' dihexylsexithiophene, non-substituted sexithiophene and α-α' dihexylsexithiophene, confirming the increased conformational freedom of the β–β' dihexylsexithiophene system. On the other hand, substitution on the α position enhanced the cohesive forces between the conjugated molecules. This was mainly caused by the hydrophobic-lipophilic interactions existing between alkyl chains. Furthermore, X-ray measurements showed long range order for the α substituted sexithiophene compared to the non-substituted form, whereas the β substituted sexithiophene did not show any crystallinity. The crystallinity of each molecule correlated with its measured hole mobility. Hole mobilities of 0.05 cm^2/V.s. and 0.002 cm^2/V.s. were obtained the α substituted sexithiophene and non-substituted

sexithiophene respectively, whereas the β substituted sexithiophene did not show any charge transport behavior. Consequently, alkyl substitution has proven effective in improving the structural organization of molecules on the mesoscopic scale, resulting in highly ordered solid architectures, and thereby improving hole mobilities.

Additional studies on the impact of alkyl side chains on the crystallinity and charge transport were conducted using thiophene oligomers substituted with n-hexyl, n-decyl, n-dodecyl and bulky cyclohexyl side chains at the α position as shown in Figure 1-6c.[48] It was observed that the modified molecules aligned themselves with their long molecular axis perpendicular to the substrate, while unsubstituted thiophene oligomers render randomly oriented thin films. Bulky cyclohexyl functionalized quarterthiophenes in particular showed good solubility in common organic solvents, allowing the fabrication of OFETs through drop casting. Drop cast samples demonstrated hole mobilities of 0.06cm^2/Vs, a value 3 times higher than the di-*n*-hexyl substituted quarterthiophenes.

Small organic molecules were substituted with alkoxy derivatives to increase their solubility as well as to promote ordering in the solid state. A derivative of disc shaped hexabenzocoronene (HBC) was functionalized with four dodecyloxy- side chains as illustrated in Figure 1-6d.[49] Though its aromatic core is severely distorted out of planarity into a corrugated structure, the molecule was found to self-assemble into two dimensionalcolumnar structures due to the tetra-n-dodecyloxy substitutients. Solution processed OFETs fabricated with dodecyloxy- functionalized HBC showed hole mobilities of 0.02 cm^2/V.s. with an on/off ratio of 10^6.

Another synthetic strategy to control the solid state ordering in organic molecules involves the incorporation of halogen atoms. Halogen atoms such as chlorine and/or

bromine were attached on tetracene molecules as shown in Figure 1-6e. The halogen substituted tetracene derivatives were all soluble in common organic solvents, facilitating the growth of single crystals. Single crystal X-Ray diffraction patterns of dihalogen derivatives showed a face-to-face slipped $\pi-\pi$ stacking motif, and mono-halogen substituted derivatives displayed a herringbone type packing motif. The intermolecular distance between neighboring molecules was determined to be 3.49 Å for the dichlorotetracene, resulting in hole mobilities of 1.6 $cm^2/V.s$.[50] This can be attributed to the ability of halogen groups to promote co-facial π stacking through the formation of β sheets between the layers, thus increasing the hole mobility of dichlorotetracene by promoting π-π interactions.[51]

Yet another tool for controlling molecular order in organic materials relies on heavy atom substitution, which has been found to enhance intermolecular orbital overlap in aromatic units by reducing intermolecular spacing. Phenyl end capped benzodithiophene derivatives, 2,6-diphenylbenzodichalgenophenes, have been prepared by Takimiya *et al.* as a prototypical class to study the effect of heavy atom substitution, as shown Figure 1-6f.[52] All three molecules showed moderate OFET charge transport properties when deposited under vacuum. An improved hole mobility of 0.17 $cm^2/V.s$. was obtained for the heavier selenium derivative, in stark contrast with the hole mobility of 0.018 $cm^2/V.s$. obtained for the sulfur derivative.

1.1.3.2 Molecular Order and Charge Transport in Polymers

As illustrated with the examples in section 1.1.3.1, the simple strategies of synthetic chemistry can be powerful tools to improve not only the solubility, but also to promote molecular order in thin films, of small molecules and oligomers. Polymers,

because they are larger in size than small molecules, are limited in terms of their packing arrangements, due to increased requirements for conformational freedom. As a result they tend to form small crystals surrounded by amorphous material. Additionally, polymers exhibit a polydisperse nature, which limits their long range ordering. The connectivity between the ordered domains and the amorphous domains is also an important factor in determining their charge transport properties, increasing the complexity of the analysis of their microstructures.

Poly(3-alkylthiophenes) have been benchmark polymers to study the molecular ordering in conjugated polymers due to their simple synthesis and scalable procedures as suggested by Rieke[53] and McCullough.[54-57] Polythiophenes were synthesized by electrochemical methods and found to be insoluble, impeding the possibility of device applications. Alkyl substituents on the 3 position were applied to increase the polythiophenes' solubility and self-assembly.[58] As seen in Figure 1-7a, poly(3-alkylthiophenes) with increasing lengths of alkyl chains(four to twelve carbons) were synthesized. A non-monotonic dependence of charge carrier transport properties was measured by OFETs prepared by spin casting. The average hole mobilities reported were: 1.2×10^{-3} $cm^2/V.s.$ for *n*-butyl, 0.01 $cm^2/V.s.$ for the *n*-hexyl, 2×10^{-4} $cm^2/V.s.$ for the *n*-octyl, 6.6×10^{-5} $cm^2/V.s.$ for the *n*-decyl and 2.4×10^{-5} $cm^2/V.s.$ for the *n*-dodecyl functionalized poly(3-alkylthiophenes). Additionally, in order to evaluate the microstructural characteristics of these polymers, two dimensional grazing incidence X-ray diffraction measurements were performed by drop casting n-hexyl, n-octyl and n-dodecyl poly(3-alkylthiophenes).[59] As seen in Figure 1-7c, the n-hexyl functionalized poly(3-alkylthiophene) derivative displayed long range order, as evidenced by the spots

on the q_z axis, as well as an edge-on orientation on the substrate, as derived from the arc in the q_{xy} axis. The n-octyl and n-dodecyl functionalized derivatives displayed less order, as evidenced by diffuse and weaker arcs in the q_z and q_{xy} axes. The π–π stacking distances were calculated to be 3.74 Å for poly(3-hexylthiophene) and 3.90 Å for the poly(3-dodecylthiophene) derivative.

In this context, the regioregularity or irregularity caused by the relative arrangements of alkyl chains, further determines the molecular order of poly(3-alkylthiophenes). Alkyl chains can be arranged head-to-tail (H-T) and head-to-head (H-H), as shown in Figure 1-7b. The H-H arrangement brings steric repulsion between the alkyl chains, which causes twisting of the thiophene rings. When this happens, it results in reduced intermolecular interactions of the π orbitals, therefore resulting in random orientations of the polymer chains. For instance, regioregular poly(3-hexylthiophene) (P3HT) adopts a lamellar packing structure with preferential edge-on orientation on the substrate[60], resulting in charge mobilities exceeding 0.1 $cm^2/V.s$.[60-63] By contrast, increasing the amount of H-H arrangements in the regioregular P3HT induced a face on orientation on the substrate resulting in charge carrier mobilities of only 10^{-4} $cm^2/V.s$.[59]

Furthermore, molecular order can be controlled through tuning the molecular weight of the polymer. Studies on P3HT have shown that the number average molecular weight is a key parameter for controlling mesoscopic and microscopic order.[64] Figure 1-8 shows the AFM phase images for a 3.2 kDa (Figure 1-8a) and 32 kDa (Figure 1-8b) number average molecular weight regioregular P3HT. Low molecular weight regioregular P3HT presented with a fibrillar morphology, with rod-like crystallites, well suited for crystalline stacking through self-assembly.

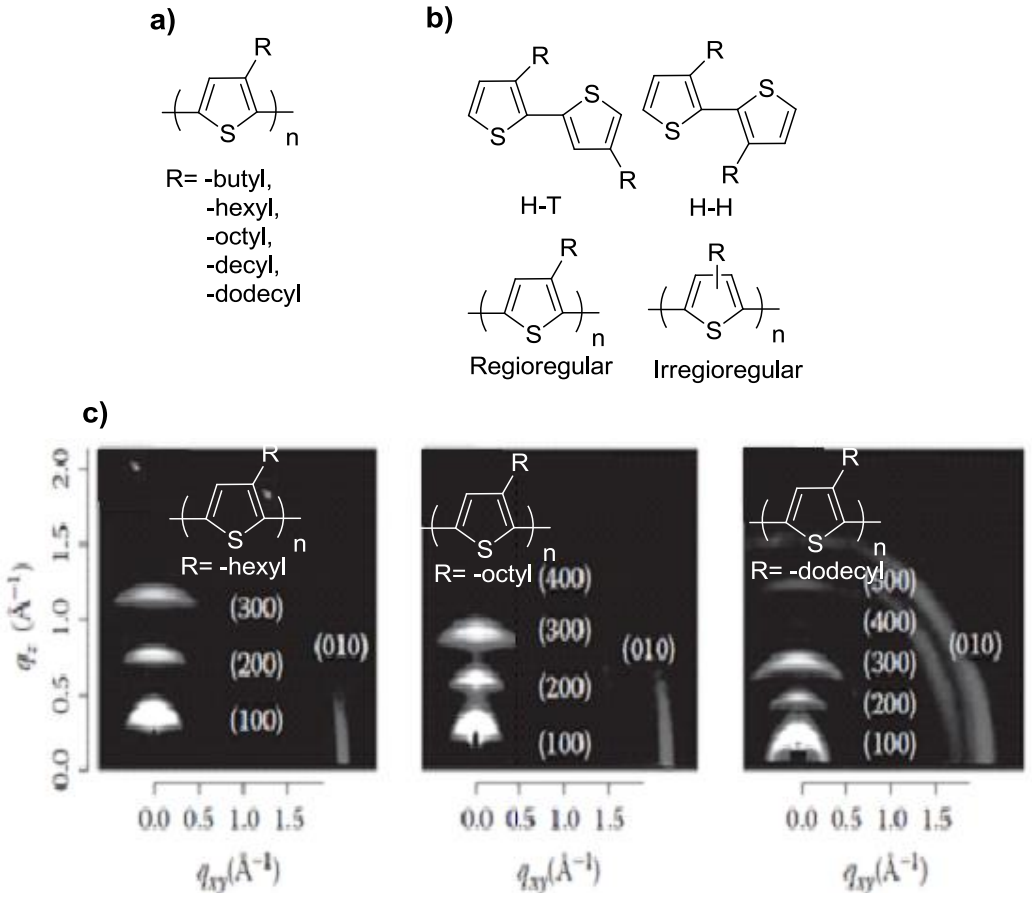

Figure 1-7. Control of molecular order in poly(3-alkylthiophenes). a) Poly(3-alkylthiophenes) functionalized with different length alkyl chains. b) Regioregular and irregular poly(3-alkylthiophenes) obtained from H-T and H-H couplings. c) Drop cast two dimensional grazing incidence X-ray diffraction patterns for drop cast poly(3-hexylthiophenes), poly(3-octylthiophenes) and poly(3-dodecylthiophenes). (Adapted with permission from Locklin)

Figure 1-8 shows the AFM phase images for a 3.2 kDa (Figure 1-8a) and 32 kDa (Figure 1-8b) number average molecular weight regioregular P3HT. Low molecular weight regioregular P3HT presented with a fibrillar morphology, with rod-like crystallites, well suited for crystalline stacking through self-assembly. Increasing the molecular weight to 32 kDa resulted in isotropic nodules, resulting in less crystallinity, due to their relatively immobile long polymer chains, which restricted their rearrangement into highly packed fibers. One would expect that highly crystalline, low molecular weight polymers

would have a higher hole mobility compared to less crystalline, high molecular weight polymers, however the charge transport is three orders of magnitude higher in the high molecular weight P3HT. This can be attributed to the presence of grain boundaries formed between highly crystalline polymer fibers in the low molecular weight polymer. Grain boundaries act as trapping sites for holes, leading to reduced charge transport. In the high molecular weight polymer, grain boundaries are smoothed out by connections between the ordered domains that provide pathways for charge transport. The low molecular weight P3HT lacks this kind of network architecture.

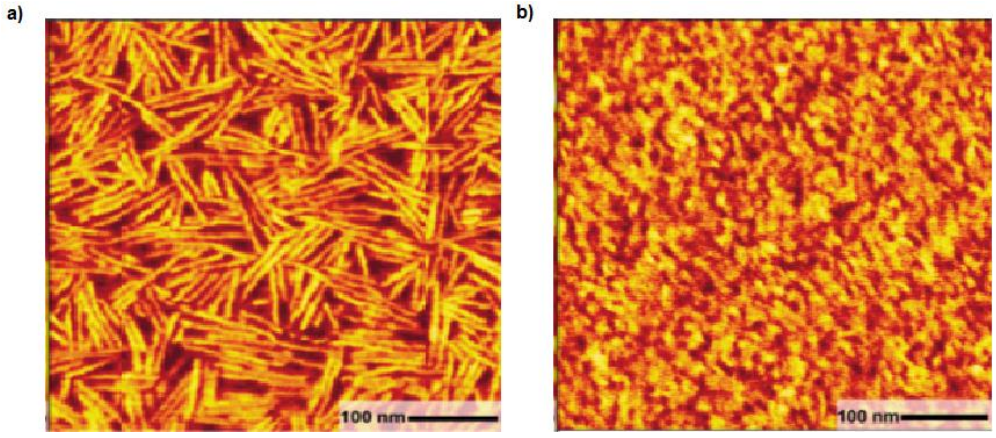

Figure 1-8. AFM phase images for different molecular weight P3HT. a) Low molecular weight (3.2 kDa) b) High molecular weight (32 kDa). (Adapted with permission from Frechet)

X-ray analyses have been performed on PCPDT-BTD copolymers substituted with *n*-hexadecyl alkyl chains, as shown in Figure 1-9.[65] A charge carrier mobility of 0.17 cm^2/V.s. was achieved with a 13 kDa molecular weight PCPDT-BTD copolymer, while a PCPDT-BTD copolymer with 65 kDa molecular weight presented with a hole mobility of 0.67 cm^2/V.s. Thus the higher molecular weight PCPDT-BTD copolymer demonstrated improved charge transport by almost 4-fold. However, macroscopic ordering, as observed through X-ray diffraction data, for PCPDT-BTD contradicts those results found

for P3HT. The high molecular weight polymer exhibited distinct spectral peaks in its X-ray diffraction pattern, as shown in Figure 1-9a, while the low molecular weight polymer yielded a completely amorphous diffraction pattern. This data was further supported by the pronounced reflections in 2D-WAXS scans performed using extruded fibers of the high molecular weight polymer (Figure 1-8b). These reflections are absent in the low molecular weight polymer (Figure 1-9c). These findings clearly contradict the aforementioned results regarding the correlation between molecular weight and crystallinity found for different molecular weight P3HT samples and warrant further study.

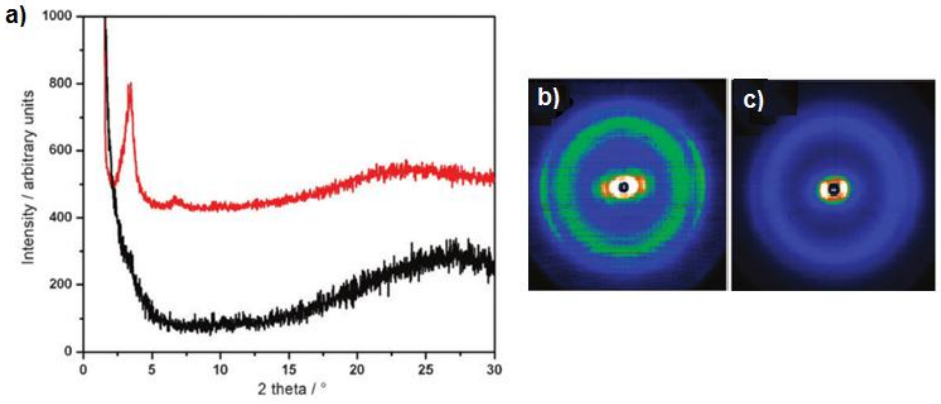

Figure 1-9. X-ray analyses of PCPDT-BTD for different molecular weights. a) X-ray diffraction pattern for high molecular weight (56 kDa) PCPDT-BTD (red line) and low molecular weight (13 kDa) PCPDT-BTD (black line).Two dimensional wide angle X-ray scattering patterns for b) high molecular weight (65 kDa) PCPDT-BTD c) low molecular weight (13 kDa) PCPDT-BTD. (Adapted with permission from Muellen)

1.2 Polymer Synthesis

This section is dedicated to the most common synthetic methods for the preparation of conjugated polymers. Important details on these polymerization methods are discussed in conjunction with the control of molecular weight, polydispersity and chemical purity of these materials.

1.2.1 Oxidative Polymerization

The first method developed to generate conjugated polymers was through oxidative polymerization, which can be accomplished through either chemical or electrochemical processes. Oxidative polymerizations are advantageous in that they do not require expensive reagents and involve shorter reaction times to produce high molecular weight polymers. For chemical oxidative polymerizations oxidants such as $Fe(III)Cl_3$, $Fe(III)(OTs)_3$, $SbCl_5$ and $NOPF_6$ can be used in organic solvents.[66-70] By far, anhydrous $Fe(III)Cl_3$ is the most commonly used oxidant. However, it produces large quantities of HCl during the rearomatization via dissociation of two protons. It can be speculated that the generated HCl can overoxidize the growing polymer chains and cause molecular defects.[71, 72] In addition, McCarley *et al.* observed that multiple chlorine end groups are added during the polymerization, which could limit the polymerization and also effect the purity of the polymer.[72] In fact, the growing polymer is in oxidized form and needs to be reduced with hydrazine in order to obtain a neutral polymer. Also, the oxidized polymer is complexed with $FeCl_4^-$ and has a lower solubility than its neutral form.[73] Moreover, large amounts of Fe residues can be buried in the polymer network which could be detrimental to the performance of the polymer in device applications.[74, 75]

Despite the challenging pros and cons of oxidative polymerizations, when the conditions are well adjusted, it is possible to obtain high molecular weight polymers through these processes. Anderson's group has shown the effects of changing the solvent in oxidative polymerizations from chloroform to orthodichlorobenzene (ODCB).[76] They claim that ODCB solubilizes the oxidized polymer better than chloroform solvents. A thidiazoloquinoxaline-bithiophene copolymer was prepared by $Fe(III)Cl_3$ oxidation to

yield an Mn of 240 kDa in ODCB. The same polymer yielded a Mn of 14 kDa when chloroform was used as the solvent. Furthermore, the rate of addition to the solvent is important, as adding the oxidant all at once causes very low molecular weights.[70] However, applications of these methods are limited, as oxidative polymerization is only effective for monomers with low oxidation potentials.

1.2.2 Metal Catalyzed Polymerizations

Palladium reagents and catalysts provide numerous possibilities for carbon-carbon bond formation in conjugated polymers through Stille, Suzuki-Miyaura, Heck, Sonogashira, Negishi, Kumada and Hiyama coupling reactions.[77] Pd catalysts are tolerant to many functional groups, such as carbonyl and hydroxyl groups. Therefore no protection step is needed before the coupling reaction. In addition, they are insensitive to moisture, basic conditions or oxygen.[78, 79]

The most common sources of Pd(0) catalysts are $Pd(OAc)_2$, $PdCl_2(PPh_3)_2$, $Pd(PPh_3)_4$,and $Pd_2(dba)_3$. The first two sources, $Pd(OAc)_2$ and $PdCl_2(PPh_3)_2$, require the addition of electron-rich phosphine ligands to form Pd(0). Common phosphine ligands include PPh_3, $P(o\text{-}tol)_3$, $P(t\text{-}bu)_3$, PCy_3.[80] These ligands are electron-rich phosphines that enable the oxidative addition step in the polymerization process by donating electrons to an oxidized Pd center. The bulky groups can also accelerate the reductive elimination step through the reduction of steric congestion in the complex. Moreover, they can be used to increase the catalytic life/activity and turnover numbers of the Pd catalysts.

For example, $P(o\text{-}tol)_3$ can be used in coupling reactions through the formation of the Herrmann complex with a $Pd_2(dba)_3$ catalyst, as shown in Figure 1-10.[81] The complex has an increased catalytic life because it is stable in air and moisture, however,

precursors to the complex must be kept in an inert environment to prevent the oxidation of the phosphine ligand.

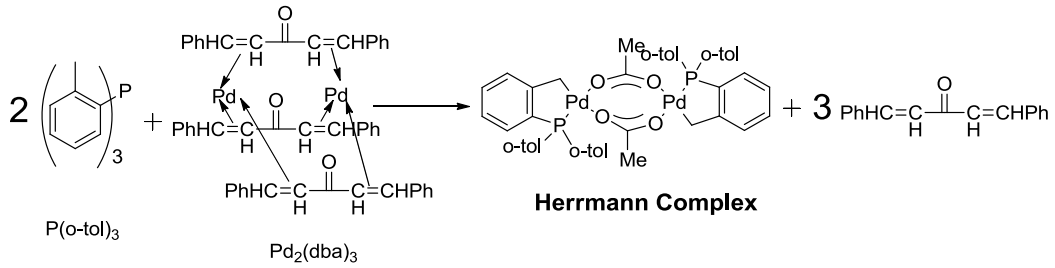

Figure 1-10. Formation of Herrmann complex with $Pd2(dba)_3$:$P(o\text{-}tol)_3$ catalyst system.

The basic steps for the Pd catalyzed reactions include oxidative addition (OA), transmetallation (TM) and reductive elimination (RE) in order to form a catalytic cycle. A Stille coupling procedure utilizing these steps is outlined in Figure 1-11. Oxidative addition involves the addition of an X-Y molecule to Pd(0) species. The single bond between the X-Y is broken, and two new single bonds are formed by using Pd nonbonding electrons. Thus, the oxidation state of Pd(0) increases by two leading to Pd(II). The process can be summarized as; Pd(0) + X-Y→ X-Pd(II)-Y. During the OA step, two of the ligands dissociate from the catalyst system to free vacant coordination sites. As the Pd metal is oxidized during the OA step, increased electron density on the Pd atom accelerates this reaction. Sigma-donor ligands, such as the phosphine derivatives mentioned previously, are particularly attractive for this purpose. On the other hand, π-acceptor ligands do the opposite: they inhibit the OA step. It is worth noting that, the nature of the halogen or pseudohalogen atom bonded to the sp^2 carbons facilitates the OA step in this order; C-I > C-Br >>> C-Cl>>C-F.[82]

In the transmetallation step, Ar-Pd-X species react with organometallic compounds of M'-R (where M'= Mg, Zn, B, Al, Sn, Si depending on the name reaction).

The driving force here is the electronegativitity difference between the M' and the Pd. M' is comprised mostly of main group elements, which are more electropositive than the palladium metal. This step is called transmetallation and can be summarized as:

Ar-Pd-X + Y-M'-R→ Ar-Pd-R + Y-M'-X

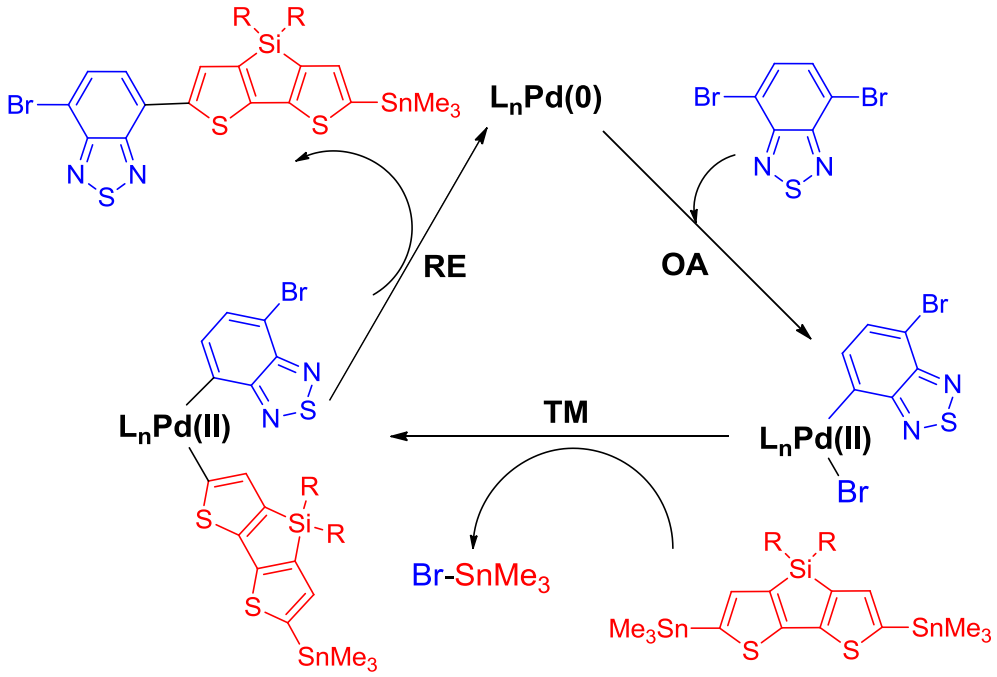

Figure 1-11. Catalytic cycle scheme as in Stille coupling.

The next step, reductive elimination, is complementary to the oxidative addition step. A unimolecular dissociation occurs, forming the original Pd(0) catalyst. The ligands that dissociate must be in *cis* configuration. The loss of two ligands results in the coordination and formal oxidation state of Pd(0) from Pd(II). Bulky phosphine ligands assist this step by bringing the two organic groups on palladium closer together. The recovered Pd(0) catalyst is now active and undergoes the OA step again, fulfilling the catalytic cycle.

The Stille reaction was first reported by Kosugi-Migita and Stille separately.[83, 84] It involves coupling reactions between organostannanes with arylbromides with the

advantage of organostannanesare compatible with other functional groups. The preparation of organostannanes is straightforward however; using stoichiometric amounts of organostannanes is a major drawback. There are several methods for the preparation of aryl organostannanes. Aryl halides can be reacted with butyllithium to form aryllithium, which can be further quenched with R_3SnCl. Another method was discovered by Eaborn *et al.* by reacting arylhalides with hexabutyldistannane (Bu_6Sn_2) and a Pd catalyst system.[85] In this case, hexamethyldistannane (Me_6Sn_2) is preferred over hexabutyldistannane as it can facilitate the transmetallation step.[86] Murata *et al.* have suggested a Pd catalyzed reaction of aryliodides with tributyltin hydride in ambient conditions, using potassium acetate as a base to generate organostannanes.[87]

Suzuki coupling involves the reaction of organoborons with arylhalides.[88-90] Unlike Stille reactions, which utilize hazardous organostannanes,[91] Suzuki reactions use organoborons, which bear low toxicity. In addition, boronic acids/esters are stable with respect to changes in heat and moisture and exposure to air. Thus, a large number of organoboranes are commercially available. Suzuki coupling conditions are advantageous as they are compatible with many functional groups and run in mild reaction conditions. On the other hand, the aryl group bonded to the boron atom is less nucleophilic, making the transmetallation step more difficult. To circumvent this problem, bases must be added to generate -ate complexes in which boron is quaternized in order to facilitate the transmetallation step. The arylboranes can be easily prepared by reacting aryllithium or arylmagnesium species with the corresponding trimethylborate, followed by hydrolysis. Alternatively, arylboranes can be prepared through the Pd catalyzed coupling between arylhalide with bis(pinacolato)diboron.[92] Simple arenes can

be reacted with pinacol ester derivatives by iridium or rhodium catalysts to generate the arylborane, without requiring bromination or lithiation steps, in high yields via direct borylation.[93, 94]

To summarize, the preparation of the precursors for Stille and Suzuki couplings, the selection of phosphine ligand and the mechanism of these reactions have been discussed in order to highlight important parameters governing polymerization reactions. When the aforementioned precursors are difunctionalized with the appropriate halide and the corresponding organostannane or organoboron derivative, it is possible to create A-B type alternating polymers. In this dissertation, as detailed above, the $Pd_2(dba)_3$:$P(o\text{-}tol)_3$ catalyst system has been utilized to produce high molecular weight polymers. This system has been chosen because of its high catalytic life and high turnover number. The ratio of $Pd_2(dba)_3$ catalyst was chosen as 2-4% mol with respect to one mole of monomer. In addition, the amount $P(o\text{-}tol)_3$ was chosen by doubling the amount of Pd catalyst. These amounts were sufficient to generate high molecular weight polymers in just hours, but the reactions were stirred over 3 days to ensure polymerization yields near 100%. This was effective in achieving polydispersities of 2-3 before any purification step. Toluene was selected as the solvent because it allowed for the samples to be heated at temperatures of 90 ^{o}C, while maintaining the polymer solubility in the reaction mixture. For Suzuki polycondensations, phase transfer catalysts such as Aliquat 336 have been used to facilitate the mixing of organic and negatively charged species. Schluter and coworkers have shown a polyfluorene homopolymer synthesized with Aliquat 336 that exhibited a number average molecular

weight (M_n) of 48 kDa.[95] Without this phase transfer catalyst the same polymer resulted in only a 9 kDa M_n.

Stille and Suzuki polycondensations producing high molecular weight conjugated polymers have been described in the literature. A patent has claimed the synthesis of a spiropolyfluorene polymer with a M_n of 267 kDa using toluene, water, K_3PO_4 and 0.025 % of the $Pd_2(dba)_3$:$P(o\text{-}tol)_3$ catalyst system using Suzuki polycondensation conditions.[96] The same polymer has also been shown to have a M_n of 410 kDa when prepared from ultrapure monomers.[95] On the other hand, Stille polycondensation has produced polymers with M_n over 100 kDa. In 2010, the Andersson group reported a copolymer with a M_n of 100 kDa synthesized using pyrazino[2,3-g]quinoxaline and trithiophene with the $Pd_2(dba)_3$:$P(o\text{-}tol)_3$ catalyst system.[97] A 207 kDa number average molecular weight copolymer based on phthalimide has been reported by Guo *et al.*[98] Recently, Bao and coworkers reported an isoindigo-bithiophene copolymer with a M_n of 138 kDa using the same catalyst system in a microwave assisted Stille polycondensation.[99]

In addition to Stille and Suzuki polycondensations, which proceed via step growth, a new method involving chain growth mechanism was suggested by Yokoyama *et al.*[100] This polymerization process is illustrated in Figure 1-12. The polymerization starts with the formation of a Pd complex with benzene, which acts as an initiator. The transmetallation occurs with the AB type monomer. Then, the metal migrates over the π part of the fluorene and adds itself oxidatively in between C and Br atoms. The species obtained is similar in structure to the initiator. Through the sequential addition of the monomer,a benzene end capped polyfluorene was obtained. The mechanism of

polymerization has been confirmed as a chain growth process, resulting in a M_n of 18 kDa with low polydispersities (1.3-1.4).

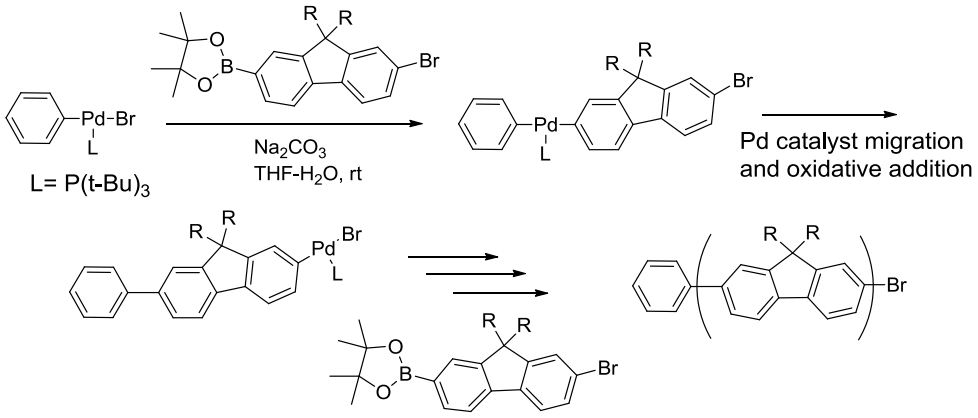

Figure 1-12. Proposed mechanism on the chain-growth Suzuki polymerizations.

A new method of carbon-carbon formation between aromatic units, called Direct Arylation, provides another alternative to Stille and Suzuki couplings.[101-103] This method eliminates the necessity of synthesizing the organostannanes or organoborons needed for Stille and Suzuki polycondensations, thus lowering the number of steps in the polymerization process. Further, by eliminating these precursors, this process avoids the use of the toxic materials used in conventional metal catalyzed polycondensations. Lemaire and co-workers have succeeded in synthesizing P3AT derivatives using this method, via direct arylation using $Pd(OAc)_2$, K_2CO_3 base and stoichiometric amounts of tetrabutylammoniumbromide as illustrated in Figure 1-13a.[104] The resulting polymers displayed regioregular structures with low molecular weights with M_n of approximately 6 kDa, and with PDI close to 2. Wang *et al.* were successful in obtaining a higher molecular weight P3HT with a M_n of 31 kDa and a PDI of 1.6 using Hermann's catalyst.[105] The regioregularity was calculated as 98 % with a polymer yield of 99%. The Leclerc group has recently shown a comparison of this polymerization with Stille

polycondensation as depicted In Figure 1-13b.[103] The Stille product showed a M_n of 9 kDa with a 71% yield, while direct arylation afforded the same polymer with a M_n of 56 kDa and a yield of 96%.

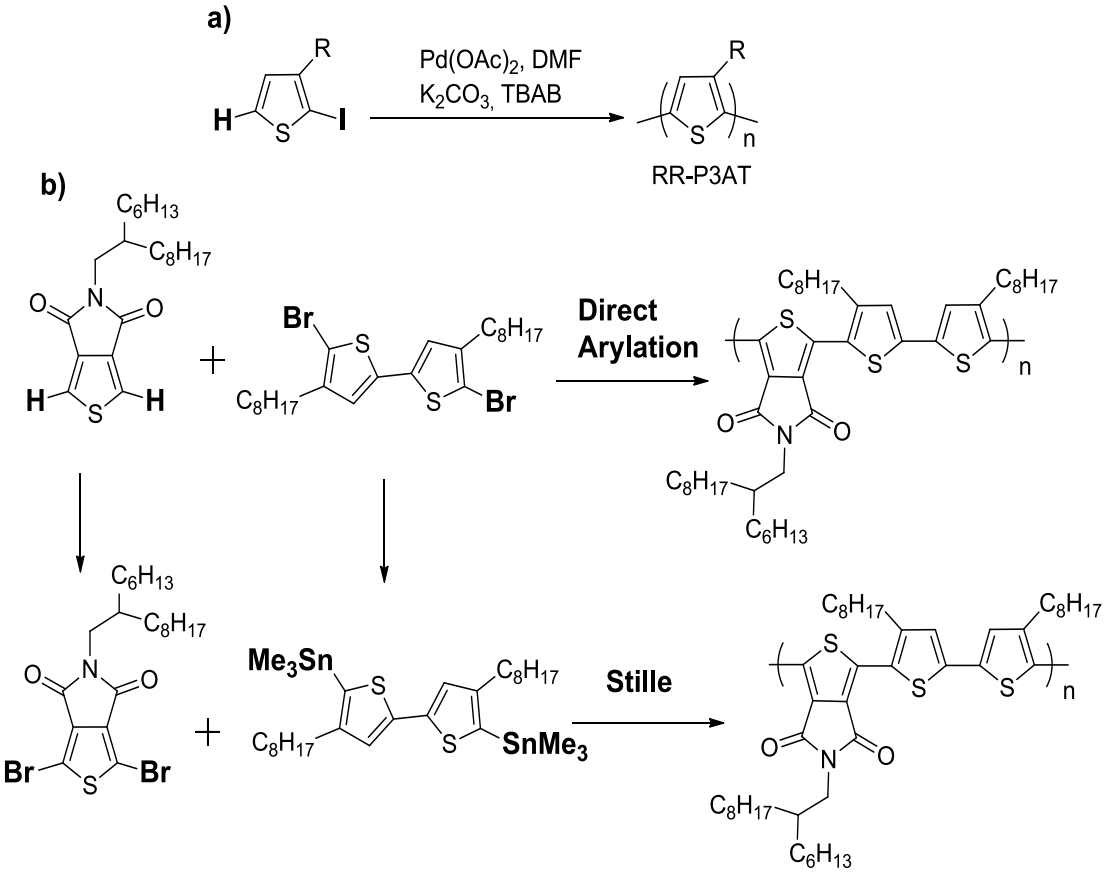

Figure 1-13. Direct arylation method for the synthesis of conjugated polymers.a) Direct arylation synthesis of poly(3-alkylthiophenes) b) Comparison of direct arylation and Stille polycondensation for generating the same thienopyrroledione based polymer.

1.2.3 End Group and Stoichiometric Control

In Section 1.1.3.2 the importance of molecular weight on crystallinity and performance has been discussed for conjugated polymers. In order to properly control the molecular weight in step-growth type polycondensations, extended reaction times, strict stoichiometric balance between the bifunctional monomers and carefully designed catalyst systems are required. In this regard, reaction time and stoichiometric balance

are emphasized in this section, particularly as they pertain to Stille and Suzuki polycondensations. The Carothers equation predicts the number average degree of polymerization as; $X_n = (1+r)/(1+r-2rp)$ for the polymerization of bifunctional monomers, where *r* denotes the stoichiometric imbalance and *p* represents the extent of reaction.[106] For polymerizations with carefully weighed, ultrapure bifunctional monomers in stoichiometric amounts, $r = 1$ and the equation becomes $X_n = (1)/(1-p)$.Thus, the polymer's molecular weight is dependent only on the conversion of the functional groups as determined by *p*. This explains why Stille and Suzuki polycondensations are run for at least 72 hours to ensure the completion of the reaction. For polymerizations with a high degree of nonstoichiometry, the polymer will have a low molecular weight. For instance, if bifunctional monomers are not carefully weighed, a 1 mol% excess of one monomer would lead to $X_n = 201$ when *p* is 100%. In reality, *p* never reaches unity, hence the same case with $p = 98\%$ results in $X_n = 40$. Another scenario arises when one of the bifunctional monomers has monofunctional impurities. This is true for many Stille reaction precursors in which the purification of ditin monomers is difficult, and monotin monomers may still be present. This not only results in a stoichiometric imbalance, but also the average functionally will be lower than 2. This is the worst case scenario and will dramatically lower the molecular weight. In practice, Suzuki reaction monomers - boranates/boronic acids- are crystalline solids that can be purified with several recrystallizations or using column chromatography. However, ditin monomers decompose during column chromatography, and trying to purify them by recrystallization may lead to decomposition by light and heat. Amb *et al.* have

suggested the utilization of reverse phase HPLC columns for large scale purifications of ditin monomers of dithienogermole.[107]

Stoichiometric imbalance can be intentionally applied to end cap step growth polymers. The polymerization proceeds until one monomer is completely exhausted. When this happens, all the chain ends will have the same functional group that is present in the excess monomer. Another strategy is to intentionally add a small amount of a monofunctional monomer. The monofunctional monomer will limit the polymerization, as the growing chains will have no functional groups to resume the polymerization. Yet another strategy relies on, post-end capping reactions. In this strategy, a Stille or Suzuki polycondensation is run with stoichiometric balance. After ensuring sufficient reaction time, monofunctional monomers are added sequentially. This method has been applied by Leclerc for carbazole based polymers[108] and by Schluter for the preparation of polyarylenes.[95] The end capping group was a monofunctional benzene moiety. As benzene hydrogen chemical shifts would overlap with the aromatic backbone units, their characterization is difficult by ^{1}H NMR. Recently Bazan and coworkers claimed the utilization of XPS measurements to analyze the absence of Sn and Br atoms after end capping with monofunctional thiophene via Stille polycondensation, claiming that the absence of these atoms implies successful endcapping of the polymers.[109] Soon after this work was published, Marks group attempted to obtain XPS spectra on these polymers, however their results were inconclusive with regards to the absence of Sn and Br on the chain ends.[110]

1.3 Processing Methods

As conjugated polymers are integrated into high performance devices, new processing techniques are needed so that improved device architectures can be

realized with conjugated polymers. In particular, solution processible polymers are of interest for industrial applications. The methods used to deposit these polymers dictate the crystal growth mechanism, and as a result determine device performance of the polymers. Therefore, in addition to investigating polymer synthesis methods, it is also important to consider polymer processing techniques. This section examines the small scale and large scale processing methods and discusses important parameters.

1.3.1 Small Scale Processing Methods

Popular processing methods for depositing conjugated polymers onto relatively small substrates include spin coating, drop casting, dip coating and spray casting. In spin coating, a thin film is formed while solution is added over a spinning substrate.[111] During this process, the film dries rapidly and evenly over the surface. As the polymer does not have sufficient time for self-assembly, long range directional alignment is uncommon with this method. The morphology of the film and also charge transport properties are dependent on the spinning rate, polymer solution concentration and the choice of solvent.[59, 112] Sirringhaus and coworkers showed that P3HT exhibits higher crystallinity, and an order of magnitude higher hole mobility, when processed from a high boiling point solvent such as 1,2,4-trichlorobenzene compared to a low boiling point solvent such as chloroform.[63] During the process, most of the polymer solution does not remain on the substrate; therefore a more economic method such as drop casting is desirable when material is limited. In drop casting, the evaporation of the solvent occurs over a longer time span resulting in “coffee rings”; no directional alignment of the polymer is provided through this method.[113]

The effect of processing conditions, such as thermal annealing, solvent selection and deposition method, have been studied by two dimensional grazing incidence x-ray

diffraction as seen in Figure 1-14.[59] It is obvious that regioregularpoly(3-octylthiophene) displays different crystallinity and molecular orientation on the substrate depending on the processing condition used for its deposition. Drop casting yields poly(3-octyl)thiophene molecules that have long range order, as proved by the (100) peaks in the q_z axis. These molecules prefer an edge-on structure on the substrate as evidenced by the (010) peak in the q_{xy} axis for the chloroform, toluene, THF and dichloromethane solvents. On the other hand, spin casting does not yield the same long range order for chloroform solutions, and results in a face-on orientation for both chloroform and toluene solutions. When a volatile solvent is selected, such as dichloromethane, long range order is still absent in spin cast samples, but molecules adopt an edge-on structure, similar to the drop casting results. Upon thermal annealing, long range order can be recovered for all of the solvents and edge on orientation is preferred in all cases except for THF solutions.

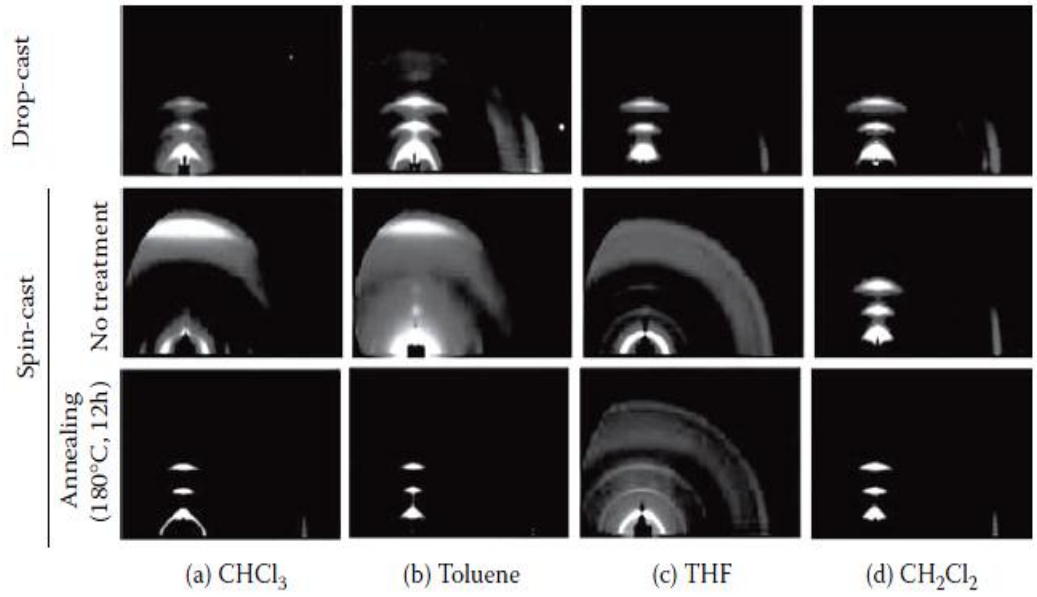

Figure 1-14. Two dimensional grazing incidence X-ray diffraction patterns for Poly(3-octylthiophene) processed from drop casting and spin coating from different solvents. (Adapted with permission from Locklin)

Another method for depositing polymer films is through dip coating, in which a substrate is immersed in a polymer solution, then drawn out at a specific rate such that the solvent evaporation happens at the rate of crystallization. This method provides homogenous thin films in the dip coating direction. If thicker films are desired, multiple layers of polymer can be coated on the substrate by repeating the process. Muellen and coworkers have shown that by depositing a PCPDT-BTD copolymer via dip coating results in improved long range ordering compared to films obtained through spin coating.[65]

Another deposition technique, spray casting, involves forming polymer solution droplets and subsequent deposition on a surface, resulting in homogenous microstructures.[114] This method offers the ability to select flexible, soft or flat substrates. The pressure, the solvent concentration and the angle of spraying are critical in determining the thickness of the material. Although it yields rough surfaces, spray casting is the most widely applied method for depositing conjugated polymers for electrochromic devices.[31, 115] One of the few reports of applying this method for polymer solar cells has shown power conversion efficiencies of 2.8% for a P3HT:PCBM blend from a dichlorobenzene solvent[116] and 3.2% when chlorobenzene was used.[117] Separately, the Yang group has demonstrated the preparation of a multi junction solar cells with active layers composed of P3HT:PCBM and dithienosilole-benzothiadizole copolymer:PCBM by spray coating which yield PCEs of 2.3 %.[118]

1.3.2 Large Scale Processing Methods

The aforementioned methods -except spray coating- are mostly applied in the lab-scale, on small substrates. These techniques are not easily scalable to the larger substrates needed for real life applications. Techniques such as ink-jet printing, screen

printing, slot die coating and combined roll-to-roll printing have been developed which can deposit polymers over large areas in a timely and costly manner. Interested readers may look at the reviews by Krebs and coworkers on these techniques.[119, 120] These methods are preferable to test optoelectronic device performances in solar cells that have sizes closer to commercial products.

Screen printing is a conventional, versatile technique used in industry for creating shapes and texts notable for its zero-waste solution processing.[121] It has been applied to deposit solar cells, field effect transistors and light emitting diodes.[122-124] The process involves the deposition of a film by painting a polymer solution onto a screen to create a pattern. It requires a highly viscous and low volatile polymer solution. Additionally, as the polymer solution is exposed to air, it is important that the polymer not dry out during the process. In 2009, Krebs *et al.* have prepared solar cells with this method in ambient conditions, and introduced the modules to the public.[125]

Ink-jet printing is akin to the process used in table top laser ink-jet printers. It uses ceramic piezoelectric printheads, which allow different ink formulations with a variety of solvents to be used.[126-128] During the deposition process, the printheads have no contact with the substrate, and therefore a many kinds of substrates are compatible with this method. While it can fabricate ultrasmooth pixels with high resolutions (300 dpi), the printing speed is slow. Nevertheless, Hoth *et al.* have demonstrated solar cells based on P3HT:PCBM with an output of 3% PCE with this technique.[129]

In the slot-die coating technique, a polymer solution is filled in a coating head and pushed through a slot by pressure with no loss.[130] It allows deposition of low viscosity polymer solutions into stripe patterns. The polymer film thickness is highly dependent on

the flow rate of the solution and the substrate velocity. Blankenburg *et al.* have demonstrated P3HT:PCBM solar cells prepared by this method with 1.7% PCEs under AM 1.5 conditions.[131] They were able to optimize production of 10 m^2/h polymer solar cells.

The Krebs group in RISO has dominated the field of large scale processing polymer solar cells by combining all the techniques above in a roll-to-roll process. Figure 1-15 outlines each step taken to deposit the electrodes, hole and electron transport layers, as well as the active P3HT:PCBM. In the first step, a striped pattern is applied onto ITO substrates by screen printing a UV curable etch resist. Next, the ITO was etched, washed, and allowed to dry. Then, ZnO nanoparticles in chlorobenzene were slot die coated onto the striped ITO pattern.

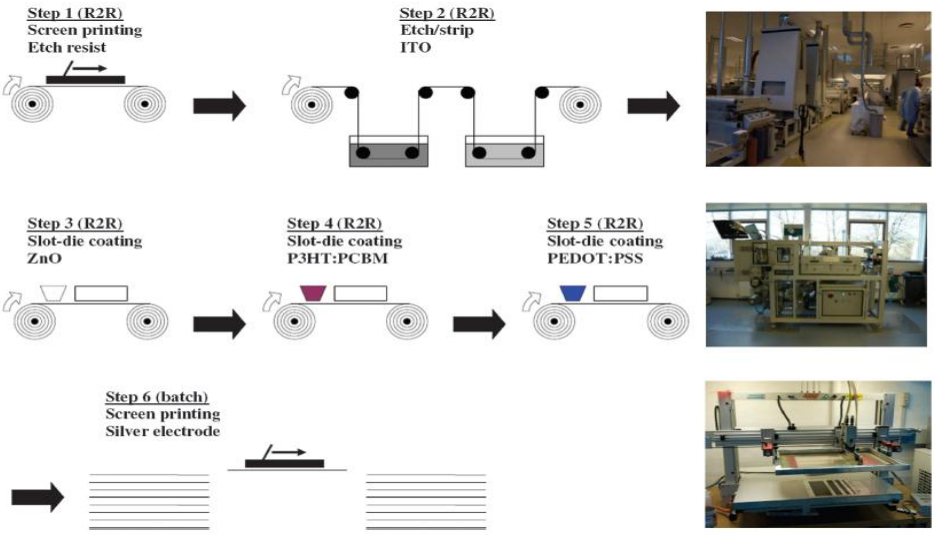

Figure 1-15. Illustration of six fabrication steps of deposition of organic solar cells components via roll-to-roll process. (Adapted with permission from Krebs)

This was followed by deposition of the active layer, consisting of P3HT:PCBM in dichlorobenzene, using slot die coating. After this layer was allowed to dry, PEDOT:PSS in isoproponal was slot die coated on top. Lastly, silver paste was screen printed, and

the samples were dried in an oven. In this regard, they have shown in numerous publications how to optimize each step and the required device geometry.[132-135] By following such steps the Krebs group was able to generate PCEs of 2.1% when the deposition of each layer is performed in air.[119]

1.4 Selected Device Applications

This section is dedicated to the description of selected examples of state-of-the-art advances in organic field effect transistors and organic photovoltaics. Fundamentals of device design and parameters are also discussed.

1.4.1 Field Effect Transistors

The basic building block of a field effect transistor is the Metal Oxide Semiconductor (MOS) capacitor, comprised of an insulator sandwiched between two conducting metals. A metal gate electrode, used to modulate the current, is covered with a dielectric layer and a semiconducting polymer film is deposited along with source and drain electrodes in intimate contact with the polymer. This particular kind of architecture is known as a bottom gate-top contact FET. Most FET devices operate in what is known as enhancement mode, where the device is in an off state when zero voltage is applied to the gate electrode. Increasing the potential applied to the gate creates an accumulation of charges at the semiconducting polymer/insulator interface. When a sufficient amount of charge builds up at the interface, an inversion layer is formed, creating a conducting channel between the source and drain electrodes. The potential existing between the source and drain electrodes, V_{SD}, obeys the basic Ohm's Law relation to the current between these electrodes, $V_{SD} \alpha I_{SD.}$ The performance of FETs is determined by measurement of the charge carrier mobility, μ. In the saturation regime, the mobility is given by the equation: $I_{SD} = W/2L\ \mu_{sat}C_i(V_G-V_T)^2$ where *W* denotes

the transistor channel width, L denotes the transistor channel length (the distance between source and drain electrodes), μ_{sat} denotes the charge carrier mobility, C_i denotes the capacitance of the insulator, V_G denotes the voltage applied at the gate electrode and V_T denotes the threshold voltage, the voltage that is needed to turn the transistor on.

State-of-the-art large area electronic displays utilize field effect transistors that use amorphous silicon as the semiconducting material. Amorphous silicon has charge carrier mobility greater than 0.1 cm^2/V.s., however high temperatures (greater than 350 ^oC) and high vacuum equipment are needed for processing. This not only increases the manufacturing cost, it also prevents the application of these materials onto flexible plastic substrates. In this instance, organic semiconductors are advantageous as they can be processed from solutions in ambient conditions, on even plastic substrates. However, they need to have charge carrier mobilities exceeding 0.1 cm^2/V.s. in order to compete with current display technology. Carefully designed conjugated polymers have shown great progress in terms of charge carrier mobilities by using simple solution processing techniques. Figure 1-16 shows the polymers with the highest performances. Regioregular P3HT has been the most widely studied material, with hole mobilities as high as 0.1 cm^2/V.s reported in top contact devices.[136] Following a more careful design, in order to decrease the density of alkyl chains, bithiophene moieties were incorporated between 3-hexylthiophene units. Ong *et al.* have shown hole mobilities of 0.1 cm^2/V.s with PQT-12.[137] Further, derivatives of poly(2,5-bis(3-alkylthiophen-2-yl)thieno[3,2-*b*]thiophenes)s (PBTT) have been introduced by McCulloch *et al.*[138] FETs based on these polymers have shown hole mobilities up to 0.6 cm^2/V.s. after annealing, in top

gate OFET device architectures. Yet more promising results have been obtained with the introduction of donor-acceptor type polymers for high performance OFETs. A phthalimide based copolymer, PhBT12 designed by Guo *et al.,* resulted in mobilities up to 0.28 $cm^2/V.s$,[98] while a diketopyrrolopyrrole-quarterthiophene based copolymer, PDQT, achieved 0.89 $cm^2/V.s$., attributed to lamellar packing on the substrate with an edge-on orientation.[139] In this particular example, the strong diketopyrrolopyrrole acceptor interacted with the neighboring donor-acceptor units, resulting in improved molecular order through extensive intermolecular interactions.

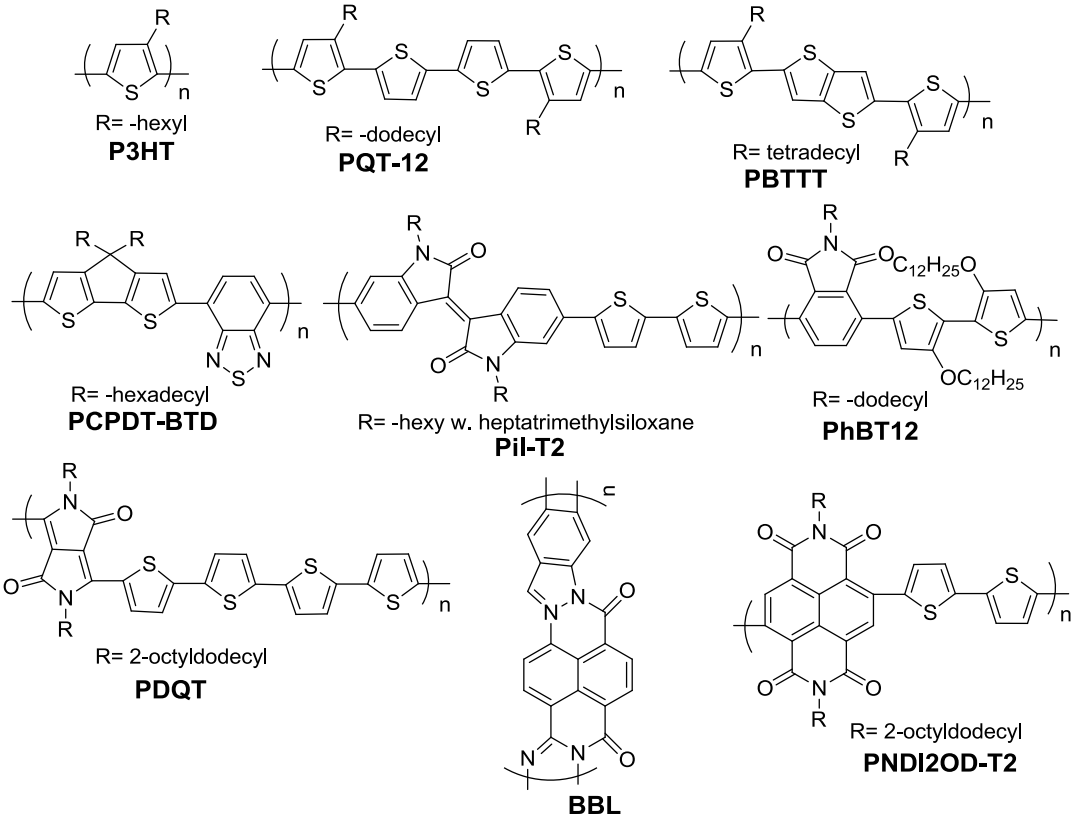

Figure 1-16. Representative hole and electron transporting polymers exceeding 0.1 $cm^2/V.s$.mobilities in OFET devices.

Much improvement has been observed by Muellen and coworkers by casting the PCPDT-BTD polymer via dip coating.[113] This method has increased the hole mobility of

0.17 cm^2/V.s.obtained by spin casting, to values as high as 1.7 cm^2/V.s. Finally, the current state-of-the-art highest charge carrier mobility that has been reported thus far was obtained by Mei *et al.* in 2011.[99] By employing an isoindigo-bithiophene copolymer, PII-T2, with siloxane pendant groups (these groups increase the attractive $\pi-\pi$ interactions by forcing polymer chains closer), they were able to obtain a mobility of 2.5 cm^2/V.s.

The aforementioned examples present holes as the dominant charge carriers. On the other side, electron transporting materials are of interest for incorporation into p-n junction diodes, acceptor molecules in the organic solar cells and in complimentary organic circuits. Compared to p-type polymers, the development of n-type materials has lagged behind, with just a few examples exhibiting μ_e exceeding 0.1 cm^2/V.s. This is due to the environmental instability of most n-type polymers due to electron interactions with oxygen and water in air. Nevertheless, a ladder type electron deficient polymer, BBL, has been synthesized and devices prepared by spin coating have shown electron mobilites of up to 0.1 cm^2/V.s.[140, 141] A very high molecular weight (250 kDa) naphthalenedicarboximide-bithiophene copolymer has also been tested in air and ambient conditions and found to yield stable electron mobilities of 0.85 cm^2/V.s.[142]

1.4.2 Photovoltaics

Bulk heterojunction (BHJ) organic photovoltaics (OPVs) can be classified into two subgroups depending on whether they consist of small molecules or polymers. Small molecule OPVs bear the advantage of straightforward synthesis, high purity that can be obtained by recrystallization, and multiple choices of device fabrication processes. Devices can be made by thermal evaporation of small molecules under high vacuum or

by processing from solution. Recent progress in this research field has resulted in power conversion efficiencies (PCEs) close to 7%.[143, 144] Despite the exciting results with small molecules, the film quality is still not well controlled in these devices, limiting further improvements. On the other side, polymer based OPVs provide many advantages. Firstly, polymer film deposition via solution processing is much more easily controlled than for small molecules because of the wide variety of solvents that can be used for processing. Secondly, polymers have higher absorption coefficients than small molecules, leading to less material consumption when making the ink formulations. Thirdly, they do not require the expensive high vacuum equipment necessary for thermal vapor deposition of small molecules.

Figure 1-17 shows the basic mechanisms occurring at the microscopic level to generate photocurrent in photovoltaic devices. Upon exposure to light, excitons are formed within the polymer. In order to create more excitons, a polymer must absorb as much light as possible in the visible spectrum. The excitons then travel to the donor/acceptor interface, where they are separated into electrons at the acceptor, and holes at the donor, if they do not decay via radiative or non radiative processes (described by the recombination rate) before reaching the interface. Therefore, in conventional solar cells, the thickness of donor and acceptor layers has to be very thin to ensure the maximum charge collection. When the charges reach the electrodes, electrons are collected at the cathode and holes are collected at the anode. The cathode is usually a metal with a low work function such as aluminum and the anode is usually a transparent metal oxide such as indium tin oxide (ITO).

The bulk heterojunction concept developed by Heeger and coworkers, in which donor and acceptor materials are blended together to form a continuous interlayer structure, as shown in Figure 1-17.[145] Electrons and holes generated in solar cell devices only have lifetimes of 10-50 fs and diffusion lengths of around 10 nm. Thus many devices are limited by large recombination rates before charge carriers can be extracted. The BHJ architecture is particularly effective for minimizing the recombination rates of solar cell devices. In this structure, interpenetrating layers of material provide a spatially distributed interface, thus ensuring that all photogenerated excitons are within the diffusion length of a donor-acceptor interface. Thus, the morphology of the donor-acceptor blend is critical to the dissociation and transport of the charge carriers.

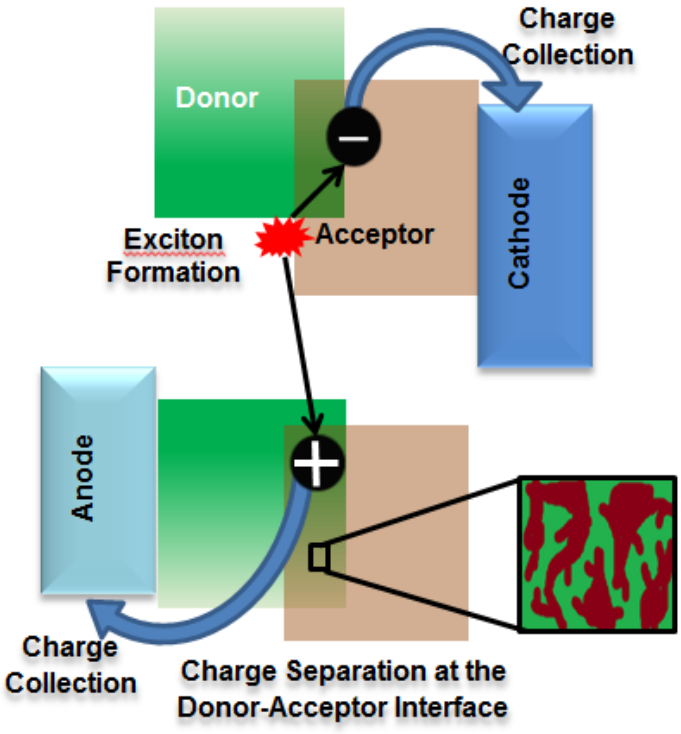

Figure 1-17. Schematic illustration of the electronic processes (exciton formation, charge separation and charge collection) in a bulk heterojunction organic solar cell and the bicontinuous interlayer between the donor and the acceptor molecule

Many groups have used conjugated polymers as the donor material for generating charge carriers in their devices, and used a variety of acceptor molecules including PCBM derivatives, PC[60]BM, PC[70]BM and the ICBA. PCBM derivatives have stood out as the best choice of n-type material as they possess strong electronegativity and high electron mobilities.

The driving force for charge separation is the energy difference of donor and acceptor LUMO levels. When the charges are separated they travel to the electrodes through the donor and acceptor materials. For efficient charge collection at the electrodes high charge carrier mobilities of the donor and acceptor materials are required. Otherwise, charges will be trapped at the donor and acceptor interface and will recombine. In summary, when developing polymer solar cells the most important parameters to consider are the morphology of the donor/acceptor blend, the charge carrier mobilities in the materials, and the energy differences between the donor and acceptor LUMO levels.

When testing the performance of OPV devices, power conversion efficiencies (PCEs) obtained from the *J-V* curves such as the one shown in Figure 1-18, provide a quantitative means of describing the effectiveness of the solar cell. The PCE's can be expressed by the following equation where V_{OC} denotes the energy difference between the donor HOMO level and acceptor LUMO level, J_{SC} denotes the short circuit current and is directly related to the absorption characteristics of the donor polymer, *FF* denotes the fill factor defined as the maximum power output divided by the product of V_{OC} and J_{SC}.

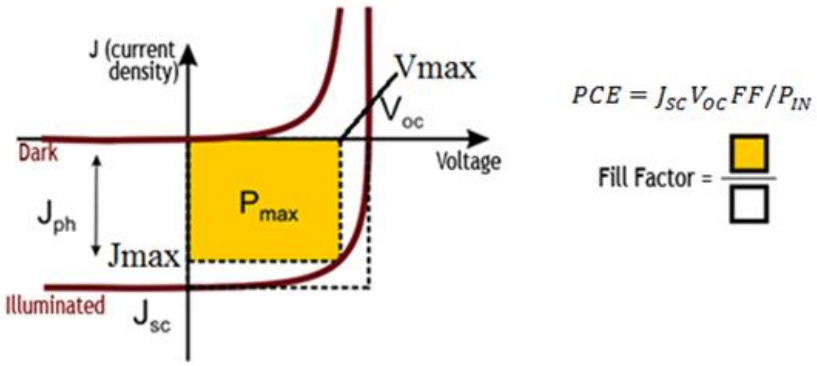

Figure 1-18. Representative J-V curve obtained from an organic solar cell and the evaluation of important parameters from the curve.

An ideal solar cell is one that has a high V_{OC}, J_{SC} and high FF values. It is a synthetic chemistry issue to satisfy all of these parameters. Low band gap polymers yield high J_{SC} values due to high coverage of the visible spectrum, however their energy levels can often lead to low V_{OC} values and sometimes cause reduced charge separation. A compromise of these parameters has been shown in the literature, where polymers resulted in PCE values of above 5.9 % as depicted in Figure 1-19. Of all the polymers studied, regioregular P3HT has been the benchmark polymer for solar cell applications where its use in devices led to PCEs of 6.5 % when blended with indene-C_{60}bis adduct (ICBA). The device structure was composed of ITO/PEDOT:PSS/P3HT: indene-C_{60}bisadduct (ICBA) (1:1, w/w)/Ca/Al.[146] The HOMO level of regioregular P3HT is approximately -5.2 eV and LUMO levels is -3.3 eV. An increase in solar cell PCE has been attributed to the ICBA acceptor molecule, which has 0.17 eV higher LUMO level compared to PCBM. After optimizing fabrication procedures, solar cell PCE values reached efficiencies of 4-5 % when P3HT was blended with PCBM.[147, 148] While the V_{OC} can be increased for P3HT by this approach, low J_{SC} values limit the output current. This is due to P3HT's absorption profile in the visible region.

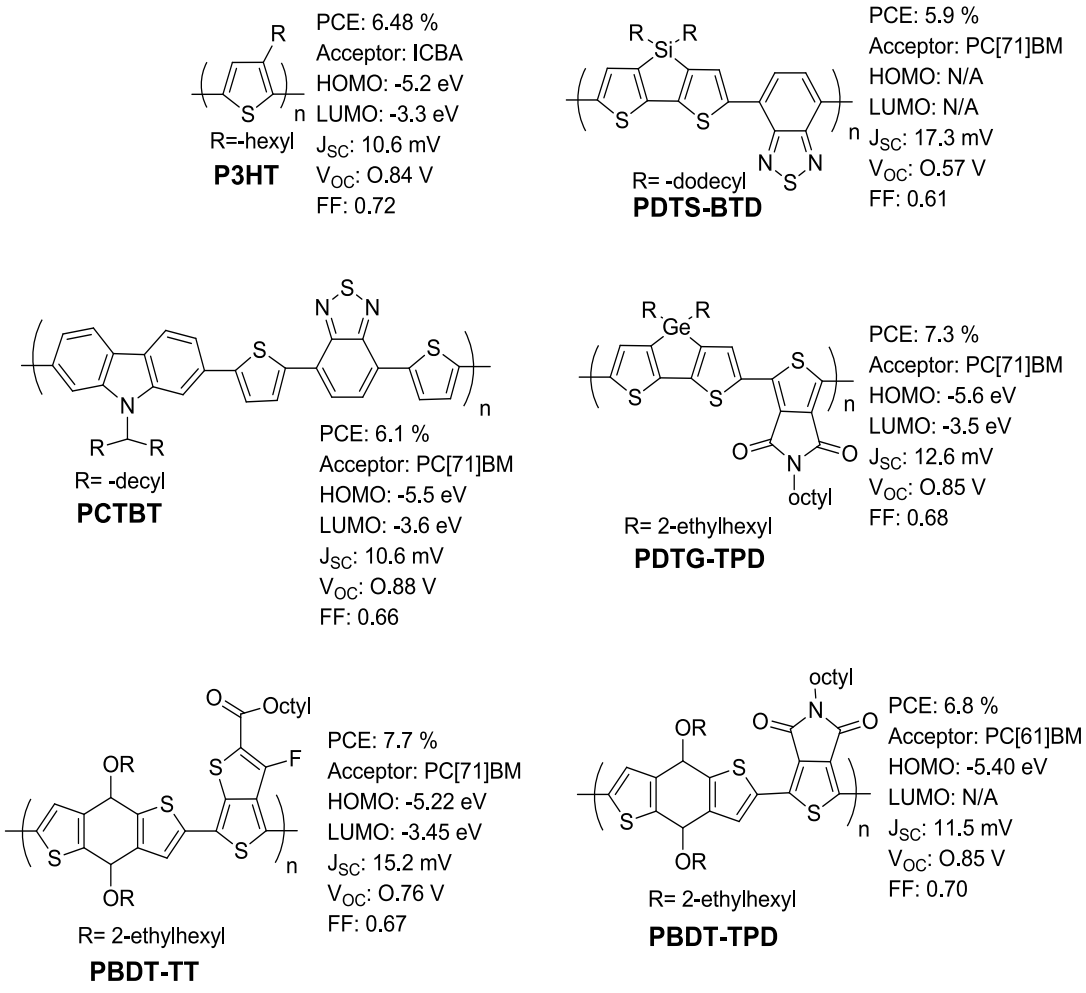

Figure 1-19. Representative high performing OPV polymers with their solar cell parameters.

It only absorbs visible light with wavelengths less than 650 nm, transmitting the rest of the visible spectrum. Thus, to cover more light in the visible spectrum, low band gap polymers have been created via the push-pull synthesis strategy based on fused aromatic ring systems such as dithienosilole, dithienogermole, benzodithiphene, and carbazole, for increased conjugation along the backbone. The Leclerc group has worked on carbazole-bithienothiadiazole (PCTBT) copolymers to obtain low HOMO energies in pursuit of high V_{OC} values.[108, 149] OPVs employing PCTBT copolymers as the active material have reached PCEs of 6.1 % by this approach. The Yu group has

developed fluorinated thienothiophene acceptors in order to provide decreased bond length alternation in the polymer backbone, by aromatization of the quinoıd form in the thienothiophene unit. Despite having higher HOMO energies compared to PCTBT polymers, their polymer enjoyed high J_{SC} values of 15.2 mA due to their longer wavelength absorption in the visible spectrum, leading to PCE's of almost 7.7 %.[150, 151] Benzoditihiophene has been popular as it is a planar molecule, which fuses benzene with two thiophenes, allowing for the incorporation of solubilizing alkyl chains on it. When coupled with the thienopyrrolodione acceptor, the copolymer yielded a performance of 6.8%.[152] Bazan and coworkers have used a dithienosilole based copolymer decorated with n-dodecyl groups for enhanced solubility.[144] Solar cells prepared using 1-chloronaphtalene additives during processing achieved PCE's of 5.9%. Last year, Amb *et al.* introduced the germanium atom bridged fused thiophene system, dithienogermole, in the pursuit of increasing attractive interactions between polymer chains due to the presence of the heavy Ge atom.[107] When this new monomer was coupled to a thienopyrroledione acceptor, the afforded polymer displayed PCEs of 7.3% in an inverted solar cell structure.

1.5 Thesis of This Dissertation

Synthetic organic chemistry hosts an infinite number of choices of molecule combinations and methods to generate high molecular weight, high performance materials. As discussed in the previous sections, organic chemistry has its own style to resolve and surpass limitations on the performance of conjugated polymers for optoelectronic applications. Challenges that are currently being addressed include scalability, color, purity, the nature of end groups, high charge carrier mobilities and intrinsic molecular order in deposited films. These challenges are thought to be critical

for prospective conjugated polymers that might find their place in daily life applications. Hence, this thesis approaches these issues with synthetic organic chemistry tools through structure-property relationships

Chapter 2 summarizes the basic polymer characterization methods used to analyze the purity of polymers. Polymer purification processes are later examined for the purposes of controlling the purity and molecular weight of the polymers. Then, physical characterization methods such as X-ray methods are introduced in order to study the molecular order in the polymers.

In Chapter 3, approaches to control green colored, aesthetically pleasing, polymers are discussed in conjunction with the scalability of these polymers. The same polymers are made with two different polymerization methods (oxidative polymerization *vs*. Stille polycondensation), and the difference of performances of solar cells prepared using these polymers is discussed. Even though, the molecular weights obtained using the two polymerization methods are similar, both polymers require different PCBM blend ratios, thus emphasizing the importance of the synthesis techniques on polymer properties. In addition, these polymers were used in the production of large scale organic solar cells, previously only studied using P3HT. In this context, the performance difference between the lab scale solar cells versus the large area solar cells is addressed. Lastly, an attempt to obtain green colored polymers by employing APFO type polymers is outlined along with its performance in electrochromic, light emitting and photovoltaic devices.

Chapter 4 details the synthesis of dithienosilole and dithienorgermole based polymers with benzothiadiazole, thienopyrroledione and phthalimide acceptors. Six

polymers were obtained via a 1% stoichiometric imbalance approach where the distannylated monomer was added in slight excess. Then the polymers were end capped by adding 4-iodotoluene to control the end groups. All polymers afforded moderate molecular weights, higher than 20 kDA, using this method. Their absorption and electrochemical behaviors are analyzed to highlight structure-property relationships in pursuit of understanding the effect of the heavy atom substitution (germanium versus silicon atom) in the fused thiophene ring. Further, their OFET performances are evaluated in conjunction with the X-ray analyses to determine the effect of the heavy atom as it pertains to polymer applications.

Chapter 5 focuses specifically on the characterization and analysis of toluene end groups on a dithienogermole-benzothiadiazole (DTG-BTD) copolymer. DTG-BTD polymers, one end capped with toluene moieties and the other left with bare hydrogen atoms, were characterized by ^{1}H-NMR, 2D-NMR and MALDI-MS. XPS and ICP analyses are also conducted to examine the purity of the polymers. These end groups have led to higher charge transport and increased molecular order.

CHAPTER 2
EXPERIMENTAL METHODS AND CHARACTERIZATIONS

2.1 General Synthetic Methods

All chemicals were purchased from commercial sources and used without further purification unless otherwise noted. Reactions were run in dry argon atmosphere under strict Schlenk conditions with oven dried glassware equipment. Specific details describing the synthesis and purification of the compounds used in this dissertation are given in the experimental sections of Chapter 3-5. As a note, Vogel's Textbook of Practical Organic Chemistry has been extensively used as a reference for the synthesis and purification of the compounds discussed throughout this dissertation. Additionally, Preparative Polar Organometallic Chemistry by L. Brandsma and H.D. Verkruijsse has been used as a reference book for handling the strong organometallic bases (butyllithium and Grignard reagents).

2.2 Purification of Polymeric Materials

The purity of polymerization products can be critical to their performance in optoelectronic applications. Impurities can arise due to unreacted starting materials, low molecular weight oligomers, unwanted end groups, oxidized polymer species, chemically doped polymer species, and metal residues. As the list gets longer, the importance of purification becomes more prominent. For example, residual Pd can limit the intensity of emission and cause changes in the spectral properties of polymers, which can be detrimental to their use in LED applications.[95] In photovoltaics, residual Pd decreases the fill factor and PCE values, as shown independently by Razumov *et al.* and Seki *et al.*[153, 154] On the other hand, the effects of heavy metals on organic field effect transistor performance are still under debate. Parneix *et al.* prepared P3HT via

the GRIM method, and fractionated the polymer after washings with methanol, hexane and chloroform.[155] They observed an increase in the OFET performance in the fractions with larger amounts of metal residues, where the metal acted as a dopant to the polymer. By contrast, McCulloch and coworkers applied various washings (acetone, petrol ether and methanol) and chemical treatments (silica, thiol-silica and thiourea-silica) on a poly[(2,5-bis(3-decylthiophen-2-yl)thieno[2,3-b]thiophene] polymer obtained by Stille polycondensation.[156] The amounts of metal residues after each procedure were determined and OFETs were prepared from each sample. They were able to decrease the metal residues of Pd from 3000 mg/kg to 600 mg/kg and of Sn from 12000 mg/kg to 300 mg/kg. However, polymer hole mobilities were not affected by these procedures and no improvement in the OFET performance was observed. For the Pd catalyzed polycondensations, removal of palladium impurities can be efficiently performed by adding a complexation agent -known as a Pd scavenger- diethylammonium diethyldithiocarbamate introduced by Krebs *et al*.[157] The complexation scheme is outlined in Figure 2-1. The Pd scavenger has a great affinity to bind to palladium(0), and the resulting complex is soluble in most organic solvents including methanol, chloroform and light petroleum. Solubility in methanol is rather important as precipitation onto methanol and washing with methanol in Soxhlet extraction are commonly applied processes. However, Schluter and coworkers warn that this kind of palladium scavenger is not effective in removing palladium species that are chemically bonded to polymers.[95]

For the oxidative polymerizations, hydrazine monohydrate is added to reduce the resulting polymer, which has previously been oxidized during the reaction. Next, the polymer solution is added to a pure methanol bath. Low molecular weight oligomers,

starting materials and salts (*e.g*. tin halides for Stille couplings) can go into the methanol phase while the polymer precipitates out. Precipitated polymer can then be separated by ultracentrifugation or simple filtration over a nylon membrane. Many impurities can be removed from the polymer this way, and can be tracked easily by the change in color of the methanol phase. However, continuous washings with different solvents are still needed to remove the impurities trapped in the polymer network.

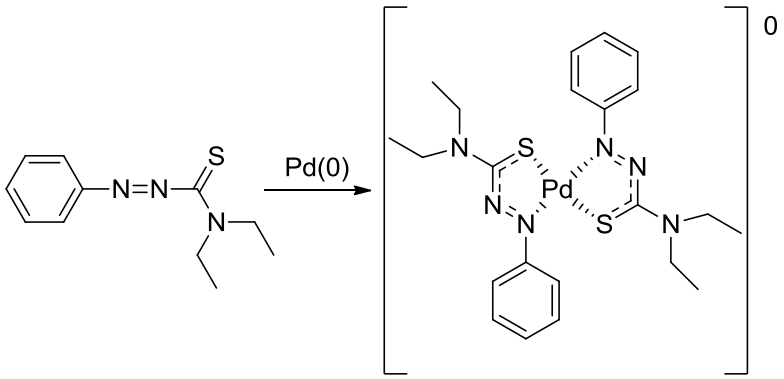

Figure 2-1. Pd scavenging by using diethylammoniumdiethyldithiocarbamate

Soxhlet extraction involves continuous washing of the polymer with desired solvents to extract the residual unwanted oligomeric species, unreacted monomers and salts. Figure 2-2 shows each washing step in a soxhlet extractor. The precipitated polymer is collected in a thimble and washed with hot methanol, acetone and hexane to remove the low molecular weight oligomers, salts and catalyst residues. Then the polymer is collected with hot chloroform to obtain the high molecular weight polymer. Finally, the solution is precipitated from methanol to collect the polymer as a solid. Parneix *et al* .have made a detailed study on the efficacy of soxhlet extraction as a method for removing impurities from P3HT using methanol, hexane and chloroform.[155] After each washing, the amount of residual catalyst and the number average molecular weights (M_n) of polymer samples were measured. It was observed that the M_n increased

and the PDI was reduced as the low molecular weight oligomers were removed. Furthermore, the sequence of solvents used was found to be an important parameter in the purification process.

a)

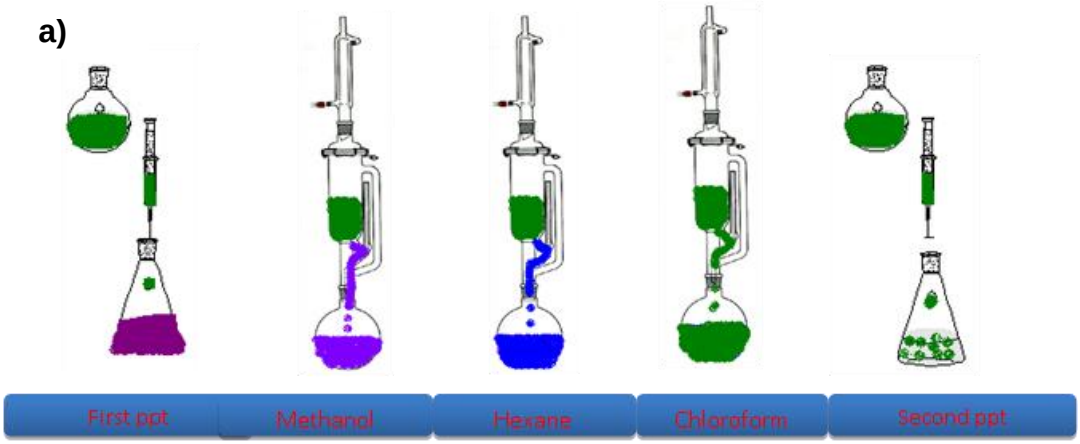

b)

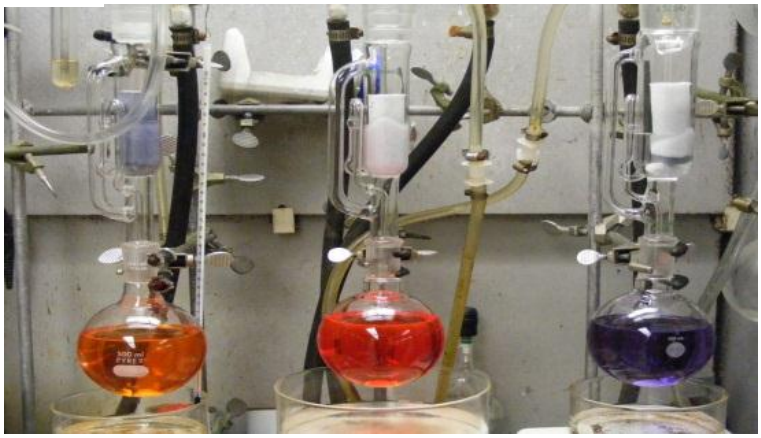

Figure 2-2. Demonstration of soxhlet extraction process. a) Soxhlet extraction sequence b) Different colors of washings for the low molecular weight polymers

In general, methanol was chosen as the first solvent as it is a “poor” solvent that does not dissolve most polymers, but does however dissolve polar species. This was followed by water and acetone washings for Suzuki couplings to remove salts and low molecular weight species. After acetone, washing with hexane was performed to conclude the removal of low molecular weight oligomers. Finally, the polymer was

extracted using chloroform to dissolve the moderate molecular weight species. The dissolved polymer in chloroform was then recovered by precipitation from methanol. Any polymer left that was not soluble in chloroform could be further washed with chlorobenzene. A comparative study has been carried out during the purification of non-end capped DTG-BTD [NE(DTG-BTD)] polymers to study the effect of Soxhlet extractions on the polydispersity and molecular weight. The results are presented in Table 2-1. After the polymerization, the crude polymer was precipitated into methanol and collected in a thimble, this fraction is labeled NE(DTG-BTD)-1. Then it was washed with methanol. A small amount of this sample was taken and the molecular weight parameters were measured by GPC, this portion is labeled NE(DTG-BTD)-2. Next, the polymer was washed with acetone (NE(DTG-BTD)-3), hexane (NE(DTG-BTD)-4) and chloroform (NE(DTG-BTD)-5). After each washing, the polymer's PDI decreased from 3.11 to 2.66 through removal of the low molecular weight species. At the same time, Mn values increased from 19.9 kDa to 28.1 kDa.

Table 2-1. GPC estimated molecular weights in THF after each solvent washing for NE(DTG-BTD) polymer with Soxhlet extraction.[a]The values might not be correct due to large amount of impurities.

Polymer	M_n (kDa) THF	M_w (kDa) THF	PDI
NE(DTG-BTD)-1[a]	26.7	83.1	3.11
NE(DTG-BTD)-2	19.9	59.8	3.00
NE(DTG-BTD)-3	21.1	57.9	2.73
NE(DTG-BTD)-4	20.7	49.4	2.37
NE(DTG-BTD)-5	28.1	74.9	2.66

.

Thus, through soxhlet extractions we were able to obtain higher molecular weight polymers with relatively narrow polydispersities. Soxhlet extraction based polymer purification is a prominent method in the literature for lab-scale prepared polymers.

However, it is a time consuming process (3-5 days) which makes it impractical for commercial applications

2.3 Materials Characterization

2.3.1 Structural Characterization

The polymers were characterized using a Mercury 300 or Inova-2 500 MHz NMR spectrometers using deuterated chloroform. Chemical shifts were referenced to 7.27 ppm for residual $CDCl_3$ peaks. High temperature (373 ^{o}K) H NMR (500MHz) spectra were obtained by Dr. Manfred Wagner of the Max Planck Institute for Polymer Research, Mainz, Germany. NMR experiments were conducted using a Bruker Avance III 500 (11,7 T) with a 5 mm z-gradient BBFO ^{1}H/X probe. The proton (1D and 2D) and carbon spectra (1D and 2D) were measured in $C_2D_2Cl_4$ at 373^{o}K and the spectra were referenced as follows: for the residual C_2HDCl_4-(H)-$d_1\delta(^{1}H)$ = 5,95 ppm and $C_2D_2Cl_4\delta(^{13}C)$ = 74.1 ppm. ^{1}H,^{1}H NOESY 2D method was applied via the dipolar coupling. The mixing time was 200ms. The frequency sizes were 6000 Hz in both dimensions (f1 and f2) with a relaxation delay of 1,2s. 2D ^{1}H,^{13}C-HSQC experiments were carried out by 8192 points in f2 and 512 points in f1.

Inductively Coupled Plasma (ICP) analyses were completed at the University of Florida Geology Department by Dr. George Kamenov. Elemental analyses were conducted by the University of Florida, Department of Chemistry spectroscopic services. MALDI mass spectra were acquired by Dr. Tracy D. McCarley at Louisiana State University with a Bruker Daltonics Ultraflextreme MALDI TOF/TOF mass spectrometer operated in linear mode. The matrix used was trans-2-[3-(4-tert-butylphenyl)-2-methyl-2-propenylidene]malononitrile (DCTB).

2.3.2 Polymer Molecular Weight Characterization

Gel permeation chromatography (GPC) was performed at 40 °C using a Waters Associates GPCV2000 liquid chromatography system with an internal differential refractive index detector and two Waters Styragel HR-5E columns (10 μm PD, 7.8 mm i.d., 300 mm length) using HPLC grade THF as the mobile phase at a flow rate of 1.0 mL/min.Calibrations were done against narrow molecular weight polystyrene standards (Polymer Laboratories; Amherst, MA). Alexander Pemba is acknowledged for his efforts in taking the GPC measurements for this research. GPC measurements in trichlorobenzene at 135 ^{o}C were performed at the Max Planck Institute for Polymer Research, Mainz, Germany using a refractive index detector with calibrated against polystyrene standards.

2.3.3 Thermal Characterization

Polymer thermal stability measurements were taken using thermogravimetric analysis (TGA) on a TA Instruments TGA Q1000 Series in nitrogen. The TGA samples (2 mg) were typically heated to 25 °C to equilibrate to a constant mass, and then heated at a heating rate of 10°C/min to a maximum temperature of 600°C.

2.3.4 Electrochemical Characterization

Electrochemical measurements were performed in a three-electrode electrochemical cell consisting of a counter electrode, reference electrode and working electrode immersed in a supporting electrolyte solution. A platinum wire or a Pt flag, acted as the counter electrode; Ag/Ag^{+} acted as the reference electrode. Two different types of working electrode were used depending on the application. The working electrode was either a platinum button (0.02 cm^2) electrode purchased from Bioanalytical Systems when used for CV and DPV measurements, or an ITO-coated

glass slide (7x50x0.7 mm, sheet resistance, Rs 8-12 Ω/sq) purchased from Delta Technologies when used for spectroelectrochemistry. Corrware software used to control a potentiostat/galvanostat from EG&G Princeton Applied Research model 273A. The polymer films were solution drop cast onto the Pt button electrode and air-brush sprayed on the ITO-coated glass slide from 1 mg/mL polymer solution in toluene. For CV measurements, the working electrode was cycled 5 times at a 50 mV/s scan rate to break-in the films before doing the electrochemical characterization. The supporting electrolyte was 0.1 M $TBAPF_6$/PC solution and it was used for all CV, DPV and scan rate dependent CV measurements. The electrolyte solution was purged with solvent saturated argon for 30 min before electrochemical measurements and a blanket of argon was present at all times.

For electrochemical characterizations, cyclic voltammetry (CV) and differential pulse voltammetry (DPV) were employed. CV relies on ramping the applied potential at a working electrode in both forward and reverse bias while measuring the current. The important parameters to note in CV are cathodic and anodic peak potentials (E_{pc}, E_{pa}) and the peak currents. (i_{pc}, i_{pa}). The peak separation between the cathodic and anodic peak potentials (E_{pc}, E_{pa}) ΔE_p is important in terms of characterization of the electron transfer processes whether they are electrochemically reversible or irreversible. In DPV measurements, a series of discrete potential amplitudes (10mV-100mV) is pulsed stepwise. After each pulse, the potential goes back to a slightly higher voltage which is called step size (1-2mV) resulting in a staircase shape. The current is measured before the application of pulse and at the end of the pulse and the difference in currents is correlated to the applied potential. By doing so, the capacitive or charging current is not

measured which is still present in CV measurements. Thus, DPV curves become more symmetric with a higher signal to noise ratio, resulting in better defined onsets of oxidation and reductions. DPV has been used to determine the HOMO and LUMO levels of the samples. The oxidation onset and reduction onset are related to HOMO and LUMO levels respectively. As all measurements are referenced to the Fc/Fc^{+} redox couple, the energy levels can be calculated by adding -5.1 eV to the oxidation and reduction onsets relative to the vacuum level. Even though some sources in the literature use -4.8 eV for Fc oxidation potential, this discrepancy has been well discussed in the dissertation of Barry C. Thompson[158] and recently by Bazan and coworkers.[159]

2.3.5 Optical Spectra Characterization

UV-VIS absorption spectra were obtained from a Varian Cary 500 Scan UV-VIS-near-IR spectrophotometer using 1 cm x 1 cm x 5.5 cm quartz cells manufactured by Starna Cells, Inc. Solution spectra were measured in dilute polymer solutions in toluene or chloroform to give an optical density of 0.8. Thin film spectra were recorded by spraying a hot polymer solution in either chloroform or toluene on ITO glass to such a thickness that would yield an optical density of 0.8.

2.3.6 Spectroelectrochemistry

Spectroelectrochemistry has been often employed in our research group to calculate the optical band gap, the energies of the polaron and bipolaron states and investigate the electrochromic behavior of polymers under redox processes. For spectroelectrochemistry experiments the air-brush sprayed polymer films on ITO were immersed in quartz cuvettes of 1 cm path lengths containing 0.2 M LiBTI/PC electrolyte solution. Copper tape was used to make contact between the ITO electrode and the

potentiostat connection cables. The electrolyte solution was purged with argon for 30 min before electrochemical measurements were taken, and the film was cycled 10 times with a 50 mV/s scan rate using CV measurements.

2.3.7 Two Dimensional Wide Angle X-Ray Scattering (2D-WAXS)

Structural characterizations by 2D-WAXS have been performed at the Max Planck Institute for Polymer Research. The experiments have been conducted with the help of Dr. S. Reddy Puniredd. In 2D-WAXS experiment, a polymer fiber is placed in the field of an X-ray beam to study the level of organization in the material. The fiber preparation process is shown in Figure 2-3a. The polymer fibers are prepared by filament extrusion process using a home built extruder, in which polymer powder is heated at a point where it can undergo plastic deformation. Then, the polymer is extruded through the nozzle by a constant motion of the piston inside the cylinder. A number of parameters control this mechanical processing such as the velocity of the piston, diameters of the cylinder and the shape of the die. The extruder is capable of processing polymer fibers with a 0.7 mm diameter. (Figure 2-3b)

The extruded fiber is placed inside the X-ray chamber perpendicular to the incident X-ray beam along with its extrusion direction. As seen in Figure 2-3c, the position of reflections in the X-ray pattern give information about the level of organization in the polymer. Two pieces of information can be obtained from the resulting X-ray pattern as shown in Figure 2-3c. The outermost reflections indicate π–π stacking and the innermost reflections show the intermolecular distances or lamellar distances. The intensity of the π–π stacking reflections corresponds to the crystallinity of the polymer.

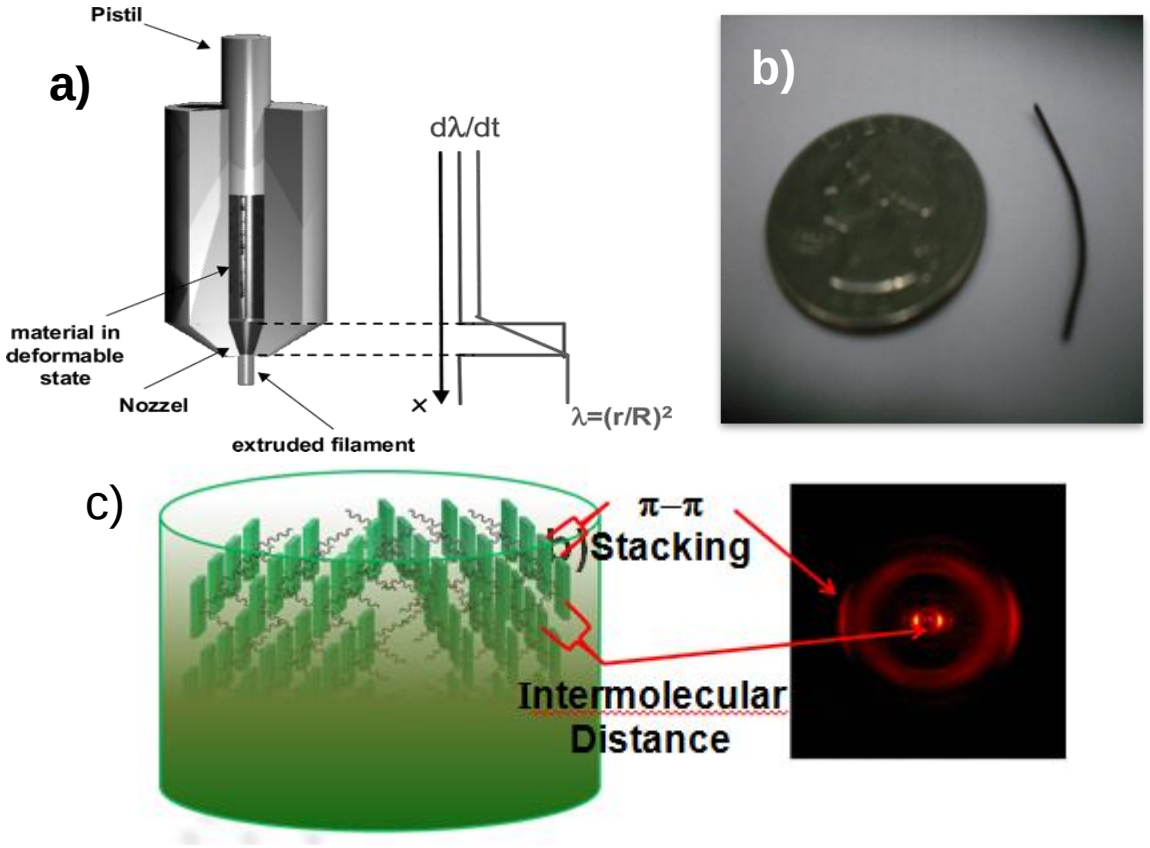

Figure 2-3. Preparation and analysis of a polymer via 2D-WAXS. a) Schematic illustration of extrusion process. (Adapted with permission from Muellen, Copyright 2005 American Chemical Society) b)The extruded polymer fiber prepared and comparison with a US quarter. c) Representation of an extruded fiber and the aligned polymer chains along the extrusion direction as well as relating π–π stacking and intermolecular distances in an obtained X-ray pattern.

The intermolecular distances (or chain-to-chain distance) are found in the equatorial plane of the scattering pattern as the chains aligned are aligned perpendicular to the incident beam. The length and bulkiness of the side chains attached to the polymer backbone rules the extent of intermolecular distanced. Also, an amorphous halo can be seen in the X-ray pattern which is related to the isotropic side chains. The 2D-WAXS measurements discussed in this dissertation were performed by a rotating anode (Rigaku18 kW) X-ray beam source with a pinhole collimation and a 2D

Siemens detector. A double graphite monochromator for the Cu-Kα radiation (l=0.154 nm) is used.

2.3.8 Grazing Incidence Wide Angle X-Ray Scattering (GIWAXS)

The presented GIWAXS data in the Chapter 4 and 5 have been obtained at the Max Planck Institute for Polymer Research, Mainz, Germany via a home built X ray source (a rotating Cu-anode operating at 50 kV/200 mA (Cu Kα, λ = 1.5418 Å)) orienting the substrate surface at or just below the critical angle for total reflection with respect to the incoming X-ray beam (~0.2°), The GIWAXS data were acquired using a camera comprising an evacuated sample chamber with an X-ray photosensitive image plate. The experiments were performed by myself and data analysis was carried out by Dr. Sreenivasa Reddy Puniredd.

In the GIWAXS method, X-rays impinge on the surface of the polymer film at a small grazing angle (below the critical angle typically 0.2^{o}) and are scattered in plane and out of plane X-rays are detected.[161, 162] The polymer thin films are deposited by drop casting or spin coating and placed horizontally on the stage. The incidence angle (α) rules the X-ray penetration depth, scattering intensity and the nature of scattering. It can be adjusted so that only scattering from the film is obtained without the scattering from the substrate. X-rays can be scattered from the thin film as a result of the periodicity, repeat distance and orientation of the crystallites. Typical GIWAXS scattering patterns for conjugated polymers are shown in Figure 2-4. The essential peaks obtained are the result of $\pi-\pi$ stacking which is around 0.4 nm and intermolecular spacing in the direction of side chains which is around 2.0 nm. The out of plane scattering which is the result of the spacing between periodic planes and the orientation of the vector is normal to the

periodic planes give a pattern such that as illustrated in Figure 2-4a.

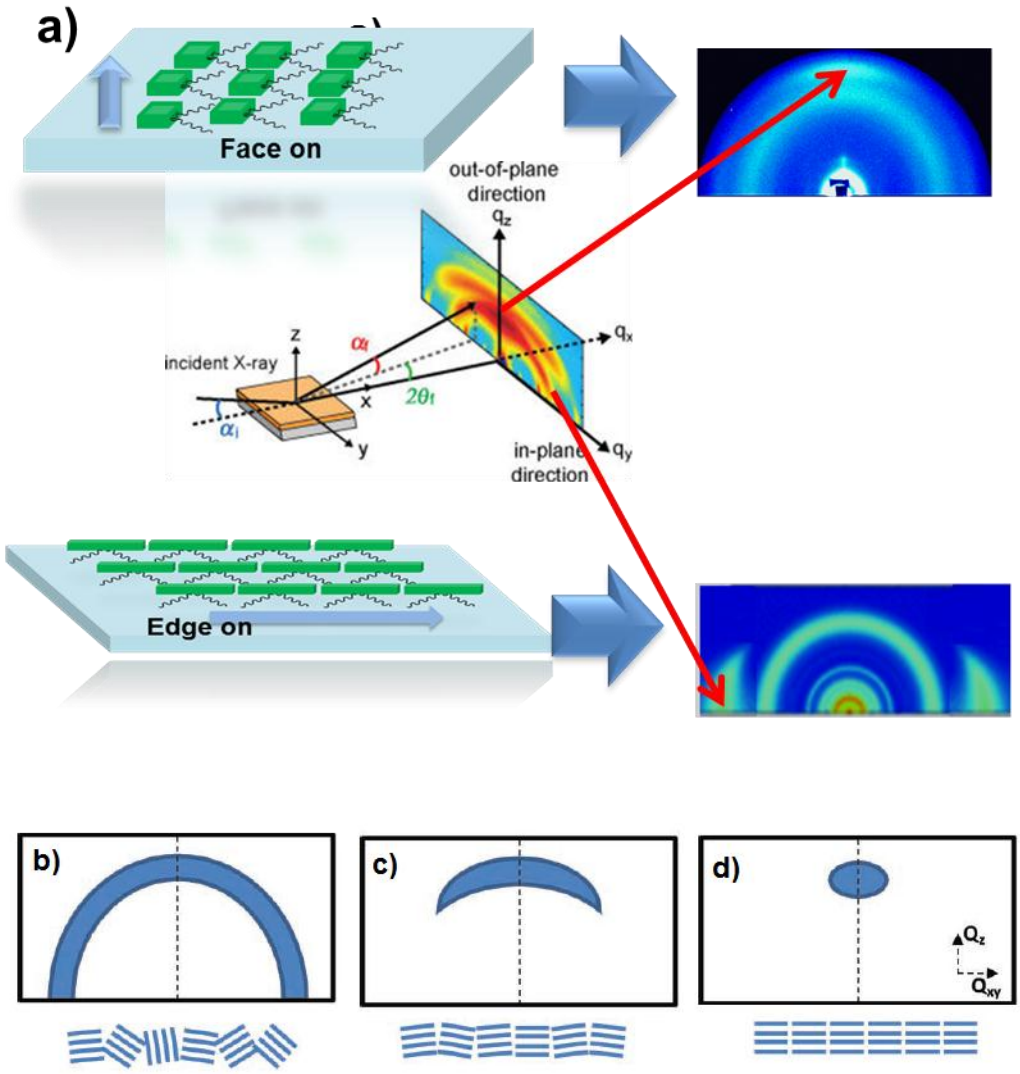

Figure 2-4. Analysis of GIWAXS patterns. a) Representation of the GIWAXS experiment and cartoons showing the X-ray pattern for face on and edge on arrangement on the substrate. b-d) The intensity and the shape of the arc at the q_z direction with the cartoons of representative ordering in the polymer chains.

Their reflections are in the q_z direction, where q_{xy}=0 indicate a face-on orientation of the polymer backbones on the substrate. In plane scattered X-rays form an X-ray pattern such as the one shown in Figure 2-5a, indicating an edge-on orientation of the polymer backbones on the substrate. In this particular orientation, the side chains are standing

vertical on the substrate creating an insulated region between the polymer and the substrate. Furthermore, the intensity of the reflections are important in terms of determination of the anisotropy in the film. Figure 2-4b-d shows the representative scenarios where the reflection diffuse from a ring to a perfect spot in the q_z direction where q_{xy}=0. A ring is indicative of a totally isotropic film where crystallites have different orientations. A diffuse arc represents an isotropic film where crystallites have higher angles in between each other. A perfect spot shows almost anisotropic film in which crystallites are perfectly aligned with respect to each other indicating a preferred crystallization axis. In addition, continuous spots on the q_z direction show the long range ordering in the film where planes of crystallites repeat each other. As a summary, a GIWAXS analysis can give valuable information including the orientation of the film on the substrate, the relative orientations of crystallites, the extent of long range ordering in the crystallites indicating anisotropy in a film, $\pi-\pi$ stacking and intermolecular distances.

2.3.9 Atomic Force Microscopy

Atomic force microscopy was used to characterize surface morphologies of the end capped DTG-BTD and non-end capped DTG-BTD polymers in Chapter 5. The experiments were done at the Max Planck Institute for Polymer Research. AFM images of the spin coated and drop cast thin films were recorded with a Multimode phase AFM NanoScope IV Scanning Probe Microscope Controller functioning in tapping mode. During the measurement, the cantilever tip was kept stationary and oscillating at 300 MHz resonance frequency while the sample was moved while scanning.

2.4 Photovoltaic Devices

All the solar cell measurements and photovoltaic device measurements are performed in the Prof. Franky So's group at the Department of Material Science of

University of Florida. The data have been kindly provided by Dr. Jegadesan Subbiah and Song Chen. Organic solar cells were designed with the bulk heterojunction device architecture. For this purpose, a 30nm layer of poly(3,4-ethylenedioxythiophene):poly-(styrenesulfonate) (PEDOT:PSS; Baytron AI 4083 from HC Starck) was spin coated on indium tin oxide (ITO)-coated glass substrates which were ultrasonically cleaned and UV-ozone-treated, prior to the process. Substrates were then baked on a hot plate at 180 °C for 10 min. Next, onto the PEDOT:PSS, the active layer blend consisting of polymer and PCBM (99% pure, Solenne BV) was spin-coated from chlorobenzene solvent with a thickness around 100-120 nm. Then, the sample was heated on a hot plate at 70 °C for 30 min. The cathode (LiF (1 nm) and aluminum (100 nm)) were then thermally evaporated under $\sim 1 \times 10^{-7}$ mbar vacuum. The whole device has 0.04 cm^2 active area. For the inverted device architecture, ZnO (35 nm) obtained by sol-gel process is spin coated onto ITO coated glass and then annealed in air for 30 min at 200 °C. The active layer blend is processed and annealed as the same way mentioned previously. Later, PEDOT:PSS (35 nm) is spin-coated onto the active layer and the components are annealed at 130 ^oC for 5 min. Lastly, silver metal (80 nm) is thermally evaporated onto PEDOT:PSS layer. The whole device has an active area of 0.04 cm^2. The solar cells are tested using a 150 W Newport ozone free xenon arc lamp as the light source in conjunction with a Keithley 4200 semiconductor parameter analyzer system. The measurements were carried out under 1000 W/m^2 AM 1.5G illumination conditions. Solar cell devices are made in nitrogen in glovebox and characterizations are conducted in ambient atmosphere.

2.5 Organic Field Effect Transistors (OFETs)

OFET devices were prepared at the Max Planck Institute for Polymer Research, device optimization and data analyses were performed by Dr. Sreenivasa Reddy Puniredd. All OFET devices discussed in this thesis were fabricated in the bottom-gate, bottom-contact architecture. The substrates used were highly doped Si acting as the gate electrode with a 200 nm thick SiO_2 dielectric layer on top and was purchased from BASF. The SiO_2 layer was then reacted with hexamethyldisilazane (HMDS) overnight at 100 ^{o}C to minimize interfacial trapping sites. Polymer thin films were fabricated by drop-casting 2 mg/mL of a 1,2-dichlorobenzene solution onto FET substrates already heated at 100 °C in nitrogen atmosphere. Next, the components were annealed at 200 °C for 60 min. Additionally, polymer thin films were fabricated by spin coating from 10 mg/mL chloroform solution at 1200 rpm for 60 s. followed by annealing at 200 °C for 60 min. The channel length (L) and width (W) are 20 and 1400 µm, respectively. 10 transistors were measured in nitrogen atmosphere and the average hole mobilities measured. All the charge carrier transport measurements are carried out by using Keithley 4200 SCS in a glove box under nitrogen atmosphere as shown in Figure 2-5.

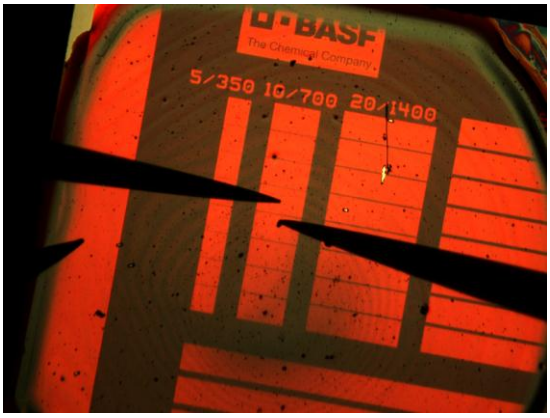

Figure 2-5. Picture of a bottom gate bottom contact OFET covered with a polymer.

CHAPTER 3
THE IMPORTANCE OF SYNTHESIS AND PROCESSING METHODS ON THE PERFORMANCE OF GREEN COLORED PHOTOVOLTAIC MATERIAL: PGREEN CASE

3.1 Introduction

Recent developments in photovoltaics have focused on integrating conjugated polymers into these devices as the active light harvesting materials. Conjugated polymers are particularly attractive due to their potential for low cost, scalable deposition onto a variety of substrates. Much progress has been made to improve the power conversion efficiencies (PCEs) of polymer based bulk heterojunction (BHJ) solar cells over the last two decades, with the highest performing devices achieving PCEs as high as 8.5%.[163] However, more advancements are still needed in the field according to one of the leading research teams, the Konarka group, which announced that to be competitive with industry standards, polymer devices would need to achieve PCE's of 10% and above.[164]

It is worth mentioning here that, development of the light harvesting materials in the academia is concomitant with the lab scale processing techniques such as spin coating and most of the reported PCE values are recorded on very small substrates with active areas of less than 0.5 cm^2. Therefore, in addition to designing new light harvesting materials, advancements must be made in large scale processing these materials, in order for polymer based solar cells to find a place in the commercial applications. In this regard, P3HT has been the benchmark polymer, yielding both a 6.5% PCE in lab scale devices when processed via spin coating, and 3% PCE when processed on a large scale by ink jet printing.[146, 129] However, as P3HT has limited light coverage above 650 nm, alternative polymers with longer wavelength absorptions are

still being sought after. As such, one of the most important criteria in obtaining high PCEs is obtaining low band gap polymers that can capture most of sun's radiation in the visible spectrum.[165] In this regard, the donor-acceptor strategy has been particularly successful.

In addition to considerations necessary for obtaining high PCEs, the color of the solar cells is often an important parameter in terms of increasing demand for commercial products. In this context, green colored polymers are desirable for aesthetically pleasing polymer solar cells that can mimic the appearance of leaves or grass. However, green colored polymers are synthetically challenging to achieve. Pierre Beaujuge's dissertation discusses the synthetic design requirements for obtaining polymers with green hues.[166] Particularly, the PGreen polymer originating from his research, financially supported by Sestar LLC, has been the starting point for the realization of aesthetically pleasing polymer cells. PGreen's structure, optical and solar cell characteristics are shown in Figure 3-1.[167, 168] The chemical structure of this polymer consists of alkylateddioxythiophenes, acting as donor moieties, and benzothiadizole, acting as the acceptor unit. The combination of these units results in dual band absorption. Dioxythiophenes were functionalized with 2-ethylhexyl side chains to ensure solubility of the target polymer. Bithiophene spacers were employed in the repeat unit structure to fine tune the band gap and induce planarity by separating the dioxythiophenes, which have bulky side chains. In the solid state, PGreen shows a dual band absorption profile, with its high energy band's absorption maximum at 448 nm, covering the blue region of the spectrum, and its low energy band's absorption at 636 nm, tailing off to 800 nm to cover the yellow-red region of the visible spectrum. The

polymer's absorption spectrum displays a trough at 501 nm, which gives the polymer its perceived green color. When blended with PCBM in bulk heterojunction (BHJ) solar cells in a 1:8 ratio, PGreen achieved a 1.90% PCE in conventional device architectures (ITO/PEDOT/PGreen:$PC_{60}BM$/LiF/Al). It is important to note here that PGreen showed a PCE of only 0.64 % when blended with PCBM in a 1:4 ratio.

a)

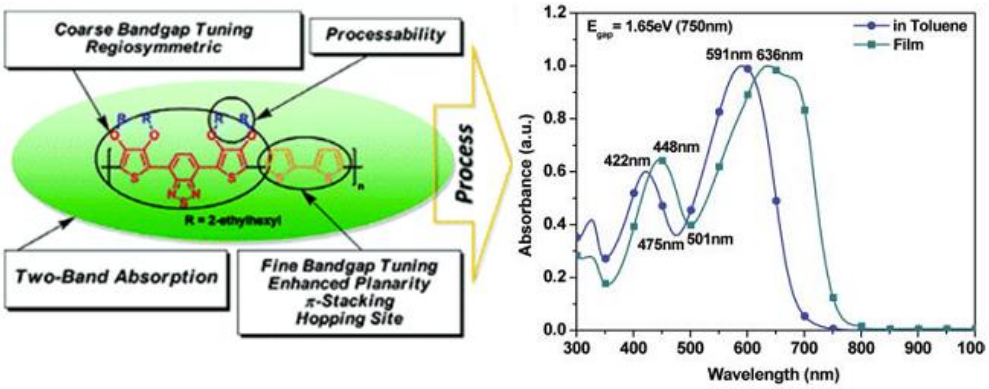

b)

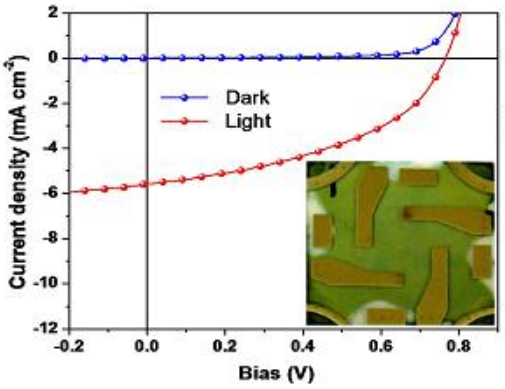

P3:$PC_{60}BM$ (%w/w)	J_{SC} (mA/cm²)	V_{OC} (V)	FF (%)	PCE (%)
1:4	1.99	0.78	41	0.64
1:6	3.93	0.77	46	1.39
1:7	4.79	0.76	46	1.68
1:8	5.56	0.77	44	1.90
1:9	3.97	0.73	35	1.00
1:10	2.10	0.71	40	0.60

Figure 3-1.Properties of PGreen. a) Design rationale and chemical composition of the PGreen with absorption profile in the visible spectrum resulting its green color. b) Solar cell characteristics of PGreen.(Adapted with permission from So, Copyright 2009 American Chemical Society)

The difference in PCE values within different mixtures was due to the higher content of PCBM, which is responsible for the increased short circuit current density (Jsc) from 1.99 to 5.56 mA/cm^2. In this context, we discuss some important challenges

that are being addressed by current photovoltaic research, with a focus how PGreen can resolve some of these issues. Scalability, reproducibility, polymer chemical quality and processing methods are the key factors that have been taken into consideration. Scalability is important, as large amounts of polymers are needed to process solar cells on the industrial scale. In this regard, though many groups have previously reported polymer yields of 100-500 mg, industrial applications require much larger amounts. Reproducibility depends on the strict control over synthetic protocols in order to generate smaller batch-to-batch differences between polymerization products. For more information regarding important protocols for polymerization and the purification methods necessary for decreasing batch-to-batch variations, the reader can refer back to Chapter 1 and Chapter 2 of this dissertation. Lastly, small scale solar cell preparations by spin coating and large scale roll-to-roll processes for processing polymer photovoltaics result in large discrepancies that need to be investigated. Through Chapter 3, we discuss the synthesis of PGreen on the gram scale using oxidative polymerizations and compare the performance of solar cells prepared by spin coating and slot-die coating. Further, effects of changing the polymerization method to Stille polycondensation in order to control the quality and purity (reduce branching and controlling end groups) of PGreen and solar cell performances are discussed. Finally, a new APFO type polymer is discussed in an attempt to generate green colored polymers. This polymer, which ultimately allowed for electrochromic, light emission, and photovoltaic activity, was chosen as an example of the careful blending of donor-acceptor moieties

3.2 PGreen by Oxidative Polymerization

PGreen was obtained from the oxidation of the monomer by dropwise addition of five equivalents of $FeCl_3$ over 2 hours, as shown in Figure 3-2. During the polymerization, dry air was passed through the reaction mixture to remove HCl generated by the reaction. The reaction was allowed to run overnight, then the oxidized polymer was reduced with hydrazine and fractionated through washing with methanol, acetone, hexane and chloroform to remove any low molecular weight species. The chloroform soluble fraction was precipitated into methanol, affording the PGreen polymer. The reproducibility of this procedure was tested by running the polymerization with strict protocols by three different researchers using the same written synthetic protocol to achieve a standard operating principle. Additionally, the scalability of the reaction was investigated by conducting the polymerization on both1 and 2 gram scales. All four polymers presented expected CHN percentages in the 0.4% theoretical limit, indicating high quality polymers with few impurities. The molecular weights were determined using a polystyrene calibrated GPC using THF as an eluent and the results are shown in Table 3-1. PGreen1 had a M_n of 57.3 kDa in a 52% yield, in agreement with the reported values. PGreen2 showed a lower M_n of only 37.3 kDa and a yield of 25% due to the fast addition of the oxidant (0.33 equivalents in 2 min.) because of a problem with the syringe pump used for adding the oxidant dropwise. Additionally, the reaction yielded a large amount of insoluble polymer, as a result of crosslinking of the unsubstituted thiophenes during polymerization. PGreen3 had a still lower M_n of 28.2 kDa due to the presence of hydrated $FeCl_3$, which was evident by its yellow color before the polymerization. Hydrated $FeCl_3$ has a lower reduction potential, thereby decreasing the extent of polymerization. Additionally, PGreen4 was run through a procedure most

similar to PGreen1, but with a 2 gram scale of polymerization, resulting in a M_n of 48.4 kDa in a 60% yield. This implies that the polymerization procedure is scalable, while yielding reproducible molecular weight results.

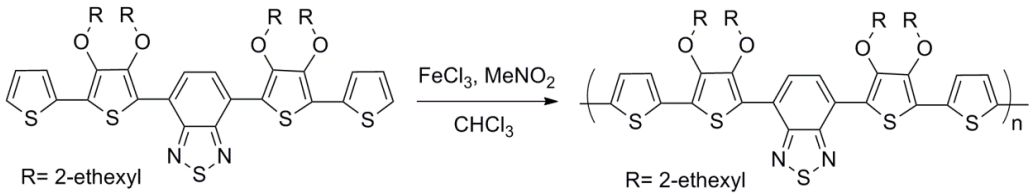

Figure 3-2.Synthesis of PGreen via oxidative polymerization.

Table 3-1. GPC estimated molecular weights in THF and elemental analysis of the PGreen series prepared by different researchers.

Researcher	Polymer	*Scale (g)*	M_n (kDa)	Yield (%)	PDI	EA Calculated (%) C	H	N
						66.49	7.65	2.87
						Experimental (%) C	H	N
Chad A.	PGreen1	1	57.3	52	1.70	66.33	7.70	2.83
Mike C.	PGreen2	1	37.3	25	1.91	66.39	7.96	2.87
Unsal K.	PGreen3	1	28.2	58	1.71	66.44	7.85	2.81
Unsal K.	PGreen4	2	48.4	60	1.83	66.21	7.71	2.70

Small scale solar cells prepared by spin coating, have been tested by Franky So's group, and large area solar cells employing slot die coating and screen printing have been fabricated by Frederic Krebs' group. The following data have been kindly provided by these groups.

PGreen1, PGreen2 and PGreen3 were integrated into solar cells with an active area of 0.04 cm^2. The solar cells had the conventional architecture (ITO/PEDOT:PSS/PGreen:PCBM [1:8]/LiF/Al) as shown in Figure 3-3a, with the active layer deposited by spin coating. The illuminated *J-V* characteristics of the bulk heterojunction (BHJ) solar cells based on each PGreen polymer (with a 1:8 ratio to

PCBM as the acceptor) are shown in Figure 3-3c and solar cell parameters are summarized in Table 3-2. Firstly, the *J-V* curves for solar cells prepared from each polymer are similar, thus indicating the reproducibility of the polymerizations. PGreen3 produced the highest PCE of 1.90 % despite its comparatively low molecular weight. PGreen1 produced a PCE value of 1.73 %, and PGreen2 produced 1.28 %. The discrepancies between the solar cell performances can be explained by the presence of defects during the oxidative polymerization. It is known that some defect structures can form due to cross linking and coupling of monomers from β positions during the oxidative polymerization.[71] In this regard, PGreen3, which resulted in low molecular weights due to the hydrated Fe(III)Cl_3, likely experienced less defects in the polymer due to the lower reduction potential of the hydrated Fe(III)Cl_3.[169] This also explains the low performance of PGreen2, which most likely had more defects in its structure due to the fast addition of the oxidant.

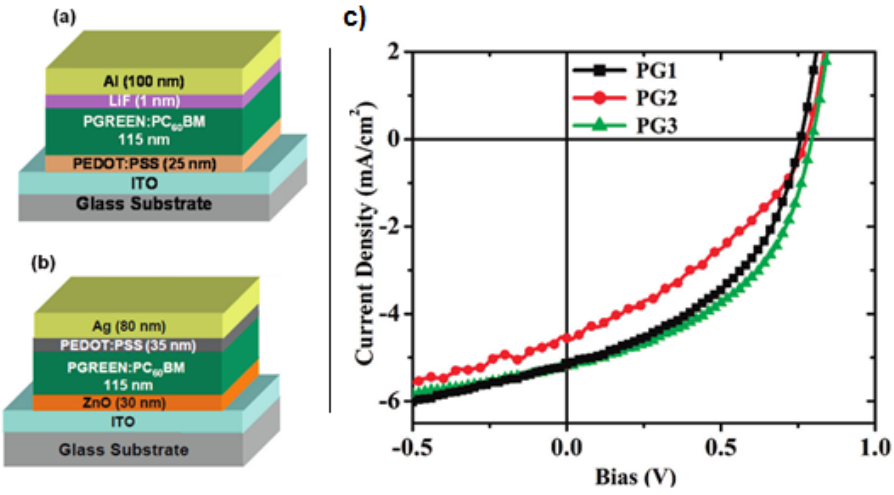

Figure 3-3.Employed solar cell architectures and performance of PGreen series. a) Conventional solar cell architecture with its components. b) Inverted soalr cell architecture. c) Solar cell characteristics of PGreen1(black), PGreen2 (red) and PGreen3 (green) (Adapted with permission from Reynolds, Copyright 2012 American Chemical Society)

Table 3-2. Summary of solar cell performance parameters for PGreen series with device structure ITO/PEDOT:PSS/PGreen:$PC_{60}BM$(1:8)/LiF/Al.

	Thickness	J_{SC} *(mA/cm^2)*	V_{OC} *(V)*	*FF*	*PCE (%)*
PGreen1	120 nm	5.16	0.75	0.45	1.73
PGreen2	120 nm	4.56	0.77	0.37	1.28
PGreen3	120 nm	5.14	0.79	0.47	1.90

Next, PGreen3 was integrated into an inverted solar cell, which is the most suitable structure for roll-to-toll processing. This architecture yields more efficient charge collection, resulting in higher currents because of the favorable morphology of the active layer electrodes.[171,172] Inverted solar cells (ITO/ZnO/PGreen3:PCBM [1:8] PEDOT:PSS/Ag) resulted in a 1.98 % PCE with just a slight increase in the efficiency compared to conventional solar cells (1.90 %). The reason the improvement was so minimal can be attributed to the very high content of the PCBM in the active layer, which could prevent favorable vertical phase morphology. As PGreen3 had the highest PCE of the tested polymers, 0.5 grams of PGreen3 were transferred to Frederic Krebs' group for large area solar cell fabrication through roll-to-roll processing. The active layers (PGreen3 and PCBM) were deposited by slot die coating, and the metal electrodes were fabricated by screen printing. First, single cells with active areas of 4.2 cm^2 were prepared in order to optimize the ratio of PGreen3 to PCBM for roll-to-toll processing. The variation of PCE values and solar cell parameters are shown in Figure 3-4. The polymer and PCBM were pumped differentially, and solar cells were tested immediately after the deposition. The highest PCEs were around 0.7 %-0.8 %, with a blend ratio of 1:1. (Figure 3-4a) When the PCBM content was kept between 30 %-80 %, the *Voc* and FF remained fairly constant, while an increase in the *Jsc* resulted in an increase in the PCE, as shown in Figure 3-4b. It is worth mentioning here that small-scale inverted

solar cells with spin-cast active layers generated PCE's of 1.98 % with a blend ratio of 1:8. The large difference between the PCE and the optimal blend ratios used in these two methods (roll-to-roll versus spin-casting) can be attributed to differences in the active layer. Thicker films of 240 nm were used for slot die coating to provide mechanically robust, defect-free coatings, as well as enhanced color intensity in the solar cells. However, thicker films resulted in less efficient charge collection, as charges buried inside polymer domains were heavily affected by recombination.

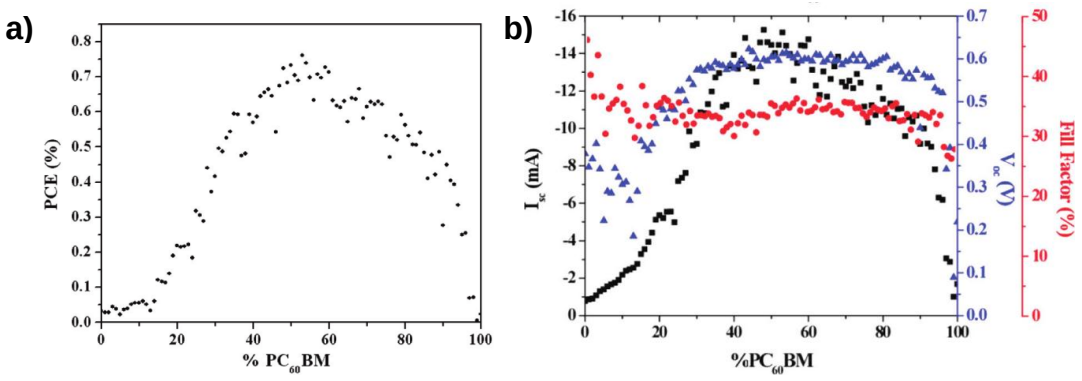

Figure 3-4. Performance of PGreen3 in large area solar cells. a) PCE optimization in 4.2 cm^2 solar cells as a function of PCBM content in the active layer blend. b) The variation of short circuit current (ISC), open circuit voltage (VOC) and FF (%) as a function of PCBM content. (Adapted with permission from Reynolds, Copyright 2012 American Chemical Society)

After optimization of the polymer-to-PCBM blend ratio, fifty 25x25 cm^2 modules, employing 12 serially connected cells, were prepared by roll-to-roll processing as shown in Figure 3-5b. The calculated active area (PGreen3 and PCBM) was 450 cm^2, adding up to 2.25 m^2 of total surface area in 50 modules. On a sunny Florida day, an open circuit voltage of 7.59 V was measured in one module. (Figure 3-5b) The PCE of each module was measured and is shown in Figure 3-5a. With the exception of modules 25-35 and 45-50, modules consistently displayed PCEs between 0.25 % and 0.3 %. The large decrease of PCE from 0.7-0.8 % in 4.2 cm^2 to 0.3 % in the large area modules can

be attributed to the increased resistance (37 000 Ω/cm^2) in the larger device due to the the many series resistances across polymer/electrode interfaces.

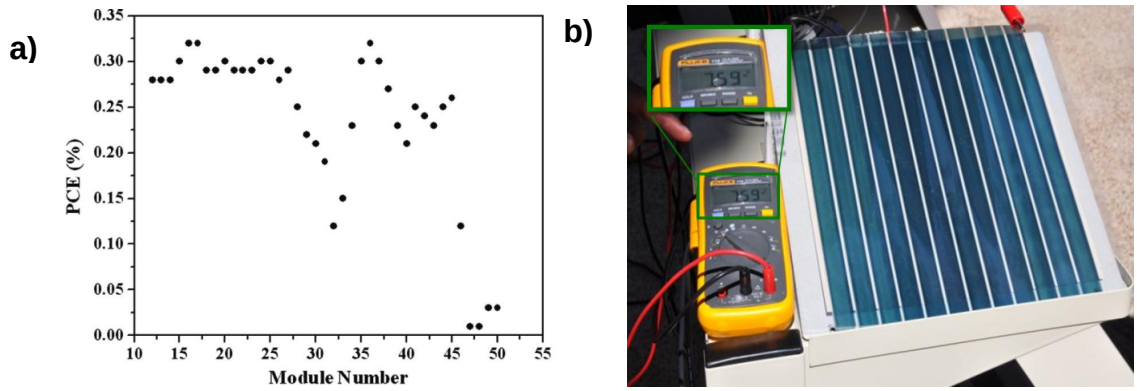

Figure 3-5. The performance of large scale processed blue-green cells. a) PCEs measured for each module. b) One of the slot die coated, inverted solar cell module in a Florida day sunshine. (Adapted with permission from Reynolds, Copyright 2012 American Chemical Society)

3.3 PGreen by Stille Polycondensation

Stille polycondensation was used for the synthesis of all PGreen samples in an attempt to minimize structural defects caused by β coupling of unsubstituted thiophenes during oxidative polymerization. This method affords not only reliable bonding, but also in enhanced control over the nature of the end groups of the polymers. Thus, PGreen was prepared from the Stille polymerization of distanylated bithiophene and dibromothiophene-benzothiadiazole-thiophene monomers by using a $Pd_2(dba)_3$:$P(o\text{-}tol)_3$ catalyst system via the scheme shown in Figure 3-6. Two different paths have been taken to control the end groups: The first includes mixing the difunctionalized monomers in a 1:1 stoichiometric balance and adding the monostannylated benzene and bromobenzene after the polymerization. The resulting product is labeled PGreenStille1. In the second method, 1% excess distannylatedbithiophene monomer was mixed with a dibromo monomer in a stoichiometric imbalance, and the bromobenzene was added to

end-cap the polymer after the polymerization. The end-capped polymer is denoted as PGreenStille2. The polymers were obtained after precipitations into methanol and washings with methanol, acetone, hexane and chloroform in a Soxhlet extractor. Chloroform fractions were precipitated into methanol, affording the polymers as black solids in a 65 % yield. The chemical purity was confirmed by elemental analysis, which showed the percentages of CHN elements in the expected 0.4% theoretical value. The molecular weights of the polymers were determined by GPC in THF, calibrated against polystyrene standards. Results are given in Table 3-3.

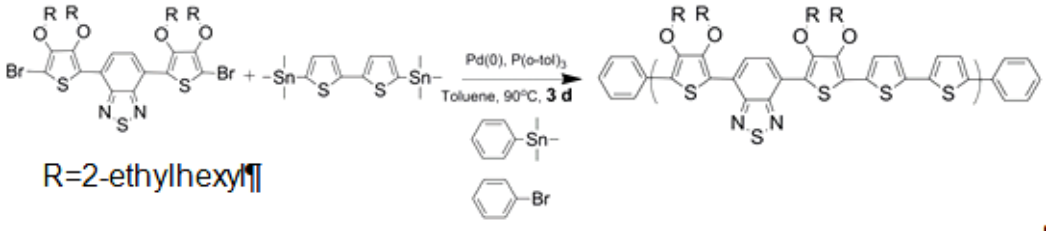

Figure 3-6. PGreen synthesis through Stille polycondensation.

Table 3-3. GPC estimated molecular weights in THF and elemental analysis of the PGreen polymers obtained through Stille polymerization.

	M_n (kDa) THF	M_w (kDa) THF	PDI	EA (Calcd/Found) C	H	N
PGreenStille1	30.5	60.9	1.99	66.49/66.52	7.65/7.73	2.87/2.72
PGreenStille2	35.1	64.9	1.85	66.49/66.12	7.65/7.76	2.87/2.75

PGreenStille2 had a slightly higher number average molecular weight (35.1 kDa) than PGreenStille1 (30.5 kDa). This could be the result of making the ditin monomer more available for the polymerization, as destannylation is commonly observed for Stille polymerizations limiting the extent of reaction in the PGreenStille1.

The polymers' repeat unit structures and the nature of their end groups were studied with matrix-assisted laser desorption/ionization mass spectrometry (MALDI-MS)

measurements. The polymers' repeat units were confirmed by MALDI-MS and the spectra shows ions up to 12000 amu.(Figure 3-7) For each polymer repeat units (n=3-10) have been confirmed with their expected masses. The residual ions in the 4500-5200 amu region have been investigated to probe the nature of the polymers' end groups. Spectra are shown in the insets of Figure 3-7. Each polymer showed peaks with 165 amu around n=5, thus identifying the end groups as either hydrogen or bithiophene. This is indicative of the loss of tin groups during polymerization due to hydrolytic destannylation.

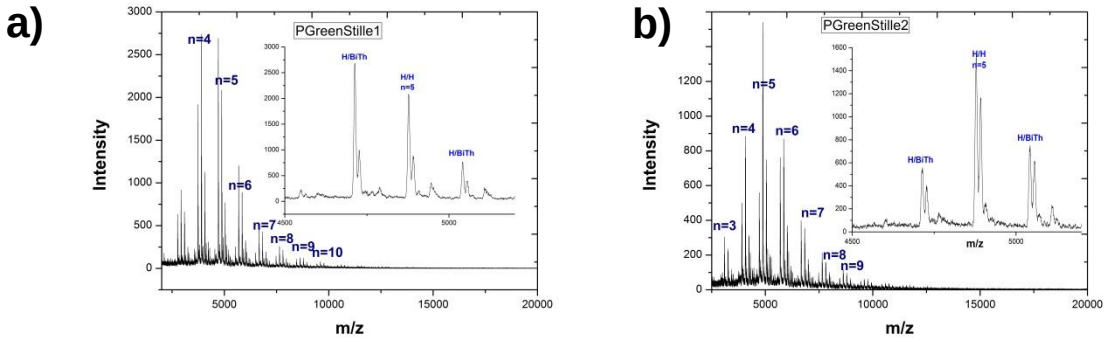

Figure 3-7. MALDI-MS of PGreenStille polymers. a) PGreenStille1 and b) PGreenStille2

Small scale solar cells prepared by spin coating, have been tested by Jagedesian Subbiah in Franky So's group, and large area solar cells employing slot die coating and screen printing have been fabricated by Frederic Krebs' group. The following data have been kindly provided by them.

Solar cells were prepared employing PGreenStille1 and PGreenStille2 in the conventional solar cell architecture (ITO/PEDOT:PSS/PGreenStille:$PC_{60}BM$(1:4)/LiF/Al). The solar cell parameters obtained are shown in Table 3-4. Similar solar cell performance was observed for each polymer, resulting in PCE's near 2.1% with a 1:4 polymer to PCBM blend ratio. PCE's were found to be independent of the active layer

thickness. It is worth noting here that, in the conventional cell architecture, the active layer blend ratio was 1:4. The Stille products consistently required less PCBM to achieve an increased PCE of 2.1%. In previously reported solar cell performance, the oxidative polymerized PGreen had a blend ratio of 1:8 resulting and a PCE of 1.90 %. Additionally, when the active layer blend was 1:4, the PCE was only 0.64 %. A threefold increase was obtained with the new PGreen polymers afforded by Stille polycondensation. This can be attributed to the lack of structural defects (often caused by crosslinking in other methods) and better defined end groups in the Stille products.

Table 3-4. Summary of solar cell performance parameters for PGreenStille1 and PGreenStille2 with different active layer thicknesses in a device structure ITO/PEDOT:PSS/PGreenStille:PC60BM(1:4)/LiF/Al. a Reported solar cell performance for the PGreen obtained by oxidative polymerization employing 1:4 polymer to PCBM ratio in the donor-acceptor blend.

	Thickness	*J_{SC} (mA/cm^2)*	*V_{OC} (V)*	*FF*	*PCE (%)*
PGreenStille1	120 nm	5.82	0.75	0.46	2.02
PGreenStille1	135 nm	6.48	0.75	0.43	2.10
PGreenStille2	120 nm	6.27	0.73	0.47	2.14
PGreenStille2	125 nm	6.46	0.73	0.46	2.19
PGreen[a]	120 nm	1.99	0.78	0.41	0.64

Solar cells were fabricated by Frederic Krebs' group using 150 mg of PGreenStille to test the solar cell performance of the polymer. The solar cells had 4 cm^2 area of the active layer with the inverted solar cell architecture while the thickness of the active layer was 240 nm. The polymer to PCBM ratio was optimized, and the best performance was obtained with a PCBM content of approximately 80 %, resulting in PCE's of 0.25 % as shown in Figure 3-8. The ratio of the polymer to PCBM in the blend was consistent with the earlier optimized 1:4 blend ratio in the small scale solar cells. It is an intriguing fact is that a threefold decrease in PCE was obtained for PGreenStille

when compared to the previously discussed PGreen3 sample, showing PCEs of 0.7-0.8 % in this particular experiment. The reason for this does not likely stem from the purity of the PGreenStille polymer, as no crosslinking is expected and the chemical elemental analysis demonstrated the high quality of this polymer. Further study is needed to confirm and justify these results.

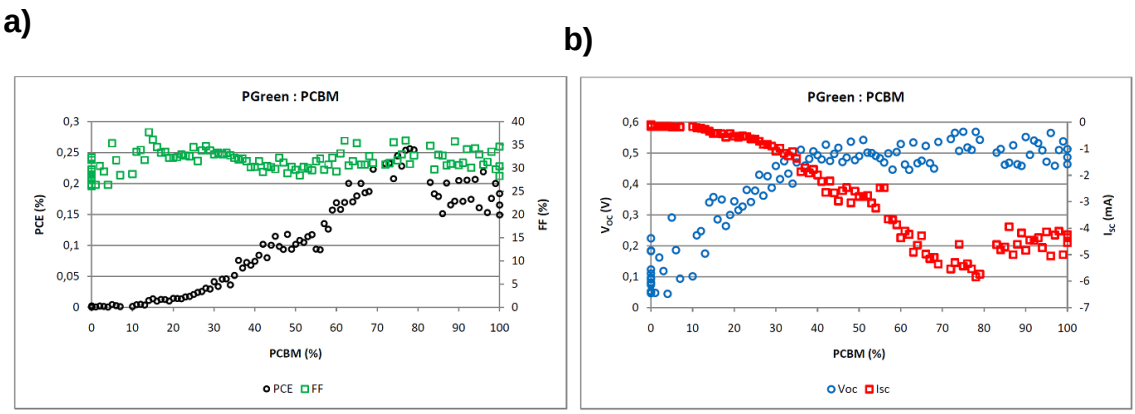

Figure 3-8. Performance of PGreenStille polymer in large area solar cells. a) PCE optimization and FF (%) results in 4.2 cm^2 solar cells as a function of PCBM content in the active layer blend. b) The variation of short circuit current (I_{SC}) and open circuit voltage (V_{OC}) as a function of PCBM content.

3.4 Conclusions on the PGreen

Conjugated polymers require scalable and reproducible polymerization methods, as well as optimized printing methods to generate aesthetically pleasing solar cells. The PGreen polymer was studied for this purpose after its synthesis was scaled to 2 grams, while still maintaining strict synthesis protocols. Slight differences in synthesis have been shown to produce different molecular weights, but reproducible solar cell performances. However, solar cell performances were affected by changes in the processing method used. Solar cells prepared by spin coating resulted in higher PCE values than those prepared by slot die coating. Employing a different synthetic method, Stille polymerization, resulted in a different polymer to PCBM ratio in the active blend.

Large area solar cells resulted in PCEs of 0.3 %. This is the first time a large scale fabrication of slot die coated solar cells has been employed using a polymer other than P3HT.

3.5 Utilization of APFO Type Polymers for Obtaining Green Color

In an effort to diversify our green colored polymer library, APFO type polymers were also synthesized and employed in solar cell devices. This type of polymer's structure is based on alternating fluorene with donor-acceptor-donor (D-A-D) units of thiophene and various acceptors.[36,30] A judicious choice of the acceptor units in the repeat unit, green and purple colored polymers were achieved. Inganas and coworkers have studied these polymers, and showed it is possible to span the entire visible spectrum by controlling the dual band absorption through incorporating different acceptor moieties in the polymer backbone. Within the repeat unit structure of APFO type polymers, the fluorene moiety determines the mobility and HOMO levels, and also ensures the solubility of the final polymer by means of the octyl side chains.

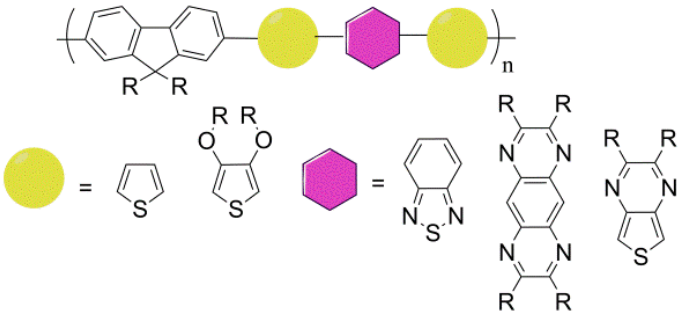

Figure 3-9. Chemical composition of APFO copolymers with different donor and acceptor units employed in the repeat unit structure. (Adapted with permission from Reynolds, Copyright 2011Royal Chemical Society)

The thiophene-acceptor-thiophene (D-A-D) unit is responsible for controlling the absorption profile and intensity, as well as tuning the HOMO and LUMO levels. In

particular, APFO3 polymers exhibited green colors and PCEs of 3.5 % when employed in BHJ solar cells.

In our experiments, we changed the thiophene donor units to dialkylated dioxythiophenes in order to increase the solubility of our polymers and enhance molecular order between the polymer chains. Additionally, dialkylated dioxythiophenes raise the HOMO levels to lower the band gap of the polymers. The other components of the repeat unit were not changed, as dioctylfluorene moieties can tune charge carrier mobility and deep HOMO levels to provide moderate *Voc* for solar cell applications. In the next sections, the new APFO-DOT polymer is discussed. It was prepared by Suzuki coupling to afford a Mn of 34.5 kDa with a 1.94 PDI. It showed purple to transmissive electrochromism, red electroluminescence and 1.66% PCE when used as the active layer in BHJ solar cells.

3.5.1 Polymer Synthesis and Characterization

The APFO-DOT polymer was synthesized via Suzuki polycondensation from the corresponding monomers using a $Pd_2(dba)_3$:$P(o\text{-}tol)_3$ catalyst system with 3 M K_3PO_4 as a base, as shown in Figure 3-10. After allowing sufficient time for polymerization, monofunctional benzene molecules were added to cap the polymer. Precipitations and a soxhlet extraction protocol with methanol, water, acetone, hexane and chloroform were then conducted to remove the low molecular weight oligomers and inorganic salts. The chloroform soluble fraction was precipitated into methanol, affording the APFO-DOT polymer as a purple solid with a 75 % yield and adequate solubility in common organic solvents at room temperature. The number average molecular weight was determined by GPC in THF as 34.5 kDa with a 1.94 PDI. MALDI-MS analysis showed

the expected repeat unit mass of 919 g/mol, indicating the presence of dioctylfluorene and dialkoxythiophene-BT-dialkoxythiophene repeat units

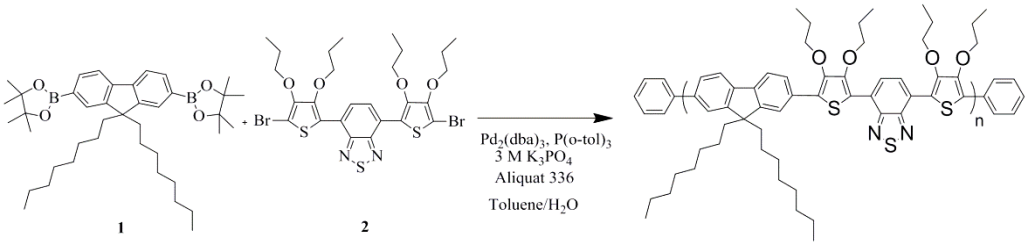

Figure 3-10. Chemical composition and synthesis of APFO-DOT copolymer by Suzuki polycondensation. (Adapted with permission from Reynolds, Copyright 2011Royal Chemical Society)

The absorption and emission characteristics for APFO-DOT are shown in Figure 3-11. Absorption studies were performed in dilute solutions and thin films. Thin film absorption measurements (black, triangles) exhibited a *ca*. 10 nm bathochromic shift compared to the solution spectrum, due to π–π stacking. Also, a characteristic dual band absorption profile was observed for the thin film spectrum due to donor-acceptor interactions in the main chain, with maxima at 390 nm and 555 nm, tailing off to 750 nm while leaving a minimum at 445 nm. The color of the polymer was perceived as purple in solution and in thin films because of the low absorbance in the blue (*ca*. 425-450 nm) and red (*ca*. 650-750 nm) regions. Furthermore, films of the polymer on glass substrates showed a broad photoluminescence band in the red to near-IR region with a maximum at 730 nm (as shown by the blue crosses in Figure 3-11a).

Electroluminescence and OLED measurements have been kindly provided by Ken Graham.

Considering the bright photoluminescence in the red to near-IR region, we investigated this polymer's performance in polymer light emitting diodes (PLEDs).

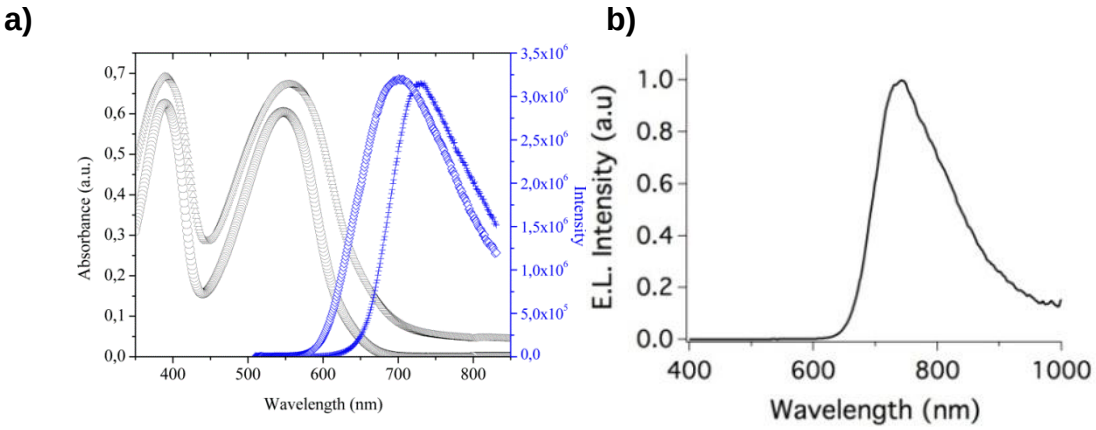

Figure 3-11. Absorption and emission characteristics for APFO-DOT. a) Absorption (in solution: circles, in film: triangles) and emission (in solution: diamond, in film: crosses) spectra of APFO-DOT. b) Electrolumnescence spectrum of a PLED based on APFO-DOT at 12 V applied bias. (Adapted with permission from Reynolds, Copyright 2011Royal Chemical Society)

The PLEDs were fabricated (ITO/PEDOT:PSS/APFO-DOT/Ca/Al) by depositing the polymer via spin coating. Sufficiently bright visible red light was obtained from the PLEDs. The electroluminescence spectra of the PLEDs is shown in Figure 3-11b. Devices exhibited strong red to near-IR electroluminescence, with an emission maximum at 742 nm, thus resulting in an appearance of a deep red color, with a significant proportion of the emission appearing in the near-IR region. The PLED characteristics are shown in Figure 3-12. The PLEDs demonstrated a maximum radiant emittance of nearly 3mW/cm^2 with external quantum efficiencies (EQEs) between 0.2 and 0.3 % at current densities between 20-1000 mA/cm^2. This result places the APFO-DOT polymer as one of the highest performing materials for PLED applications in the 700-800 nm range.

APFO-DOT showed oxidation and reduction processes observed through electrochemical characterizations by CV and DPV. (Figure 3-13ab) CV measurements

reveal the presence of redox processes between -1.8 V to 1.0 V. A peak-to-peak separation of 0.16 V is obtained with an $E_{1/2}$ of 0.68 V versus Ag/Ag^{+}.

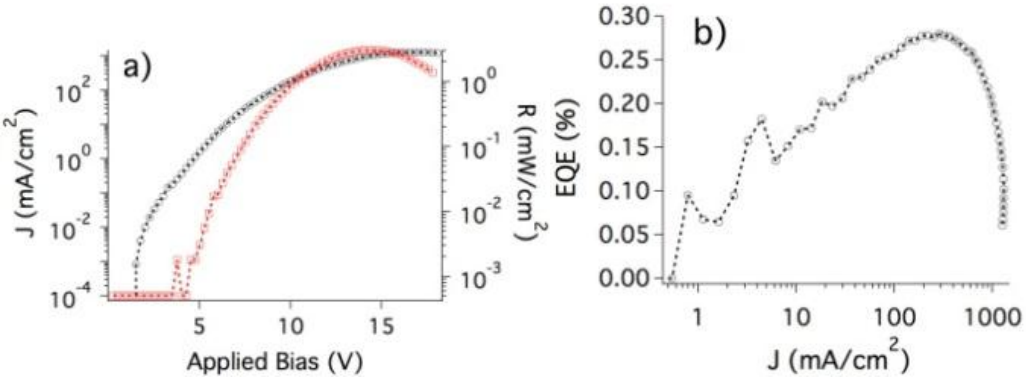

Figure 3-12. PLED properties of APFO-DOT. a) Current density and radiant emittance as a function of applied bias for APFO-DOT based PLED. b) The evaluation of EQE as a function of current density. (Adapted with permission from Reynolds, Copyright 2011Royal Chemical Society)

The small peak-to-peak separation is further studied by scan-rate dependence studies between 5 mV/s and 50 mV/s (Figure 3-13c). A linear correlation between the scan rate and anodic peak current confirms that the redox processes are surface bound. Next, DPV was used to estimate the HOMO-LUMO levels from the onsets of oxidation and reduction. The oxidation onset was 0.40 V (versus Ag/Ag^{+}), thereby bringing the HOMO level to -5.5 eV, assuming that the Fc/Fc^{+} redox couple is -5.1 eV relative to the vacuum level. The reduction onset was -1.47 eV, placing the LUMO level at -3.6 eV relative to the vacuum level. The band gap of the APFO-DOT polymer, measured simply by the taking the difference between between these HOMO and LUMO energy levels, was found to be 1.87 eV. The electrochromic behaviour and band structure were studied with spectroelectrochemical measurements as shown in Figure 3-13d. During these experiments, the APFO-DOT polymer films, spray cast onto ITO-coated glass in an argon purged 0.2 M LiBTI/PC supporting electrolyte solution, were oxidized stepwise,

and the absorption spectra were recorded. The voltage was increased slowly from -0.5 V to 0.82 V versus Ag/Ag^{+} during oxidation, while holding the potential for 5 min at each voltage increment.

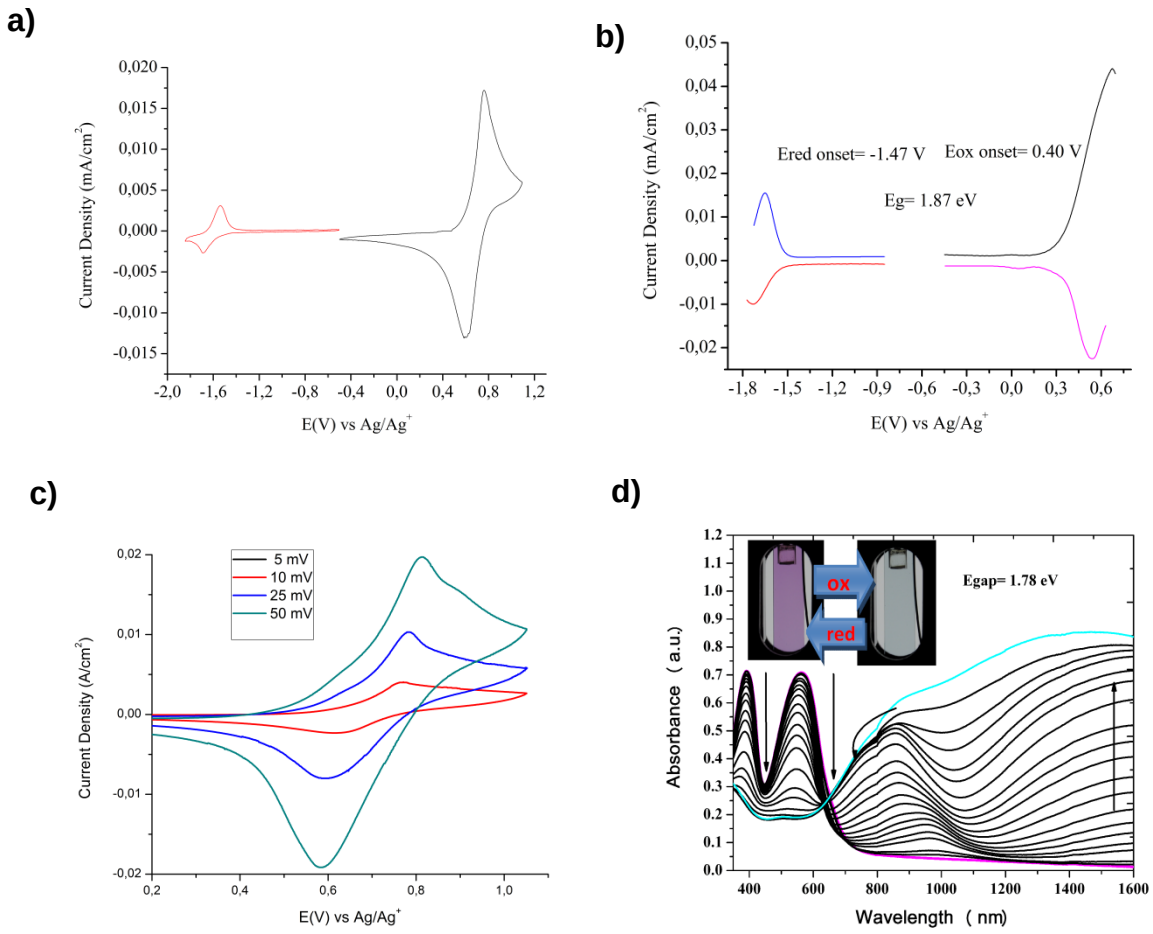

Figure 3-13. Electrochemical characterization of APFO-DOT. a) Cyclic voltammetry of APFO-DOT in 0.1 TBAPF6/PC with a 50 mV/s scan rate. b) Differential Pulse Voltammetry of APFO-DOT in 0.1 TBAPF6/PC.c) Scan Rate Dependant Cyclic Voltammetryof APFO-DOT in 0.1 TBAPF6/PC. d) The spectroelectrochemistry of APFO-DOTfilms coated on ITO glass in 0.2 M LiBTI/PC supporting electrolyte between -0.5 V and 0.82 V versus Ag/Ag+ reference electrode. Inset shows photographs of neutral and oxidized states. (Adapted with permission from Reynolds, Copyright 2011Royal Chemical Society)

Before oxidation, when the polymer was in its neutral form, at -0.5V, two absorption maxima at 562 and 391 nm with a trough at 447 nm resulted in a perceived

purple color (the purple thick line in Figure 3-13d). The absorption onset was used to estimate the optical band gap as 1.78 eV, in agreement with electrochemical measurements. Upon oxidation, the intensity of the bands in the visible region decreased and two new bands appeared in the near-IR range of the spectrum, indicating the formation of polarons and bipolarons. With a further increase of the potential up to 0.82 V, the two bands in the visible region spontaneously bleached, rendering a transmissive film, as is desirable for display applications. APFO-DOT was also employed as the active material in BHJ solar cells in the hope of achieving high *Voc*'s (>1.0 V), as were previously obtained with APFO type polymers. Solar cell characteristics are shown in Figure 3-14 with the conventional device architecture using an APFO-DOT and PC[70]BM blend.

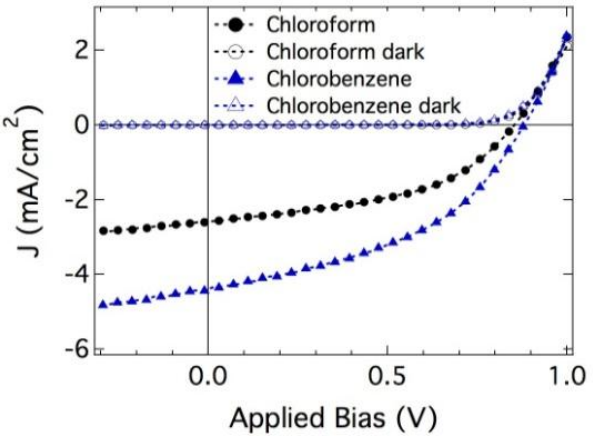

Figure 3-14. Solar cell characteristics of APFO-DOT processed from chloroform (black) and chlorobenzene (blue)(Adapted with permission from Reynolds, Copyright 2011Royal Chemical Society)

Chlorobenzene and chloroform were used as solvents for spin coating of the blend; higher results were obtained with chlorobenzene. The solar cells showed a *Voc* of 0.87 V, short circuit current density (J_{SC}) of 4.38 mA/cm^2 and fill factor of 0.43,

resulting in a PCE of 1.66 %. The low J_{SC} is attributed to the large domains of the polymer and PC[70]BM, which decreased the efficiency of charge separation.

3.5.2 Conclusions

An attempt to obtain green colored electroactive polymers by employing APFO polymers resulted in purple colored polymers due to weak absorption in the blue and red region of the visible spectrum. However, the APFO-DOT polymer based on dialkoxythiophenes showed purple-to-transmissive electrochromism upon oxidation and strong red to near-IR emission in the range of 700-800 nm, making it a suitable material for dual EC/EL devices. Dual EC/EL devices are attractive for display applications that can operate in various lighting conditions. Lastly, the polymer showed a high V_{OC} of 0.87 V with a moderate photovoltaic performance, with a PCE of 1.66%. In summary, though APFO polymers did not yield the green color initially targeted by these experiments, they may be suitable for other application such as EC/EL displays or photovoltaic devices.

3.6 Experimental Details

4,7-bis(5-bromo-3,4-bis((2-ethylhexyl)oxy)thiophen-2-benzo[c][1,2,5]thiadiazole,[167] 5,5'-bis(trimethylstannyl)-2,2'-bithiophene,[174],2,2'-(9,9-dioctyl-9H-fluorene-2,7-diyl)bis(4,4,5,5-tetramethyl-1,3,2-dioxaborolane),[30] have been synthesized according to the reported in the literature.

PGreen1 [168] 4,7-bis(3,4-bis((2-ethylhexyl)oxy)-[2,2'-bithiophen]-5-yl)benzo[c][1,2,5]thiadiazole (1.00 g,1.02 mmol) was transferred from a storage vial to a smaller vial by spatula. This was then rinsed into a 250 mL round-bottom flask with chloroform (HPLC grade, stabilized with 50 ppm pentene), and then more chloroform

was added, so that the total volume of chloroform added was 170 mL. The flask was placed in a room temperature water bath, which was maintained at a temperature of 18.8−19.9 °C throughout the experiment. Dry air was then bubbled into the solution through a stainless steel needle at a bubbling rate of 2−3 bubbles per second. The reaction was then covered by aluminum foil to limit exposure to ambient light, which was only removed periodically to check the status of the reaction. To this solution was added 4.6 mL of a 1.1 M solution of $FeCl_3$ in nitromethane via syringe pump. The pump was set at 2.3 mL/h at a syringe diameter of 13 mm, and the addition took 2 h and 20 min to complete. The reaction was then stirred for 21 h and 40 min longer. After completion of the reaction, the mixture was poured into 500 mL methanol and stirred vigorously for 10 min. The reaction was then filtered on a course paper filter, and washed with 100 mL methanol. The methanol used for washing was then discarded, and a clean flask was placed under the filter. The paper was then punctured to allow solids to flow into the flask below, and the solids were washed down with 350 mL chloroform, yielding a dark suspension with a significant amount of soluble material. Hydrazine monohydrate (10mL) was then added, and the mixture was stirred for 2 h at room temperature. The mixture was then concentrated to approximately 150 mL (rotary evaporation at room temperature), and the mixture was pipetted into 350 mL of methanol. The resulting solid was filtered onto a cellulose thimble, and extracted (via Soxhlet extraction) with methanol (16 h), acetone (12 h), dichoromethane (12 h), and chloroform (until the extract was clear, ~ 6 h). The chloroform soluble fraction was then cooled to room temperature, and 5 mL of hydrazine hydrate solution (80% in water) was added and stirred for 2 h. This fraction was then concentrated to 150 mL (by rotary evaporation, at

room temperature), pipetted into 350 mL of methanol, and the resulting solid was filtered using a nylon filter membrane (GE magna, 20 μm pore size). The solid was then placed under vacuum (~0.1 Torr) for 2 days to remove solvents, resulting in 520 mg (52%) of a dark solid. (PGreen1) Elemental Anal.Calcd %: C, 66.49; H, 7.65; N, 2.87. Found: C, 66.33; H, 7.70; N, 2.83. 1H NMR: 8.45 (bs, 2H), 7.34 (bs, 2H), 7.16 (bs, 2H), 4.05 (m, 8 H), 1.95 (bs, 2H), 1.8−1.0 (m, 34 H), 1.0−0.8 (m, 24 H). ^{1}H NMR spectra were not significantly different between batches PGreen1-PGreen4. PGreen2 was synthesized using a procedure identical to the one used to preparePGreen1, except that 0.3 mL of the Fe(III)Cl_3 solution was added over 2 min and the remainder added over 1.75 h. The temperature was maintained at 21.4−22.1 °C throughout. Yield 250 mg (25%). Elemental Anal. Found: C, 66.39; H, 7.96; N, 2.87. PGreen3 was synthesized using identical procedures as PGreen1, except that the solid Fe(III)Cl_3 used was yellow in color (hydrated), and was dispersed in nitromethane, but not all of the 4.5 g used for the stock solution could be dissolved. Elemental Anal. Found: C, 66.44; H,7.85; N, 2.81. PGreen4 was synthesized using an identical procedure to the one used to synthesize PGreen1, except the amounts of the reagents and solvents were doubled. Elemental Anal. Found: C, 66.21; H,7.71; N, 2.70.

PGreenStille1 A 100 mL flame dried Schlenk flask was charged with 4,7-bis(5-bromo-3,4-bis((2-ethylhexyl)oxy)thiophen-2-yl)benzo[c][1,2,5]thiadiazole (0.422 g, 0.434 mmol) and 5,5'-bis(trimethylstannyl)-2,2'-bithiophene (0.213 g, 0.434 mmol), $Pd_2(dba)_3$ (0.016 g, 0.017 mmol) and P(o-tol)$_3$ (0.010 g, 0.034mmol). The mixture was cycled with argon and vacuum three times. After addition of degassed toluene (25 mL), the reaction was heated to 90 ^{o}C for 3 days. This was followed by the addition of

trimethyl(phenyl)stannane (0.010 g, 0.043 mmol).The reaction was stirred for 24 hours. Then, bromobenzene (0.011g, 0.065 mmol) was added, and the reaction was stirred for another 24 hours. The reaction was cooled to room temperature and precipitated into methanol (500 mL). The precipitates were collected into a thimble and the polymer was washed with Soxhlet extraction using methanol, acetone, hexane and chloroform. The chloroform fraction was concentrated to 50 mL and diethylammonium diethyldithiocarbamate was added. After stirring for 2 hours under argon, the mixture was filtered over a 0.45 µm size polypropylene membrane onto methanol (350 mL). Precipitates were collected and dried under vacuum for 2 days to afford 0.277 g (65 %) of PGreenStille1. Elemental Anal. Found: C, 66.52; H,7.73; N, 2.72.The H-NMR data obtained for PGreenStille1are similar to those obtained for PGreen1. For PGreenStille2 the synthesis protocol was similar except, the distannylated monomer was added in 1% excess. Yield: 300 mg (65%) Elemental Anal. Found: C, 66.12; H,7.76; N, 2.75.

4,7-Bis-(5-bromo-3,4-dipropoxy-thiophen-2-yl)-benzo[1,2,5]thiadiazole (2) In a 100 mL two neck flask 4,7-Bis-(3,4-dipropoxy-thiophen-2-yl)-benzo[1,2,5]thiadiazole (0.35 g, 0.64 mmol) was dissolved in chloroform (20 mL) and N-bromosuccinimide (0.25 g, 1.4 mmol) was added in portions under a flow of argon. The reaction mixture was stirred at room temperature for 24 hours, and aluminum foil was used to shield the reaction from exposure to light. The reaction mixture turned from dark orange to ared bright color. The organic layer was washed with water and dried over magnesium sulfate. After concentration under vacuum, the product was purified via column chromatography (1:1 = Hexanes: Dicholoromethane) to yield 0.397 g (90 %) of a red oil. 8.43 (s, 2H), 4.10 (m, 8H), 1.81 (m, 8H), 1.04 (m, 12H). ^{13}C NMR (75MHz, $CDCl_3$): *δ:*

152.28, 148.19, 147.46, 127.22, 123.78, 121.14, 100.57, 75.43, 74.98, 23.39,10.65, 10.55 Elemental Anal.Calcd for $C_{10}H_{16}O_2S$: C, 59.96; H, 8,05; found: C, 59.16; H, 8.53

Poly[9,9-dioctyl-2,7-9H-fluorene-alt- 4,7-Bis-(5-bromo-3,4-dipropoxy-thiophen-2-yl)-benzo[1,2,5]thiadiazole (APFO-DOT) A 100 mL schlenk flask was charged with 4,7-Bis-(5-bromo-3,4-dipropoxy-thiophen-2-yl)-benzo[1,2,5]thiadiazole (0.225g, 0.326 mmol), 9,9-dioctyl-2,7-di(4',4',5',5'-tetramethyldioxyboralane)fluorene (0.210g, 0.326 mmol), tri-orthotolyl phosphine (4 mg, 0.0130 mmol), $Pd_2(dba)_3$ (6.8 mg, 0.00652 mmol), potassium phosphate (3.18 g, 3M in 5 mL H_2O) and a drop of aliquat 336. The flask was then evacuated and backfilled with argon several times. Toluene (5 mL) and water (5 mL) were then added under argon atmosphere, followed by stirring at 90 ^oC for 4 days. The reaction mixture turned from red to dark purple over the course of the reaction. 1-bromobenzene (0.034 mL, 0.405 mmol) was added and stirred for 1 hour, followed by the addition of 1-phenylboronic acid (0.049 mg, 0.405 mmol). After stirring for a further 1 hour, the reaction was precipitated into methanol (300 mL). Precipitates were filtered into a cellulose thimble and then washed with methanol, water, acetone, hexane and chloroform via a Soxhlet extractor. The chloroform soluble fraction was precipitated into methanol and precipitates were collected using a 20 µm pore size 47 mm diameter nylon membrane. The precipitates were washed with copious amount of water and then re-dissolved in chloroform, then the strongly complexing agent (diethylammonium diethyl dithiocarbamate) was added in order to remove any residual catalyst. After stirring for 2 hours, the mixture was filtered over a 0.45µm size polypropylene membrane into methanol (300 mL). The precipitates were collected and dried under vacuum overnight affording 225 mg (75 %) of a purple solid. ^1H NMR (300

MHz, $CDCl_3$): *δ:* 8.52 (s, 2H), 7.92 (s, 2H), 7.78 (dd, 4H), 4.09 (m, 8H), 2.18-0.65 (m, 54 H) Mn= 34,567 g/mol, Mw= 67,391 g/mol, PDI: 1.94 Elemental Analysis for repeat unit $C_{55}H_{70}N_2O_4S_3$: Calcld: C, 71,85; H, 7,67; N, 3,05; found C, 70.95; H, 8,05; N, 2,80

CHAPTER 4
THE INFLUENCE OF THE BRIDGING ATOM IN THE FUSED THIOPHENE BASED DONOR ACCEPTOR POLYMERS ON CONTROLLING MOLECULAR ORDER AND CHARGE TRANSPORT

4.1 Introduction

The donor-acceptor strategy, a method which involves alternating electron-rich and electron-poor aromatic rings in conjugated polymers, has been effective in controlling important properties of these materials such as band gap, $\pi-\pi$ stacking, light absorption, and charge transport in electroactive polymers. For examples, refer to the Chapter 1 of this dissertation. These properties are desirable for high performance, low cost, processable, organic electronic applications. In particular, an understanding of structure-property relationships in conjugated polymers is of great importance when generating rational design rules for the development of polymers for optoelectronics.

As donor moieties, fused thiophene aromatic rings bridged by carbon (cyclopentadithiophene, CPDT) and silicon (dithienosilole, DTS) have been previously employed in the repeat units of donor-acceptor type polymers in OPVs and OFETs. (Figure 4-1 and Figure 4-2) Fused thiophenes offer enhanced conjugation by forcing planarity of two thiophene units, as well as through the attachment of solubilizing chains to the bridging atom. As such, alternating copolymers of 2-ethylhexyl substituted CPDT and benzothiadizole (BDT) have been reported by Brabec *et al.,* which showed particular promise for OPV applications due to their long wavelength absorption profile.[34] These polymers showed PCEs exceeding 5% and later 5.5% by Heeger and coworkers, who employed solvent additives to optimize the polymer:PCBM blend microstructure.[175] Additionally, high charge carrier mobilities of 0.02 $cm^2/V.s$ have been achieved by Brabec group with these polymers.[176] Additionally, Muellen and coworkers

have shown that their charge carrier mobilities could be increased to 0.17 cm^2/V.s when n-hexadecyl side chains were incorporated onto the CPDT moiety to increase the length of the alkyl chains, thereby improving solubility and molecular order. This was as evident by the measured $\pi-\pi$ stacking distances of 3.7 Å between the two polymer chains.[177] Another approach was taken by Janssen group, where the acceptor moieties were changed from BDT to four different acceptors as shown in Figure 4-1.[178] This structure-property relationship study allowed them to vary the light absorption from 800 nm (for PCPDT:Q) to 1200 nm (for PCPDT:TP). The band gaps of the polymers were tuned between 1.82 eV and 1.34 eV. From the five polymers, PCPDT:BO showed the highest PCE of 2.5 % when blended with PCBM.

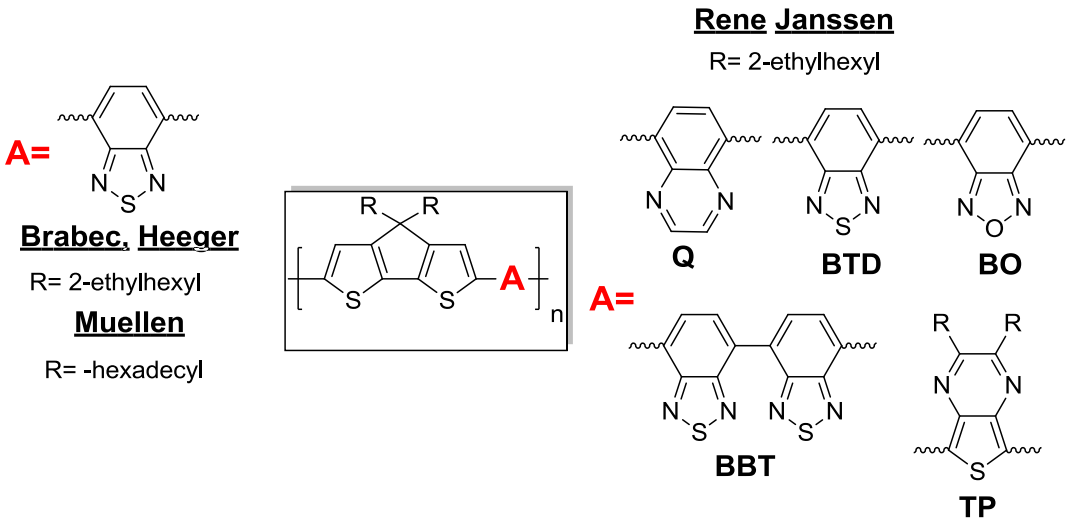

Figure 4-1.Various cyclopentadithiophene based copolymers and their chemical composition.

Following this work, new polymer designs were developed by changing the bridging atom to silicon, in place of the carbon atom, as outlined in Figure 4-2. Initiated firstly by Marks and coworkers, work to develop copolymers of dithienosilole with thiophene units resulted in hole mobilities up to 0.06 cm^2/V.s.[179] The motivation behind

this work was to take advantage of the planar DTS units' ability to reduce intermolecular interactions to yield enhanced transport properties. Inspired by this work, Beaujuge *et al.* carried out a structure-property relationship study using a series of dithienosilole-benzothiadiazole donor-acceptor polymers as shown in Figure 4-3.[180] Given the structures, the study examined the extent of $\pi-\pi$ stacking in the polymers in pursuit of achieving long wavelength absorption and high charge transport properties. Among the five polymers, dithienosilole substituted with 2-ethylhexyl chains showed the highest molecular order, which is reflected in the OFET hole mobility of almost 0.1 $cm^2/V.s$ and 4.6 % PCE obtained when blended with PC[71]BM and integrated into OPVs. In general, it was found that polymers with high molecular weights and appropriate choice of alkyl chains (2-ethylhexyl versus n-octyl) achieved high performance results. Indeed, Yang Yang, employed 2-ethylhexyl substituted DTS with a BTD acceptor based donor-acceptor polymer having an Mn of 18 kDa and yielded 5.1 % PCEs in solar cell devices.[26] This was followed by substitution of the rigid thienopyrroledione acceptor in the place of benzothiadizole, which allowed to polymer to then be functionalized with alkyl chains. Solubility of the polymers was improved with this new acceptor, resulting in molecular weights of up to 28 kDa.[181] Leclerc and coworkers achieved a PCE of 7.3 % after optimization of the polymer:PC[71]BM with solar cell parameters: *Voc* = 0.88 V, *Jsc* = 12.2 mA/cm^2, and *FF* = 0.68.[181]

Yongfang Li and coworkers studied the effects of the position and nature of the alkyl chains on the planar thiazolothiazole (TTz) acceptor.[182] The copolymers of DTS with TTz showed longer wavelength absorption when n-hexyl side chains were moved from the R1 to the R position due to reduced steric crowding. This allowed a 5.88 %

PCE for devices made with this polymer, compared to the 5.58 % of PCE for devices using the polymer with n-hexyl chains at the R1 position.

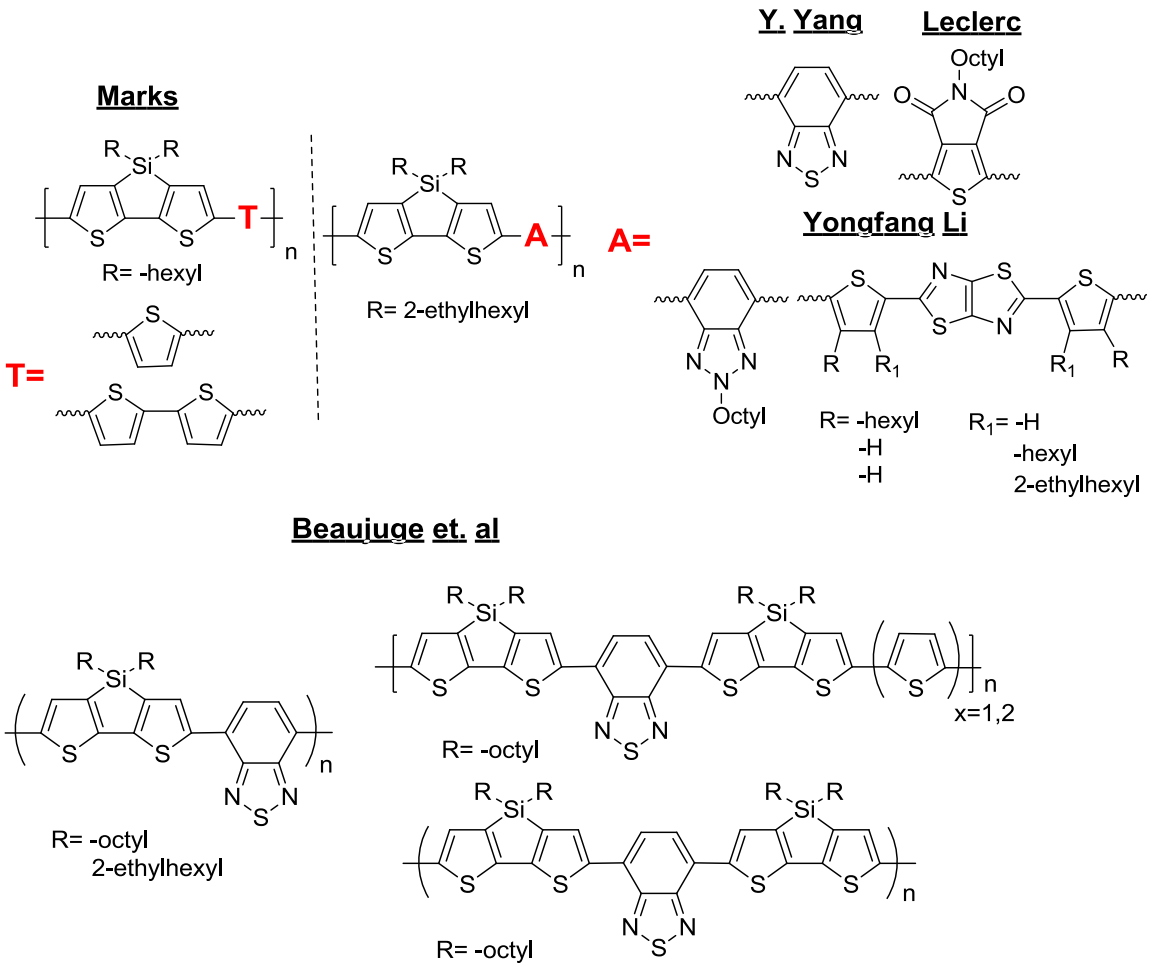

Figure 4-2.Copolymers based on dithienosilole and their chemical compositions.

Additionally, when 2-ethylhexyl side chains were substituted in place of n-hexyl the hole mobility increased to 0.03 $cm^2/V.s$.[183] To conclude all the work done on dithienosilole and cyclopentaditihiophene, Scharber and coworkers did a careful structure-property relationship study to understand the effect of substituting a silicon atom in place of a carbon atom.[184] As seen in Figure 4-3, they compared the crystallinity of the 2-ethylhexyl functionalized CPDT-BTD polymer and DTS-BTD. They found that when a silicon atom was substituted for the bridging atom, the resulting polymers

displayed higher molecular ordering. CPDT-BTD resulted in an amorphous polymer whereas DTS-BTD showed a pronounced peak at 5.2^{o} due to intermolecular interactions, and another small peak at around 20^{o} due to the $\pi-\pi$ stacking. This higher tendency to achieve molecular order is a result of the longer C-Si bonds in the fused ring system.

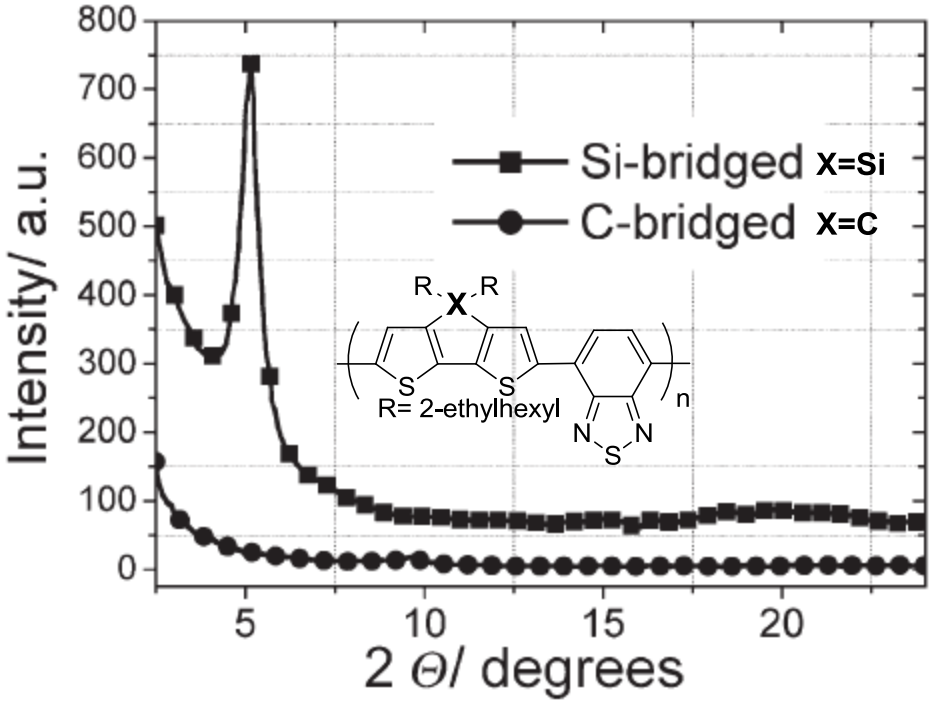

Figure 4-3. X-ray diffractograms of donor acceptor polymers of cyclopentadihiophene and dithiensilole. (Adapted with permission from Brabec.)

Continuing down along the Group 14 elements, the Ge atom bridged fused thiophenes, dithienogermole (DTG), has recently attracted a lot of attention in the polymer research community. As shown in Figure 4-4, a number of donor-acceptor type polymers based on DTG with various acceptors have been developed in the past year. Our group has reported a copolymer with a high molecular weight of 47 kDa, consisting of 2-ethylhexyl functionalized DTG with a TPD acceptor, that resulted in a 7.3 % PCE

when blended with PC[70]BM in an inverted solar cell architecture.[107] The polymer with a Mn of 16 kDa afforded a 4.1 % PCE for Leclerc and coworkers.[185] When copolymerized with a BTD acceptor, PCEs of 1.2 % and 2.9 % were obtained by Kunugi and Leclerc's groups, separately.[185, 186] Additionally, Fujita and coworkers have shown the synthesis of a DTG based copolymer with dithieno-bithiaziadizole and thiazolothiazole acceptors resulting in PCEs of 1.5 % and 2.4 % respectively.[187]

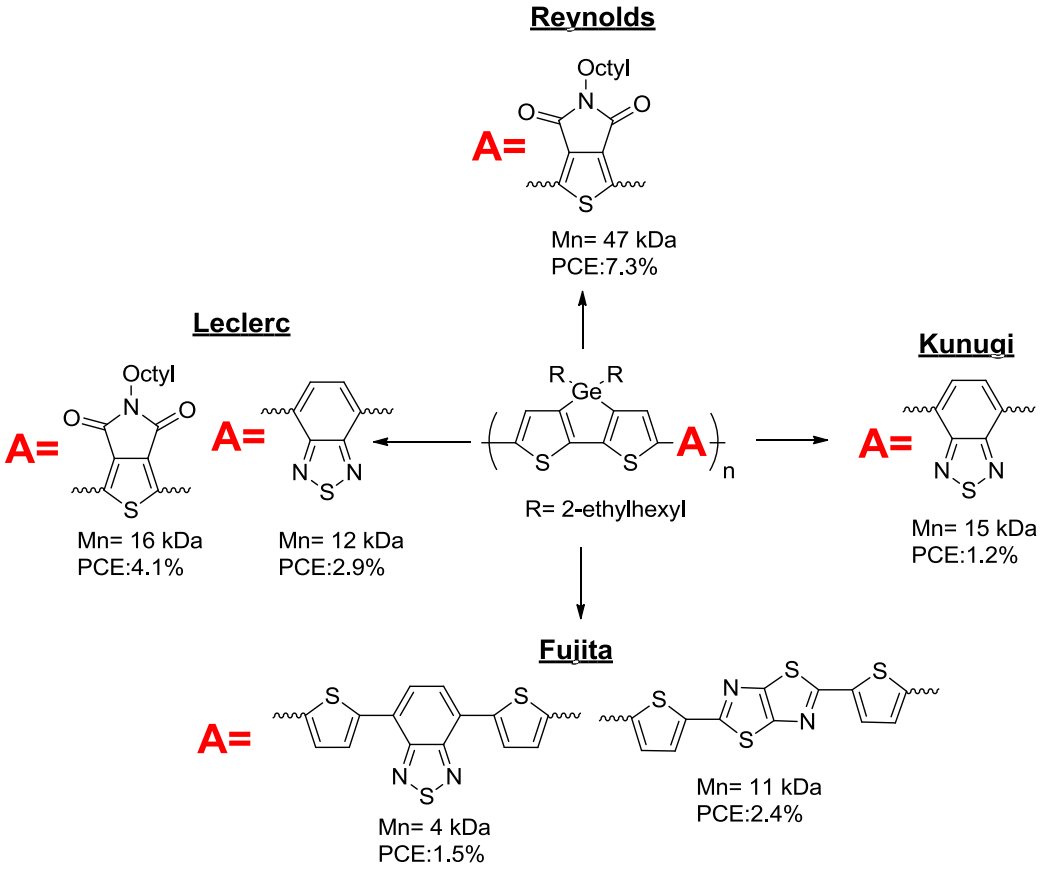

Figure 4-4.Dithigermole based donor-acceptor copolymers reported in 2011.

One reason why DTG is so attractive is due to the longer C-Ge bond (1.99 Å) when compared to the C-Si (1.87 Å) and C-C bonds (1.53 Å).[107, 188] (Figure 4-5a) The motivation for work on these polymers is that by taking advantage of the longer C-Ge bond, which can push the solubilizing chains away from the aromatic ring system,

interchain interactions between the aromatic units may be improved. Heeney and coworkers have studied the peripherally alkylated dithienogermole based polymers illustrated in Figure 4-5b.[189] They compared these Ge atom bridged polymers with Si bridged polymers and performed theoretical calculations on the length of the C-Ge bond to confirm a slightly longer bond length for C-Ge than for C-Si bonds in this particular kind of polymer.

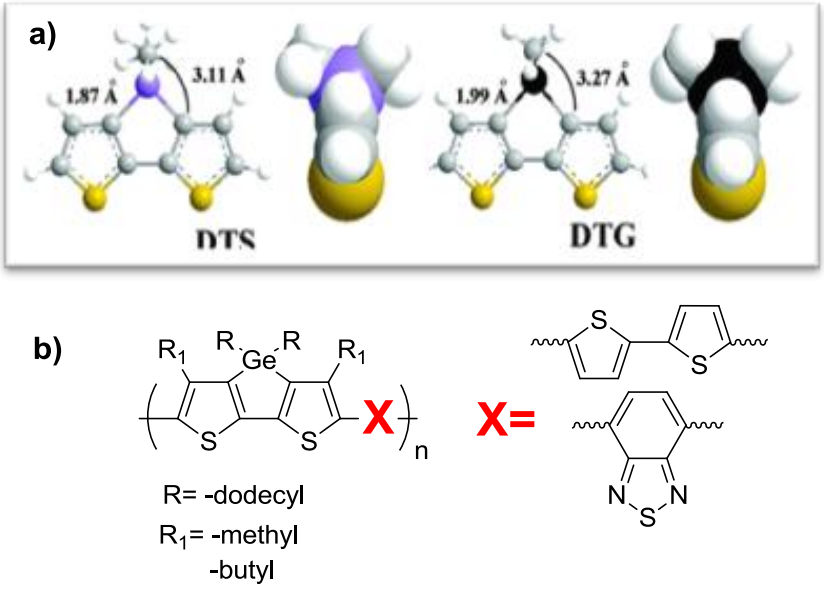

Figure 4-5. The literature examples studied the C-Ge bond lengths. a) Comparison of theoretical model structures dithienosilole and dithienogermole aromatic units. (Adapted with permission from Reynolds) b) Peripherally alkylated dithienogermole based copolymers.

In all of these cases, understanding structure-property relationships is crucial to the design of high performance polymers. In this context, we expand upon previous DTG research by changing the bridging atom from carbon in CPDT to a silicon atom in CPDT, and further to a germanium atom in DTG. For this purpose, six polymers have been designed and synthesized as shown in Figure 4-6. DTS and DTG donor units were combined with acceptor units including BTD, TPD and Pthalimide (PT) to

investigate the effect of heavy atom substitution on absorption behavior, HOMO-LUMO energy levels, molecular packing and charge transport properties. As a general rule, to ensure solubility in the final polymers, DTS and DTG monomers were functionalized with linear n-dodecyl alkyl chains, which also direct long range ordering in the solid state. We found that DTG polymers consistently have higher hole mobilities, closer π–π stacking distances, slightly longer absorptions in the visible region and higher HOMOs when compared to DTS based polymers.

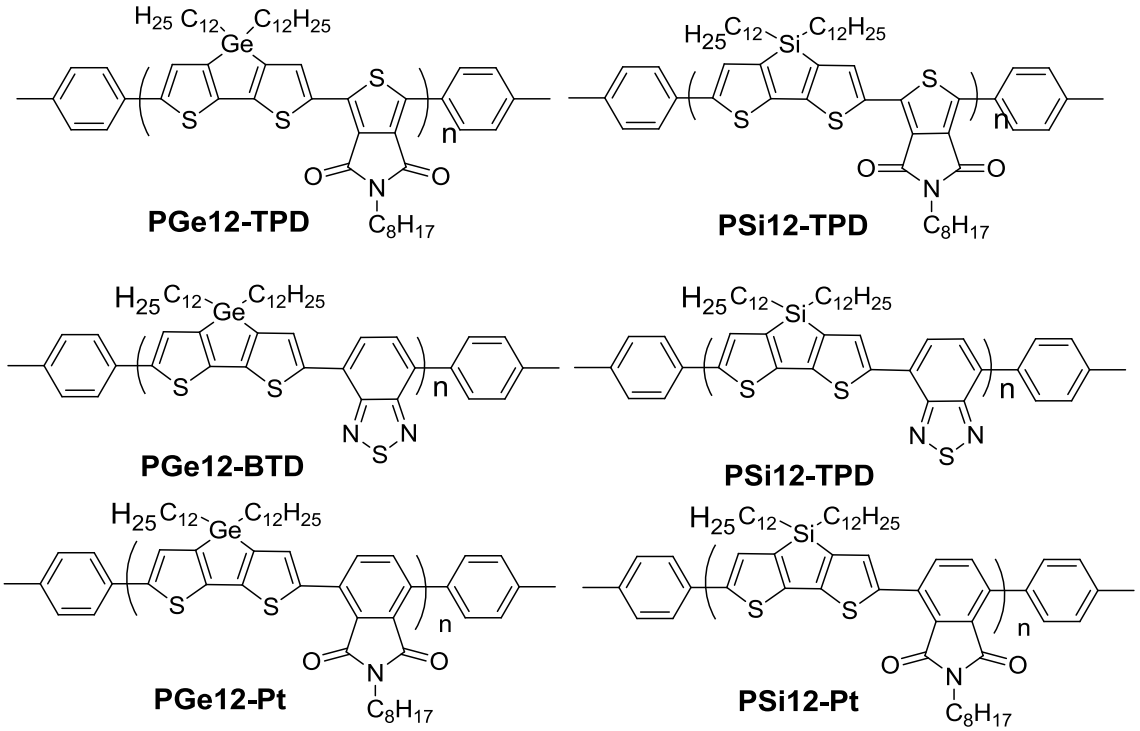

Figure 4-6. Repeat unit structures for the discussed n-dodecyl functionalized dithienogermole and dithienosilole based donor acceptor copolymers in Chapter 4.

4.2 Polymer Synthesis and Characterization

The synthesis of n-dodecyl functionalized DTG and DTS monomers is outlined in Figure 4-7. Briefly, the synthesis starts with the addition of n-dodecyl magnesium bromide onto silicon or germanium tetrachloride, yielding dichlorodidodecylsilane

/germane (**1ab**) on a 15 gram scale after purification via high vacuum distillation. Particularly, 1.7 eq. of Grignard reagent was added to decrease the possibility of substitution of the third and fourth chlorides. Subsequently, compound 1ab was added onto ditlithiated 3-3'bithiophene, which was obtained from metal halogen exchange between 3-3' dibromothiophene and n-BuLi -78 ^{o}C, affording DTS and DTG monomers. Next, these monomers were lithiated and quenched with trimethyltin chloride to obtain distannylated monomers. Purification of these compounds was carried out by passing the material through a plug of silica pretreated with triethylamine to remove the excess tin salts. As the elemental analyses results varied slightly from the theoretical values, purification of these distannylated monomers using reverse phase HPLC was attempted. However, due to the dodecyl chains, the molecules were too apolar, and formed aggregates on the non-polar column. Nevertheless, the structure of these compounds and the absence of monostannylated side products were confirmed by ^{1}H-NMR as shown in Figure 4-8. DTS and DTG monomers have two doublets at 7.20 ppm and 7.05 ppm due to the protons at the 2 and 3 positions respectively on the thiophene ring. After distannylation, the doublet at 7.20 ppm disappears completely (as shown with the black arrow in Figure 4-8), implying the successful completion of the reaction.

After the distannylated DTS and DTG monomers were obtained, Stille polycondensation reactions were performed with these monomers and the dibromobenzothiadiazole (BTD) ,1,3-dibromo-5-octylthieno-[3,4-*c*]pyrrole-4,6-dione (TPD) and diboromo-phthalimide using a $Pd_2(dba)_3$/$P(o\text{-}tol)_3$ catalyst system. One percent excess of the distannylated DTS and DTG monomers were mixed with dibromo monomers and the reactions were run at 90 ^{o}C for 3 days.

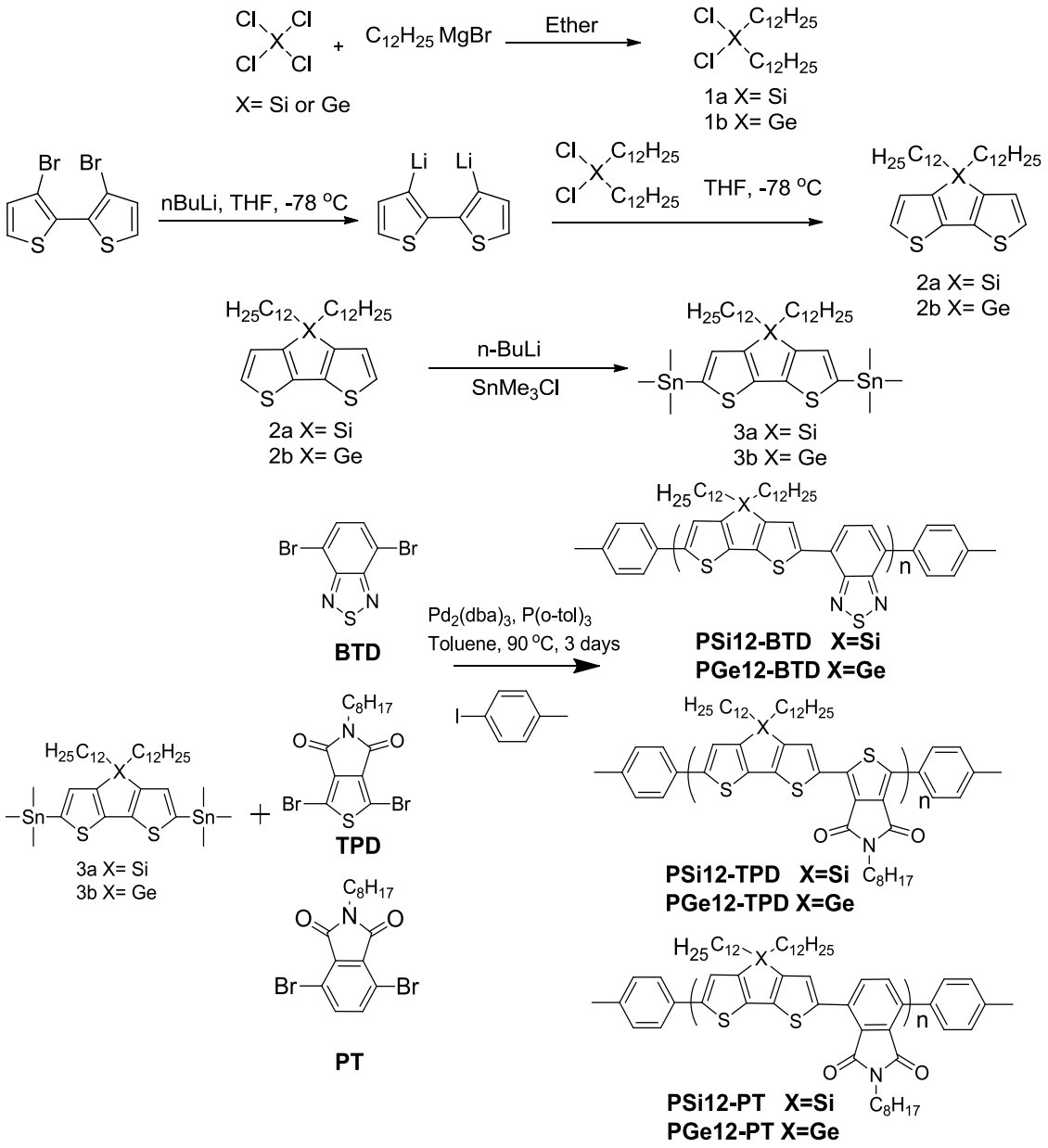

Figure 4-7. Schemes for the synthesis of n-dodecyl functionalized dithienosilole and dithienorgermole monomers and the six donor acceptor type polymers.

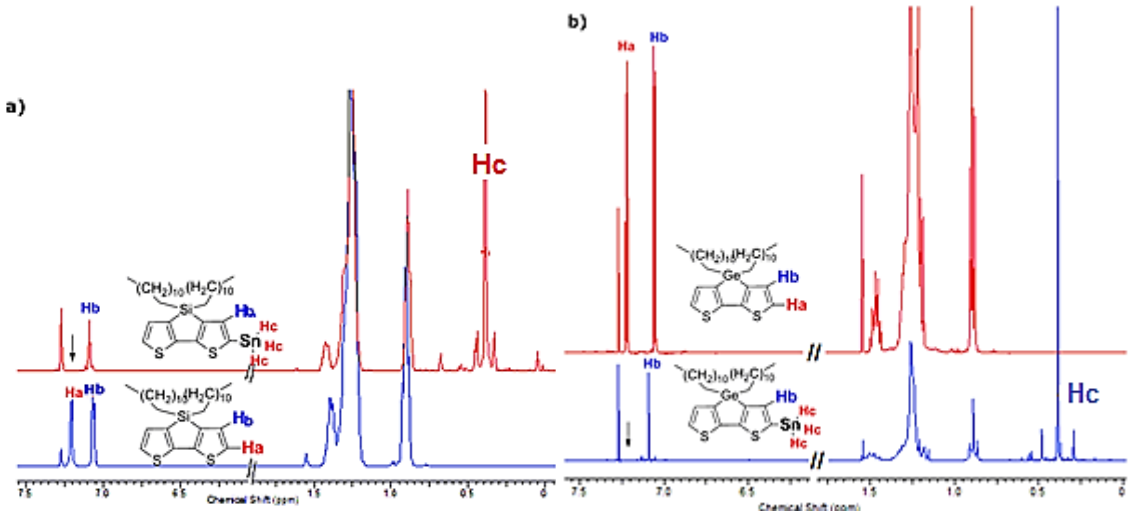

Figure 4-8. Comparison of ^{1}H-NMR spectra of the distannylated monomers and their precursors. a) dithienosilole and distannylated dithienosilole, b) dithienogermole and distannylated dithienogermole. Black arrows show the absence of Ha protons.

Subsequently, 4-iodotoluene was added in excess to end cap the polymers, and the reaction was allowed to run for another 20 hours. The polymerizations were cooled down to room temperature and precipitated into methanol. Solids were collected in a thimble and Soxhlet extractions with methanol, acetone, hexane and chloroform were carried out. A Pd scavenger was added onto the chloroform soluble fraction, and the polymers were collected from precipitation into methanol, affording polymers in yields of 65-70%. All the polymers dissolved in toluene, THF and chloroform at room temperature. The molecular weights of the polymers were determined by GPC measurements using polystyrene standards in THF. Results are shown in Table 4-1. The polymerization procedure using 1% excess ditin monomer yielded reproducible, high molecular weight polymers with M_n greater than 20 kDa (except PSi12-TPD and PSi12-PT, which both had an average number of repeat units higher than 20). PGe12-BTD resulted in the highest number average molecular weight of the polymers studied, with a M_n of 33 kDa and an average of 46 repeat units. Additionally, all polymers

exhibited the expected amounts of C, H and N in the 0.4% purity limit as shown in Table 4-1.

Table 4-1. GPC estimated molecular weights in THF and elemental analyses of the polymers.

	M_n (kDa) THF	M_w (kDa) THF	Average # of Repeat Units	PDI	EA (Calcd/Found) C	H	N
PSi12-BTD	28.5	59.8	43	2.10	68.83/68.97	8.21/9.30	4.22/3.66
PGe12-BTD	33.2	81.0	46	2.43	64.49/64.64	7.69/8.38	3.963/3.54
PSi12-TPD	16.6	35.6	21	2.14	69.91/70.22	8.54/9.24	1.77/1.65
PGe12-TPD	25.1	67.0	30	2.66	66.18/66.76	8.09/9.04	1.68/1.59
PSi12-PT	15.9	26.5	20	1.67	73.32/73.64	9.10/9.74	1.78/1.70
PGe12-PT	20.6	43.0	25	2.09	69.19/69.08	8.40/8.56	1.72/1.61

The repeat unit structures of the polymers have been confirmed by ^{1}H NMR and matrix-assisted laser desorption/ionization mass spectrometry (MALDI-MS) measurements. ^{1}H NMR data showed the expected aromatic and aliphatic proton chemical shifts for the polymer repeat units (See Experimental details). Next, we investigated the presence of toluene end groups. Toluene was selected as the end group due to the characteristic proton chemical shift (~2.2ppm) of the methyl group attached to the benzene ring. Small peaks were observed around 2.3 ppm, overlapping with broader peaks from the methylenic protons in the dodecyl chain. To circumvent this problem, in Chapter 5, PGe12-BTD is discussed specifically for the confirmation of the toluene end group by NMR measurements at 100 ^{o}C in deuterated tetrachloroethane solvent with a 500 MHz instrument. Figure 4-9 shows the selected MALDI mass spectra of PGe12-BTD, PSi12-BTD, PGe12-TPD and PSi12-TPD. Using *trans*-2-[3-(4-*tert*-butylphenyl)-2-methyl-2-propenylidene]malononitrile (DCTB) as the matrix, ions up to 10,000 u were detected using MALDI-MS. Higher mass ions were not observed due to

absence of desorption from the matrix. For each polymer, ions that correspond to oligomer series (n=2, 3, 4, 5, 6) were observed. The ions in each series were separated appropriately to indicate the expected polymer repeat units. Due to the complex nature of step growth polymerization, a number of end groups were obtained. In Chapter 5, end group analysis on PGe12-BTD is discussed in detail.

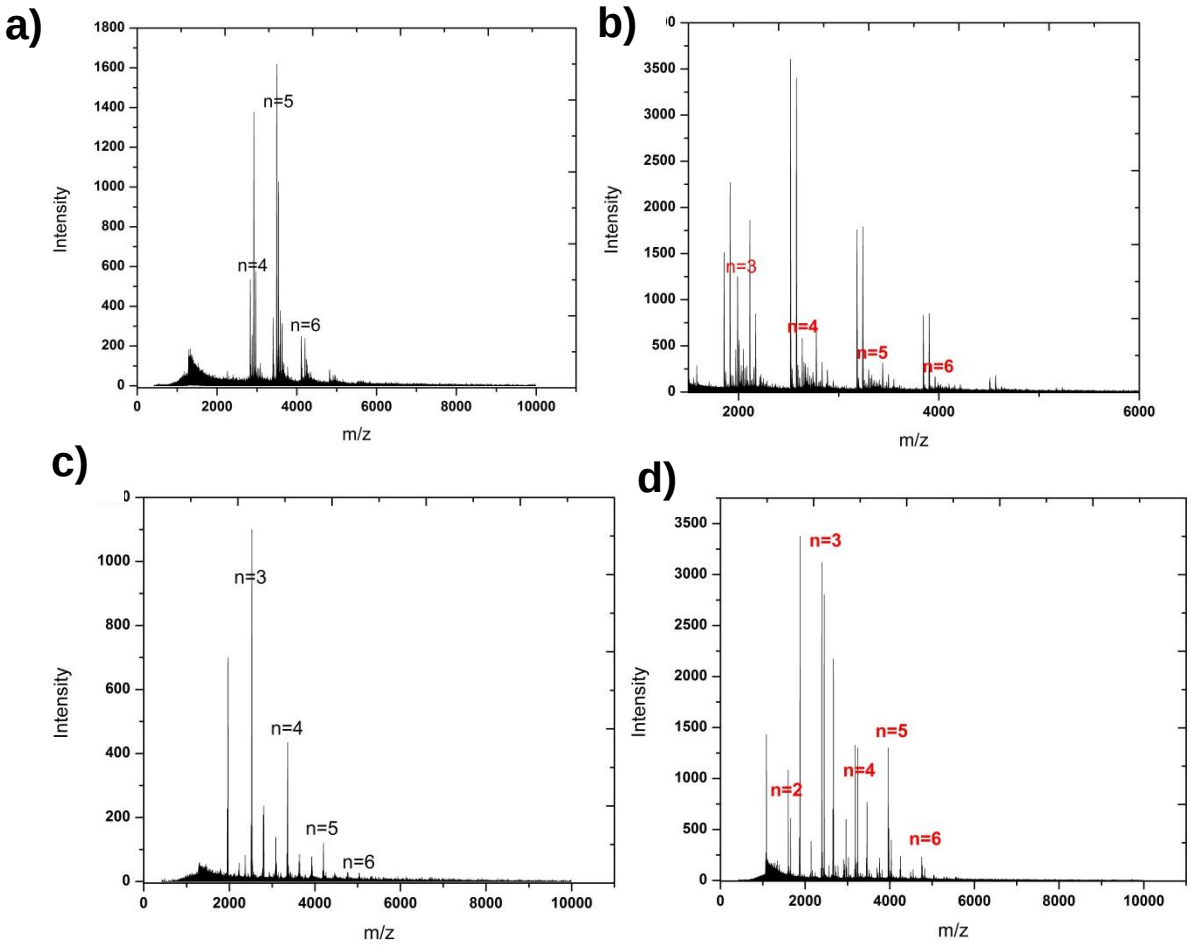

Figure 4-9. MALDI-MS of donor-acceptor polymers a)PGe12-BTD, b) PSi12-BTD, c) PG12-TPD and d) PSi12-TPD recorded using DCTB as matrix.

4.3 Optical and Electrochemical Characterization

The normalized solution and thin film absorption spectra obtained for PGe12-BTD, PSi12-BTD, PGe12-TPD, PSi12-TPD, PGe12-PT and PSi12-PT polymers are

shown in Figure 4-10, and their respective absorption parameters are depicted in Table 4-2.

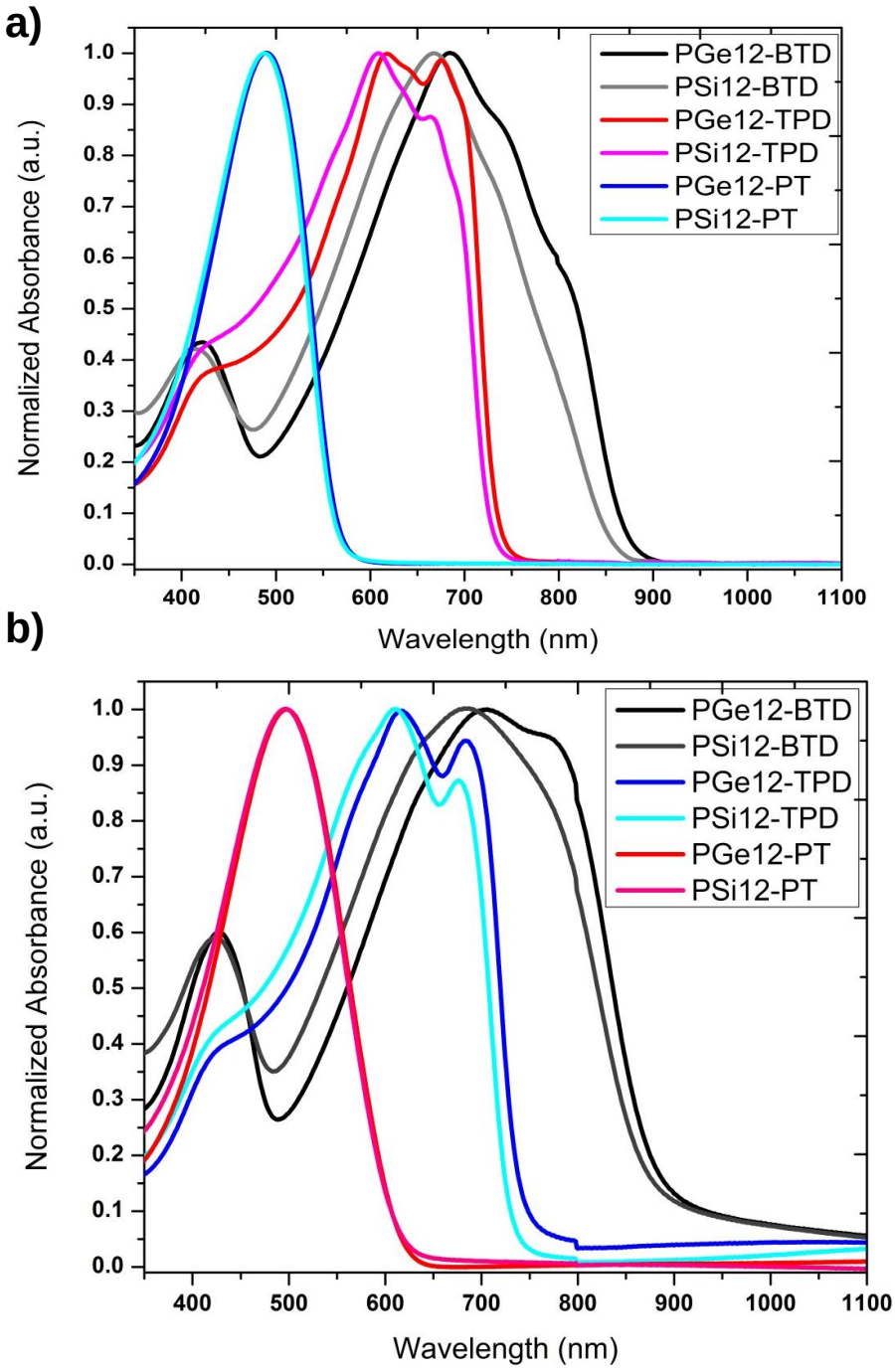

Figure 4-10. Normalized UV-VIS absorption profiles for PGe12-BTD (black), PSi12-BTD (gray), PGe12-TPD (red), PSi12-TPD (magenta), PGe12-PT (blue) and PSi12-PT (cyan) a) in dilute toluene solution and b) in thin film.

Table 4-2. Absorption parameters for polymers both in toluene and thin film with their calculated band gap energy values from the onset of absorption in thin film

Polymer	λ_{abs} *(nm) in Toluene*	λ_{abs}*(nm) Thin film*	λ_{abs} *(nm)Onset In Toluene*	λ_{abs} *(nm)Onset Thin Film*	*Eg (eV)*
PGe12-BTD	684,420	703(772),427	875	878	1.41
PSi12-BTD	667,414	685,423	854	869	1.42
PGe12-TPD	618,675,(430)	615,682,(430)	741	744	1.66
PSi12-TPD	608,664,(425)	610,676,(425)	732	736	1.68
PGe12-PT	490	497	576	623	1.99
PSi12-PT	487	496	576	623	1.99

In general, the absorption profiles show a strong dependence on the nature of the acceptor unit employed in the repeat unit. A bathochromic shift occurred when phthalimide was replaced by thienopyrroledione and subsequently by benzothiadizole, with the magnitude of this shift increasing as the strength of the acceptor increased. Additionally, with the exception of PGe12-PT and PSi12-PT, DTG containing polymers with thienopyrroledione and benzothiadiazole exhibited slightly red shifted absorption, both in solution and in thin films, compared to DTS containing polymers. In particular, in the solution spectra of phthalimide based DTS and DTG polymers, one band at 487 nm and 490 nm was observed, which corresponds to π–π^* transitions. Additionally, a trivial red shift, ca. 8 nm, was found in the absorption maxima for both polymers accompanied by a broadening of the absorption band in the thin film spectra. Incorporation of a stronger acceptor, thienopyrroledione, resulted in a bathochromic shift in the spectra compared to the spectra of phthalimide polymers. Two low energy bands appeared around 615 and 682 nm, with a merged high energy band at 430 nm for PGe12-TPD in thin film samples. PGe12-TPD showed slightly (~8 nm) red shifted onsets of absorption both in toluene and thin film samples, compared to PSi12-TPD. A stronger intramolecular interaction, due to the substitution of benzothiadizole for

thienopyrroledione, resulted in a bathochromic shift in the solution and thin film absorption maxima of DTS and DTG polymers. Benzothiadizole based polymers showed a dual absorption profile, in which the two bands were separated ca. 270 nm, leaving the blue-green region of the spectrum uncovered. Additionally, PGe12-BTD exhibited a slightly (~9 nm) red shifted absorption onset compared to PSi12-BTD both in toluene and thin film samples. These results are consistent with the analysis in the TPD based DTS and DTG polymers. Therefore, we conclude that DTG based polymers show increased aggregation tendency compared to DTS based polymers due to the longer C-Ge bonds, which push the solubilizing chains away from the aromatic units. Thus, the band gaps measured from the onsets of absorption in thin film samples resulted in slightly smaller band gap values for DTG polymers with thienopyrroledione andbenzothiadiazole. Moreover, there was a general trend that benzothiadiazole based polymers produce the smallest band gap (1.41 and 1.42 eV) compared to thethienopyrroledione (1.66 and 1.68 eV) and phthalimide based polymers (1.99 eV).

The redox processes in these polymers have been studied with cyclic voltammetry (CV) and differential pulse voltammetry (DPV) techniques. Firstly, all polymers showed oxidation and reduction processes in the 0.8 V to -1.9 V voltage range, as determined by CV experiments. The results are summarized in Table 4-3. The effect of substituting a Ge atom in the place of the Si atom, as the bridging atom, has been thoroughly investigated with DPV measurements, as shown in Figure 4-11.DTG containing polymers were found to have lower oxidation potentials than DTS containing polymers; the oxidation potentials of PGe12-BTD and PSi12-BTD differed by 270 mV.

This difference reduced to 115 mV in thienopyrroledione based polymers and 110 mV in phthalimide based polymers.

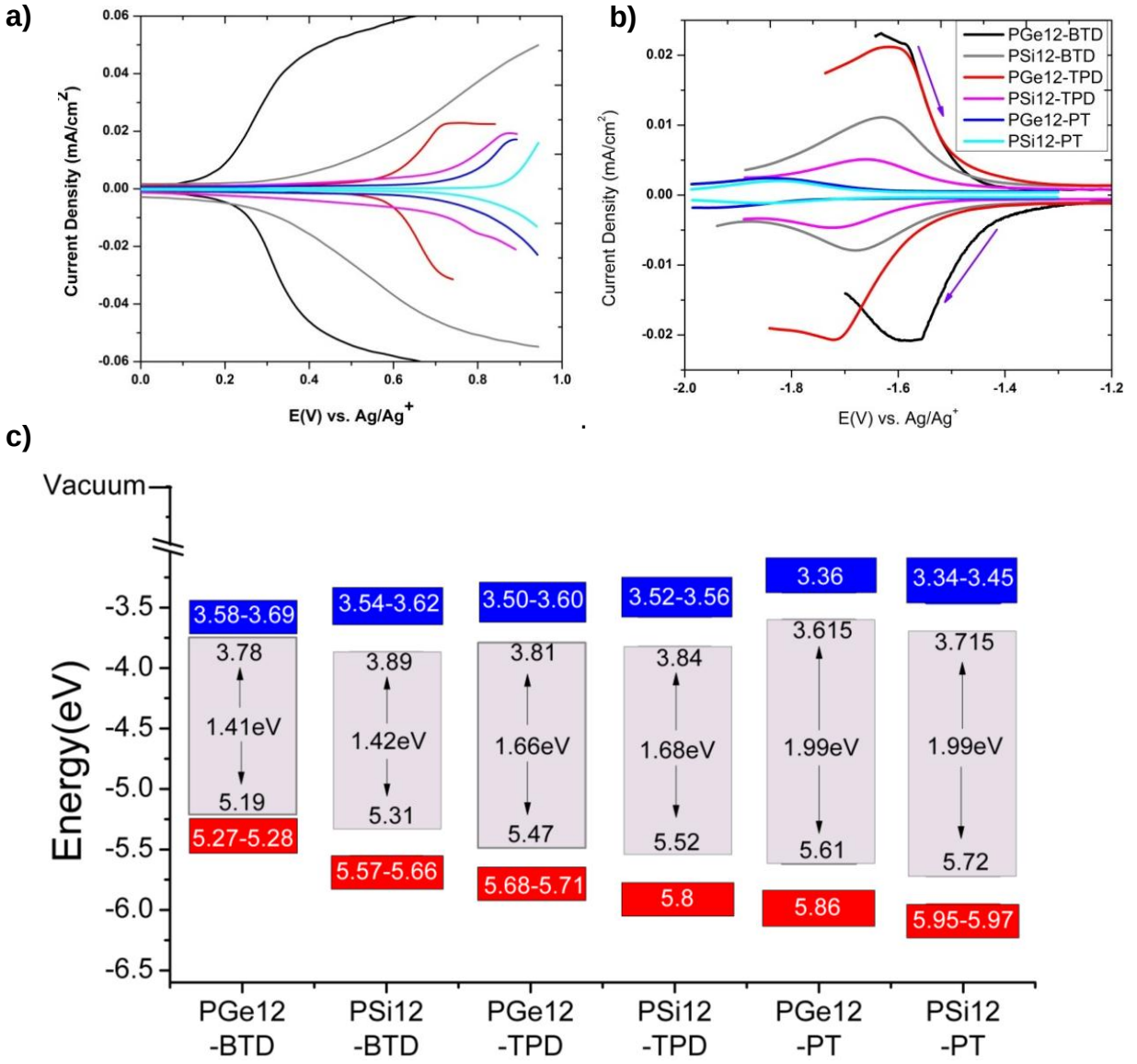

Figure 4-11. Electrochemical characterization of DTS and DTG polymers. a) Differential pulse voltammetry ((step size 2mV, step time38 ms, pulse amplitude 100 mV)for thin films of PGe12-BTD (black), PSi12-BTD (gray), PGe12-TPD (red), PSi12-TPD (magenta), PGe12-PT (blue) and PSi12-PT (cyan)under a) positive voltage bias b) negative voltage bias c) The range of HOMO-LUMO energy levels estimated by CV and DPV measurements for the DTG&DTS series. The optically estimated band gaps of each polymer are placed at the center of the DPV estimated band gaps and a second approximated HOMO and LUMO levels are defined assuming the energy levels are equidistant from the center. These are highlighted in gray rectangle areas.

Table 4-3.Estimated HOMO-LUMO energy levels and band gaps for each copolymer by cyclic voltammetry and differential pulse voltammetry.

Polymer	E_{OX} (V)		E_{RED} (V)		EHOMO (eV)		ELUMO (eV)		Eg (eV)	
	CV	DPV	CV	DPV	CV	DPV	CV	DPV	CV	DPV
PGe12-BTD	0.17	0.18	-1.52	-1.41	-5.27	-5.28	-3.58	-3.69	1.59	1.59
PSi12-BTD	0.56	0.47	-1.56	-1.48	-5.66	-5.57	-3.54	-3.62	2.12	1.95
PGe12-TPD	0.61	0.58	-1.60	-1.50	-5.71	-5.68	-3.50	-3.60	2.21	2.08
PSi12-TPD	0.70	0.70	-1.58	-1.54	-5.80	-5.80	-3.52	-3.56	2.28	2.24
PGe12-PT	0.76	0.76	-1.74	-1.74	-5.86	-5.86	-3.36	-3.36	2.50	2.50
PSi12-PT	0.85	0.87	-1.76	-1.65	-5.95	-5.97	-3.34	-3.45	2.61	2.52

Thus, it can be commented that Ge atom substitution facilitates oxidation and raises the energy of the HOMO levels between 0.1-0.3 eV. Additionally, DPV measurements show that the nature of the acceptor in the repeat unit causes the HOMO levels to become deeper. For example, a stronger acceptor, benzothiadizole was used to form PGe12-BTD with a HOMO level at -5.28 eV, while using a weak acceptor such as phthalimide resulted in PGe12-TPD with a HOMO level at -5.68 eV and PGe12-PT with a HOMO level at -5.86 eV. These results are in agreement with the estimation of HOMO energy levels from CV measurements. While this is the case for oxidation behaviors, the effect of the nature of the acceptor is even more drastic in reduction potentials. The reduction potentials decrease in this order: benzothiadiazole>thienopyrroledione>phthalimide. Thus, the LUMO levels are lower for benzothiadiazole based polymers than for thienopyrroledione or phthalimide based polymers because benzothiadiazole is a stronger acceptor. Ge atom substitution also resulted in slight changes in the LUMO levels of these polymers. PGe12-BTD yielded a 0.07 eV deeper LUMO energy compared to PSi12-BTD, and a 0.04 eV deeper level than thienopyrroledione based DTG and DTS polymers. Ge atom incorporation in the fused aromatic ring raised the HOMO energy and lowered LUMO energy levels of the

polymers. For these two reasons, DTG based polymers resulted in lower band gaps compared to DTS polymers with the same acceptor unit. The band gap reduction is depicted in Figure 4-11. DPV measurements of PSi12-BTD estimate the band gap to be 1.95 eV. A drastic reduction (0.36 eV) in the band gap is observed for PGe12-BTD (E_g= 1.59 eV). The band gap reduction is on the order of 0.16 eV for thienopyrroledione, and 0.02 eV for phthalimide based polymers. These observations are in agreement with the band gap results obtained from the onsets of thin film absorption spectra, in which DTG based polymers yielded slightly lower band gaps. It should be noted that in general, electrochemical methods resulted in higher band gaps than optical measurements, a trend commonly observed in donor-acceptor type polymers.[190]

4.4 2D WAXS and GIWAXS Characterization

The molecular organization of our polymers has been studied in bulk materials with 2D-WAXS and in thin films with GIWAXS methods. X-ray patterns are shown in Figure 4-12 and Figure 4-13. In addition, the structural information derived from these measurements is shown in Table 4-4. We find that phthalimide based DTS and DTG polymers are amorphous, as no reflections for π–π stacking or lamellar organization are evident in the extruded fiber 2D-WAXS patterns. For these polymers, there are no distinct features in the X-ray pattern, and only a vague halo is present due to the alkyl chains. (Figure 4-12e and Figure 4-12f) The lack of π–π interactions can be attributed to the distortion from planarity of the thiophene-benzene bond angle caused by steric congestion between the hydrogen on the thiophene ring and the hydrogen on the benzene unit. While this is the case for phthalimide based polymers, π–π stacking and lamellar organization of the BTD and TPD based polymers are observed as highlighted

in Figure 4-12.The outermost reflections due to π–π stacking, indicated by blue arrows, are more intense for BTD based polymers and broader and more diffuse for TPD based polymers. Thus, calculated π–π stacking distances are smaller for BTD based polymers (3.5 Å) compared to the TPD (3.6 Å) based ones. This minute decrease in the π–π stacking distance can be explained by the presence of alkyl chains on the TPD moieties, which reduce the non-covalent interactions between aromatic units. In addition to closer π–π stacking, BTD based polymers yield closer interchain distances as well. This is again due to the presence of additional alkyl chains, which fill some of the extra space between the lamellar stacks in TPD polymers. With this in mind, it can be concluded that the BTD acceptor moiety with no alkyl chains showed increased the propensity for stacking when compared to the TPD acceptor unit with alkyl chains. The effect of Ge atom substitution is more obvious in the GIWAXS patterns for thin films, as shown in Figure 4-13. PGe12-BTD exhibits a large number of reflections in the q_{xy} direction (highlighted by the yellow arrows in Figure 4-13a) compared to the PSi12-BTD polymer, which shows only one arc in the q_{xy} direction. This can be attributed to increased ordering in the polymer chain stacks of PGe12-BTD due to the presence of the larger Ge atom in DTG, in which the C-Ge bond is longer than the C-Si bond in the PSi12-BTD polymer. Additionally, PGe12-TPD shows one arc in the q_z direction, corresponding to a face on orientation of the polymer chains on the substrate. However, PSi12-TPD exhibits a strong amorphous halo and a broad arc in the q_{xy} direction, indicating that there is less ordering between its polymer chains. As seen in Table 4-4, the organization parameters obtained from thin film measurements are in agreement with the bulk measurements. The π–π stacking distances remain the same and chain-to-

chain distances generally increase slightly (except PGe12-BTD) in thin films when compared to mechanical extrusion process, due to solution processing on the substrate.

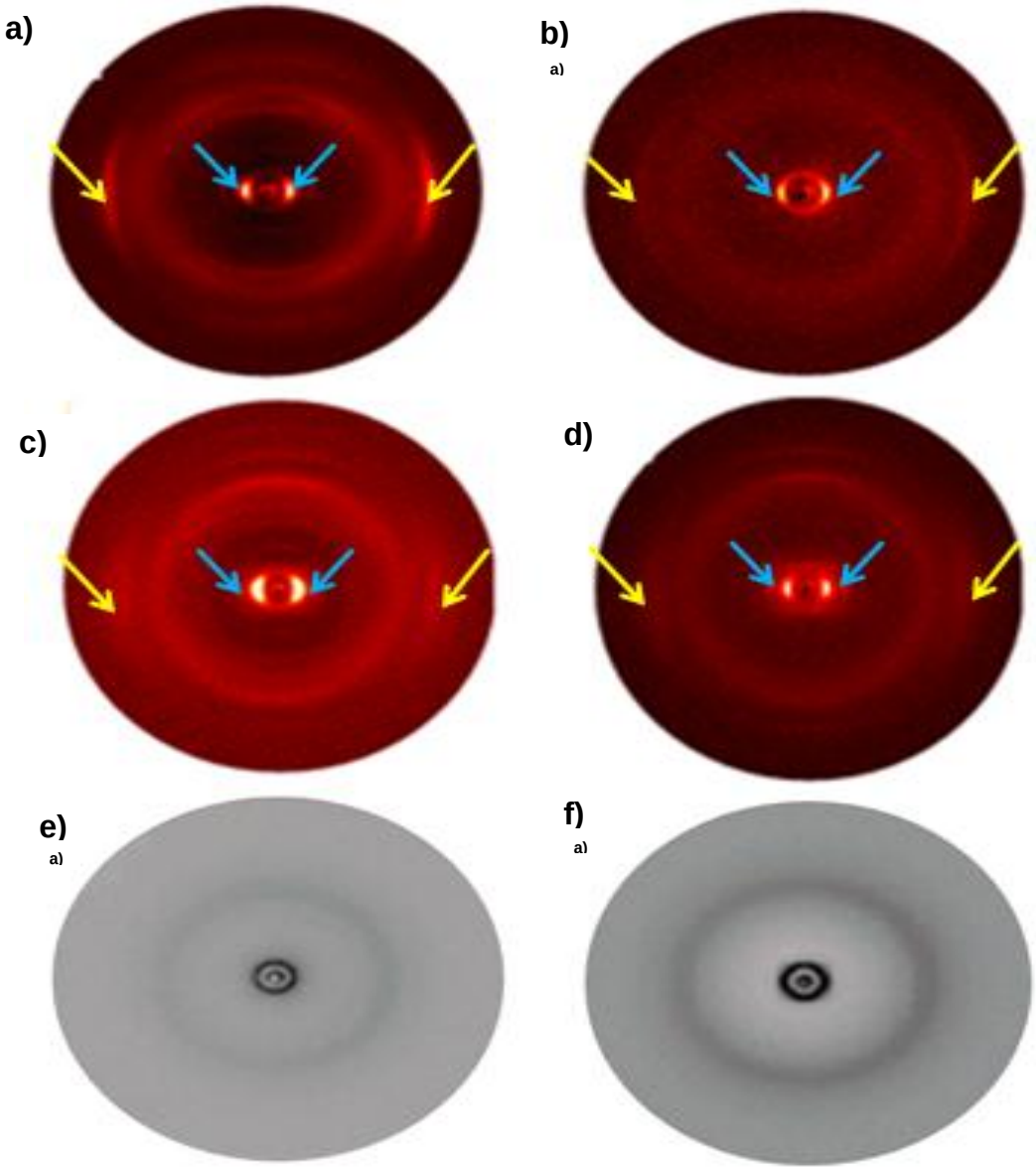

Figure 4-12. Extruded fiber 2D-WAXS patterns measured for DTS and DTG polymers. a) PGe12-BTD, b) PSi12-BTD, c) PGe12-TPD,d) PSi12-TPD, e) PGe12-PT and f) PSi12-PT at 30 ^{o}C after annealing the fibers at 200 ^{o}C. Yellow arrows show the reflections due to π–π stacking and blue arrows highlight the reflections due to lamellar interactions. The PGe12-PT and PSi12-PT patterns are shown in grayscale to increase the contrast.

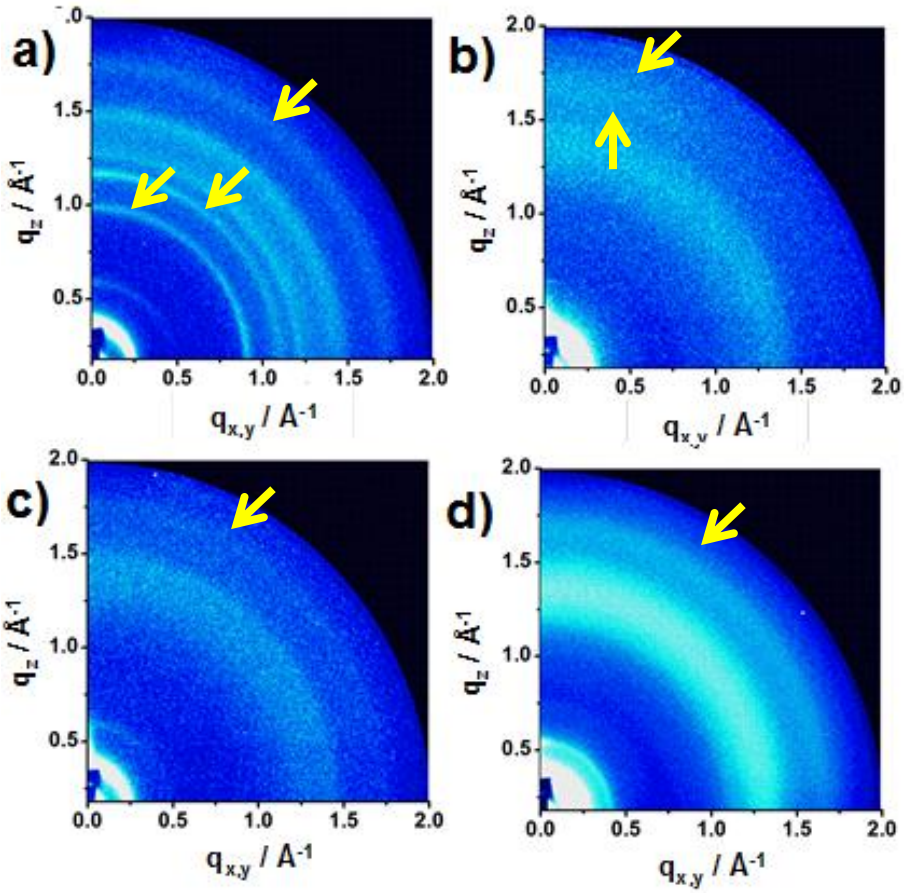

Figure 4-13. GIWAXS patterns recorded for thin films of DTS and DTG polymers. a) PGe12-BTD, b) PGe12-TPD c) PSi12-BTD and d) PSi12-TPD. Yellow arrows highlight the important reflections due to molecular organization.

Table 4-4.Structural information obtained from 2D-WAXS (bulk) and GIWAXS (Thin film) for the DTS and DTG series.

	Lamellar Spacing (Å) Bulk	*π–π Stacking(Å)* Bulk	*Lamellar Spacing (Å)* Thin film	*π–π Stacking(Å)* Thin film
PSi12-BTD	24.0	3.5	25.6	3.5
PGe12-BTD	23.5	3.5	22.4	3.5
PSi12-TPD	26.4	3.6	29.0	3.6
PGe12-TPD	25.6	3.6	27.5	3.6
PSi12-PT	NA	NA		
PGe12-PT	NA	NA		

4.5 OFET and Solar Cell Performances

OFETs were prepared in bottom gate bottom contact architecture as shown in Figure 4-14 to investigate the effects of molecular ordering on the charge transport properties of the aforementioned polymers. The polymer solutions (2mg/mL in dichlorobenzene) were drop cast onto hexamethyldisilazane(HMDS) modified Si/SiO_2 substrates followed by annealing at 200 ^{o}C for 60 min. All polymers showed holes as the dominant charge carriers in the OFET channel when negative voltage bias applied to the gate electrode, as the polymers showed only a small leakage current under positive bias. The device performances are listed in Table 4-5.The hole mobility values were calculated from the saturation regime of the J-V transfer plots for source-drain voltages of V_{SD} = -60 V with the equation mentioned in Chapter 1.Though upon first inspection an applied voltage of -60V seems high for practical display applications, the purpose of these experiments is to achieve a fundamental understanding of their charge transport properties so that advancements can be made in the field for more practical devices. On this note, it was observed that BTD based polymers had higher hole mobilities compared to TPD based polymers, correlating with the closer $\pi-\pi$ distances obtained through X-ray methods. Secondly, DTG polymers showed increased hole mobilities compared to DTS ones due to longer carbon-germanium bond lengths (compared to Si-Ge bond lengths), which improved interchain interactions by pushing away the solubilizing alkyl chains. PGe12-BTD displayed a hole mobility of 0.6 cm^2/Vs, which is almost an order of magnitude higher than the mobility of 0.075 cm^2/Vs obtained for PSi12-BTD.This result makes PGe12-BTD competitive with the high performing polymers that were discussed in Chapter 1.In TPD based polymers, PGe12-TPD

exhibited a hole mobility of 0.0075 cm²/V.s, whereas the hole mobility of PSi12-TPD was 0.0032 cm²/Vs. Surprisingly, PGe12-TPD had a hole mobility almost two orders of magnitude lower than the mobility of PGe12-BTD. This can be attributed to the unfavourable face-on arrangement of the PGe12-TPD polymer chains on the substrate. In the bottom gate, bottom contact device geometry the face on orientation of TPD polymers resulted in misalignment of their high mobility axis with the channel path, thus impeding charge carrier transport between source and drain electrodes. As a note, not shown in Table 4-5, phthalimide based polymers showed hole mobilities on the order of 10^{-6}cm²/Vs, due to their amorphous nature.

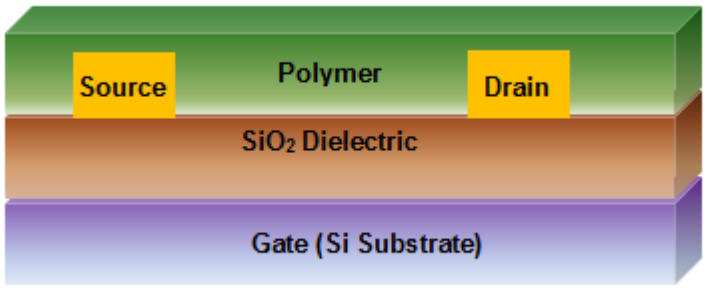

Figure 4-14. Bottom gate-bottom contact OFET architecture for charge transport measurements of the DTG and DTS polymers.

Table 4-5. Summary of holemobilities and on/off ratios and solar cell performance parameters for DTS and DTG series.

	OFET		Solar Cells			
	Hole Mobility (cm^2/V.s)	$I_{on/off}$	J_{SC} (mA/cm^2)	V_{OC} (V)	FF	PCE (%)
PSi12-BTD	0.075	10^5	4.82	0.62	0.36	1.09
PGe12-BTD	0.6	10^5-10^6	8.18	0.50	0.41	1.68
PSi12-TPD	0.0032	10^4-10^5	1.46	0.77	0.39	0.43
PGe12-TPD	0.0075	10^4-10^5	4.03	0.85	0.55	1.86

.

The solar cells results have been kindly provided by Song Chen in Dr. FrankySo's group.

The polymers were also employed in bulk heterojunction (BHJ) solar cells to evaluate the performance of DTG and DTS based polymers in light harvesting applications. BHJ solar cells were prepared using the inverted device geometry, similar to the ones discussed in Chapter 3. Devices were constructed with the following materials: indium-tin oxide (ITO)/zinc oxide/active layer (Polymer PC[71]BM) /molybdenum oxide/silver. In order to improve the morphology of the polymer: methanofullerene [6,6]-phenyl-C71-butyric acid methyl esters (PC[71]BM) blend, diiodooctane (DIO) was used as a solvent additive during the processing of the active layer. The solar cell performances were characterized using an A.M. 1.5G solar radiation source with an incident power of 100 mW/cm^2.The polymers showed power conversion efficiencies (PCEs)between 0.43 % and 1.86 %. The related solar cell parameters are shown in Table 4-5. PGe12-BTD and PGe12-TPD demonstrated higher J_{SC} values compared to their PSi12- analogues, as they have slightly longer wavelength absorption in the visible region and lower band gaps. PGe12-BTD, which had a higher HOMO level as measured by DPV measurements, exhibited lower V_{OC} values compared to PSi12-BTD, in agreement with electrochemical measurements. Moreover, DTG based polymers demonstrated higher fill factor (*FF*) values, indicating relatively better charge generation. This observation correlates with the previously discussed OFET hole mobility results of the DTG polymers, as the FF is dependent on the charge carrier mobility In general, DTG and DTS based polymers resulted in poor PCEs (0.48%-1.86%) when employed in the active layers of the solar cells. One of the reasons for this may be the extensive phase separation (even visible to the naked eye) between DTG polymers and PC[71]BM, indicative of an unfavorable blend morphology.

Larger domains of polymer were segregated from the fullerene phase, preventing excitons from reaching the polymer:fullerene interface for charge separation, thus resulting in a low external quantum efficiency.

4.6 Conclusions and Perspectives

An understanding of structure-property relationships in conjugated polymers is important for the the design of new high performance polymers for optoelectronic applications. The interplay of the many parameters governing high output photovoltaic activity (such as low E_g and deep HOMO levels) and high charge carrier mobilities (such as increased molecular organization) also require special attention. In Chapter 4, synthetic efforts have resulted in six DTS and DTG based copolymers with BTD, TPD and PT acceptors through 1% stoichiometric imbalance of the precursors in a Stille polycondensation. The polymerizations produced polymers with molecular weights reproducibly higher than 15 kDa, with the highest weight polymers reaching M_n up to 33 kDa. The six polymers were grouped into two subcategories, DTS and DTG based polymers, so that a clear trend could be obtained through the variation of the strength of the acceptor units, and for the investigation of the effects of the silicon and germanium atom placed as the bridging atom in the fused aromatic ring system. DTG polymers with Ge as the bridging atom resulted in a slightly red shifted absorption profile in the visible spectrum compared to DTS polymers. This is an important parameter in the realization of high performance photovoltaic materials, as PCEs are directly related to the solar cell J_{SC} values. Additionally, the HOMO and LUMO energies were varied through the use of different acceptor units, so that lower band gaps could be obtained. Also, higher HOMO levels and deeper LUMO levels were observed for the DTG polymers compared to DTS. Thus for applications requiring low band gap materials, DTG can be used in place of

DTS. Futhermore, the band gap was reduced from 2.52 eV for PSi12-PT to 1.59 eV PGe12-BTD. X-ray measurements, which displayed improved molecular organization for DTG based polymers, confirm that when a heavy atom -such as Ge- is introduced, stronger intermolecular interactions are observed. Improved molecular organization resulted in high charge carrier mobilities, achieving values up to 0.6 cm^2/V.s. for the DTG based polymers. On the other hand, while the polymers performed well inOFET devices, their performance in solar cells was poor due to an unfavorable phase morphology of the active layer blend with PC[71]BM. Lastly, it is worth noting here that phthalimide based polymers suffered from possible twisting of the aromatic units due to steric congestion between the thiophene and benzene protons, which is routinely observed for polymers with similar chemical backbones. Thus, completely amorphous polymers were also obtained that displayed very low hole mobilities.

4.6 Experimental Details

3,3'-dibromobithiophene, [179]4,7-dibromo(benzo[c][1,2,5]thiadiazole),[191] 1,3-dibromo(5-octyl-4H-thieno[3,4-c]pyrrole-4,6(5H)-dione)[192] and4,7-dibromo(2-octylisoindoline-1,3-dione)[193]have been synthesized according to the reported literature.

Dichlorodi-n-dodecylsilane (1a)[194] In a 1L three neck flame dried flask, $SiCl_4$ (11 mL, 16.3g, 0.096 mol) was dissolved in 300 mL THF and cooled to -78 ^oC.Dodecylmagnesium bromide solution (250 mL, 0.68 M in diethyl ether, 0.170 mol) was cannulated into the above solution over 15 min. White solid precipitates were observed immediately. The cooling bath was removed, and the mixture was stirred overnight at room temperature. Then the solvent was evaporated under reduced pressure and the crude product was suspended in hexanes (600 mL). Solids were filtered via suction filtration and the filtrate was evaporated under reduced pressure.

Crude yellow oil was distilled to afford the product as pale yellow oil (14 g, 34 %) at 190 ^{o}C under 75 mTorr. ^{1}H NMR (500 MHz, C_6D_6): δ =1.6-1.4 (m, 4H), 1.4-1.1 (m, 36H), 1.0-0.8 (m, 10H). ^{13}C NMR (125 MHz, $CHCl_3$) δ = 33.12, 32.55, 30.34, 30.24, 30.10, 29.99, 29.88, 29.83, 23.51, 23.04,20.96, 14.80

Dichlorodi-n-dodecylgermane (1b) In a 1L three neck flame dried flask, $GeCl_4$ (7 mL, 13.09 g, 0.06 mol) was dissolved in 300 mL THF and cooled to 0 ^{o}C.Dodecylmagnesium bromide solution (152 mL, 0.69 M in diethyl ether mL, 0.10 mol) was cannulated into the above solution over 20 min. White solid precipitates were observed immediately. The reaction was stirred for 4 hours at this temperature and then allowed to stir overnight at room temperature. Later, the solvent was evaporated under reduced pressure and the crude product was suspended in hexanes (300 mL). Solids were filtered via suction filtration and the filtrate was evaporated under reduced pressure. Crude yellow oil was distilled to afford the product as pale yellow oil (18.23g, 63 %) at 190 ^{o}C under 94 mTorr. ^{1}H NMR (300 MHz, C_6D_6): δ =1.6-1.4 (m, 4H), 1.4-1.1 (m, 36H), 1.0-0.8 (m, 10H)

4,4-didodecyl-4H-silolo[3,2-b:4,5-b']dithiophene (2a)[195] In a 1 L three neck flame dried flask, n-butyllithium (20 mL, 2.5M in hexanes, 0.05 mol) was dissolved in THF (400 mL) and cooled to -78 ^{o}C. 3,3'-dibromo-2,2'-bithiophene (8 g, 0.02 mol) in 50 mL THF was added dropwise into the n-butyllithium solution over 20 min, resulting in a clear yellow solution. After the addition was finished, dichlorodi-n-dodecylsilane (10.76 g, 0.02 mol) in 50 mL THF was added dropwise over 40 min,. A large amount of white precipitates were formed. The cooling bath was removed and a water bath was placed so that the reaction would warm up to room temperature. The reaction mixture was

further stirred for another hour at room temperature. The clear yellow solution turned to a brown solution over the course of the reaction. The reaction was quenched by adding a conc. NH_4Cl solution in 300 mL of water. 300 mL of hexanes was added and the organic phase was extracted and then washed with brine. The organic phase was dried over anhydrous $MgS0_4$ Evaporationof the solvent yielded a brown oil as the crude product. This product was purified via column chromatography using hexanes as a solvent affording 2.87 g (22 %) of yellow oil. ^{1}H NMR (500 MHz, $CDCl_3$): δ=7.20 (d, 2H, J= 4.5 Hz), 7.06 (d, 2H, J= 4.5 Hz), 1.44-1.34 (m, 4H), 1.32-1.18 (m, 36H), 0.96-0.86 (m, 10H) ^{13}C NMR (125 MHz, $CDCl_3$) δ = 149.55, 141.99,130.00, 125.30, 33.53, 32.31, 30.02, 29.90, 29.74, 29.58, 24.57, 23.07, 14.50, 12.24 Elemental Analysis for repeat unit C32H54S2Si: Calcld C, 72.38; H, 10.25; S, 12.08; Si, 5.29; found C, 73.65; H, 12.02

4,4-didodecyl-4H-germolo[3,2-b:4,5-b']dithiophene (2b) In a 1 L three neck flame dried flask, n-butyllithium (25 mL, 2.5M in hexanes, 0.06 mol) was dissolved in THF (400 mL) and cooled to -78 ^{o}C. 3,3'-dibromo-2,2'-bithiophene (9.44 g, 0.029 mol) in 50 mL THF was added dropwise into the n-butyllithium solution over 20 min, forming a clear yellow solution. This was followed by the dropwise addition of dichlorodi-n-dodecylgermane (14.13g, 0.029 mol) in 50 mL THF over 40 min, forming a large amount of white precipitates. The cooling bath was removed and a water bath was placed so that the reaction would warm up to room temperature. The reaction mixture was further stirred for another hour at room temperature. The clear yellow solution turned to a brown solution over the course of the reaction. The reaction was quenched by adding a conc. NH_4Cl solution in 300 mL of water. 300 mL of hexanes was added

and the organic phase was extracted and then washed with brine. The collected organic phases were dried over anhydrous $MgS0_4$ and evaporation of the solvent yielded a brown oil as the crude product. This product was purified via column chromatography using hexanes as a solvent, affording 7 g (42 %) of yellow oil. ^{1}H NMR (500 MHz, $CDCl_3$): δ=7.22 (d, 2H, J= 4.5 Hz), 7.05 (d, 2H, J= 4.5 Hz), 1.50-1.43 (m, 4H), 1.32-1.18 (m, 40H), 0.89 (t, 6H, J= 7 Hz) ^{13}C NMR (125 MHz, $CDCl_3$) δ = 147.10, 142.98,130.10, 125.07, 33.11, 32.28, 30.11, 29.99, 29.97, 29.88, 29.71, 29.53, 25.92, 23.05, 14.74, 14.47 Elemental Analysis for repeat unit C32H54GeS2: Calcld: C, 66.78; H, 9.46; Ge, 12.62; S, 11.14; found C, 68.07; H, 10.93

4,4-didodecyl-2,6-bis(trimethylstannyl)-4H-silolo[3,2-b:4,5-b']dithiophene (3a)[195] In a 100 mL flame dried Schlenk flask, 4,4-didodecyl-4H-silolo[3,2-b:4,5-b']dithiophene (1 g, 1.88 mmol) was dissolved in heptanes (40 mL). It was cooled to 0 ^{o}C, then freshly distilled TMEDA (0.65 g, 0.84 mL, 5.65 mmol) was added, followed by the dropwise addition of n-butyllithium (2.26 mL, 2.5 M in hexanes, 5.65 mmol). The resulting brown colored solution was stirred for 2 hours at 0 ^{o}C. Solid $SnMe_3Cl$ (2g, 0.01 mol, excess) was added quickly under argon flow. The reaction was stirred for another 2 hours at 0 ^{o}C, The color changed from yellow to light brown accompanied by the formation of a large amount of precipitates. Then, the solvent was evaporated under reduced pressure and the reaction mixture was suspended in hexanes. The precipitates were filtered using a plug of silica pretreated with triethylamine. The solvent was evaporated under reduced pressure, and the product was kept under high vacuum for 4 days to afford 1.52 g (95 %) of brown oil. Further purification with reverse phase HPLC

was not successful. ^{1}H NMR (300 MHz, $CDCl_3$): δ=7.09 (m, 2H), 1.46-1.38 (m, 4H), 1.34-1.16 (m, 36H), 0.92-0.84 (m, 10H), 0.38 (m, 18H)

4,4-didodecyl-2,6-bis(trimethylstannyl)-4H-germolo[3,2-b:4,5-b']dithiophene (3b) In a 100 mL flame dried Schlenk flask, 4,4-didodecyl-4H-germolo[3,2-b:4,5-b']dithiophene (1.46 g, 2.55 mmol) was dissolved in heptanes (40 mL). It was cooled to 0 ^{o}C, then freshly distilled TMEDA (0.89 g, 1.14 mL, 7.5 mmol) was added, followed by the dropwise addition of n-butyllithium (3 mL 2.5 M in hexanes, 7.5 mmol). The resulting brown colored solution was stirred for 2 hours at 0 ^{o}C. Solid $SnMe_3Cl$ (2g, 0.01 mol, excess) was added under argon flow, and the reaction was stirred for another 2 hours at 0 ^{o}C. Then, the solvent was evaporated and the reaction mixture was suspended in hexanes. The precipitates were filtered using a plug of silica pretreated with triethylamine. The solvent was evaporated under reduced pressure, and the product was kept under high vacuum for 4 days to afford 2.2 g of brown oil. (97 %) ^{1}H NMR (500 MHz, $CDCl_3$): δ=7.09 (m, 2H), 1.54-1.46 (m, 4H), 1.34-1.16 (m, 40H), 0.89 (t, 6H, J= 7 Hz) ^{13}C NMR (125 MHz, $CDCl_3$) δ = 152.96, 144.39,138.07, 137.69, 33.24, 32.28, 30.06, 30.04, 30.02, 29.99, 29.73, 29.57, 26.01, 23.05, 14.88, 14.48, -7.32 Elemental Analysis for repeat unit C38H70GeS2Sn2: Calcld: C, 50.65; H, 7.83; Ge, 8.06; S, 7.12; Sn, 26.35; found C, 52.39; H, 8,87

General Experimental Procedure for Polymerizations:Poly[DONOR-alt-ACCEPTOR)] A 100 mL flame dried Schlenk flask was charged with carefully weighed DONOR (1.01 eq), ACCEPTOR (1 eq), $Pd_2(dba)_3$ (4% eq.) and $P(o\text{-}tol)_3$ (8 % eq.). The mixture was cycled with argon and vacuum three times. After addition of 20mL of degassed toluene, the reaction was heated to 90 ^{o}C for 3 days. This was followed by

the addition of 4-iodotoluene (excess). The reaction was allowed to run for another 20 hours. The reaction was cooled to room temperature and precipitated into methanol (500 mL). The precipitates were collected into a thimble and the polymer was washed using Soxhlet extraction with methanol, acetone, hexane and chloroform. The chloroform fraction was concentrated to 50 mL, and diethylammonium diethyldithiocarbamate was added. After stirring for 2 hours under argon, the mixture was filtered over a 0.45µm size polypropylene membrane into methanol (350 mL). Precipitates were collected and dried under vacuum for 2 days to afford the title polymer.

Poly5-5'(4,4-didodecyl-4H-germolo[3,2-b:4,5-b']dithiophene)-alt-1,3(5-octyl-4H-thieno[3,4-c]pyrrole-4,6(5H)-dione) (PGe12-TPD) The polymer was obtained as 0.275 g (65 %) of a black solid. ^{1}H NMR (500 MHz, $CDCl_3$): *δ:* 8.60-7.40 (m, 2H), 3.74 (m, 2H), 1.8-0.80 (m, 65H) Mn= 28,500 g/mol, Mw= 59,800 g/mol, PDI: 2.10 Elemental Analysis for repeat unit $C_{46}H_{67}GeNO_2S_3$: Calcld: C, 66.18; H, 8.09; Ge, 8.70; N, 1.68; O, 3.83; S, 11.52 found: C, 66.76; H, 9.04; N, 1.59

Poly5-5'(4,4-didodecyl-4H-silolo[3,2-b:4,5-b']dithiophene)-alt-1,3(5-octyl-4H-thieno[3,4-c]pyrrole-4,6(5H)-dione) (PSi12-TPD) The polymer was obtained as a black solid of 0.288 g. (67%) ^{1}H NMR (500 MHz, $CDCl_3$): *δ:* 8.30-7.50 (m, 2H), 3.80-3.40 (m, 2H), 2.10-0.60 (m, 65H) Mn= 16,700 g/mol, Mw= 35,700 g/mol, PDI: 2.14 Elemental Analysis for repeat unit C46H67NO2S3Si: Calcld: C, 69.91; H, 8.54; N, 1.77; O, 4.05; S, 12.17; Si, 3.55 found: C, 70.22; H, 9.24; N, 1.65

Poly5-5'(4,4-didodecyl-4H-germolo[3,2-b:4,5-b']dithiophene)-alt-4,7-(benzo[c][1,2,5]thiadiazole) (PGe12-BTD) 0.240 g (68 %) of a black solid polymer was

obtained. ^{1}H NMR (500 MHz, $CDCl_3$): *δ:* 8.40-7.70 (m, 4H), 2.20-0.60 (m, 50H) Mn= 33,200 g/mol, Mw= 81,100 g/mol, PDI: 2.43 Elemental Analysis for repeat unit $C_{38}H_{54}GeN_2S_3$: Calcld: C, 64.49; H, 7.69; Ge, 10.26; N, 3.96; S, 13.59 found: C, 64.64; H, 8.38; N, 3.54

Poly5-5'(4,4-didodecyl-4H-silolo[3,2-b:4,5-b']dithiophene)-alt-4,7-(benzo[c][1,2,5]thiadiazole) (PSi12-BTD) The polymer was obtained as a black solid of 0.251 g. (70 %) ^{1}H NMR (500 MHz, $CDCl_3$): *δ:* 8.60-7.60 (m, 4H), 2.20-0.60 (m, 50H) Mn= 25,200 g/mol, Mw= 67,100 g/mol, PDI: 2.66 Elemental Analysis for repeat unit $C_{38}H_{54}N_2S_3Si$: Calcld: C, 68.83; H, 8.21; N, 4.22; S, 14.51; Si, 4.24 found: C, 68.97; H, 9.30; N, 3.66

Poly5-5'(4,4-didodecyl-4H-silolo[3,2-b:4,5-b']dithiophene)-alt-4,7-(2-octylisoindoline-1,3-dione) PSi12-PT The polymer was obtained as a dark red solid of 0.175 mg. (69 %) ^{1}H NMR (500 MHz, $CDCl_3$): *δ:* 7.92 (s, 2H), 7.95 (s, 2H), 3.73 (s, 2H), 1.73-0.86 (m, 65H) Mn= 15,900 g/mol, Mw= 26,600 g/mol, PDI: 1.67 Elemental Analysis for repeat unit $C_{48}H_{71}SiNO_2S_2$: Calcld: C, 73.32; H, 9.10; N, 1.78;found: C, 73.64; H, 9.74; N, 1.70

Poly5-5'(4,4-didodecyl-4H-germolo[3,2-b:4,5-b']dithiophene)-alt-4,7-(2-octylisoindoline-1,3-dione)PGe12-PT The polymer was obtained as a dark red solid of 0.357 g. (65 %) ^{1}H NMR (500 MHz, $CDCl_3$): *δ:* 7.95 (s, 2H), 7.85 (s, 2H), 3.73 (s, 2H), 1.71-0.86 (m, 65H) Mn= 20,600 g/mol, Mw= 43,100 g/mol, PDI: 2.09 Elemental Analysis for repeat unit $C_{48}H_{71}GeNO_2S_2$: Calcld: C, 69.19; H, 8.40; N, 1.72; found: C, 69.08; H, 8.56; N, 1.61

CHAPTER 5
KEY ROLE OF END GROUPS IN CONTROLLING MOLECULAR ORDER AND CHARGE TRANSPORT

5.1 Introduction

Chapter 1 to this thesis describes some synthetic methods for controlling the molecular order of conjugated polymers and the resulting effects on their charge transport properties. In this sense, end group functionalization is an efficient method for modifying the physical and electronic properties of these polymers. However, this area of research has not received considerable attention due to the difficulty of end capping reactions for conjugated polymers. P3HT has been fortunate in this regard, as there have been numerous reports of successful end capping reactions with various end groups, particularly by Grignard metathesis (GRIM) involving a chain growth mechanism.[54-57] Different functional groups such as - RCO,[196,197,198] -OH,[199] -RCOOH,[200,201] have been incorporated as end groups. Additionally, Jeffries-El *et al.* have suggested the addition of Grignard reagents of allyl, aryl, benzyl and vinyl to a growing chain of P3HT. [202] The presence of end groups is typically confirmed by MALDI-MS and ^{1}H-NMR techniques. After confirmation, the effects of these end groups on polymer performance in optoelectronic devices can then be evaluated. Chen *et al*. have synthesized hydroxyl end group functionalized P3HT in order to induce H bonding between PCBM and P3HT layers.[199] After annealing, they observe a reduction in the size of PCBM crystals along with smoother surfaces of the P3HT:PCBM film when 5% of P3HT-OH is added. When integrated into solar cell devices, this effect improved the power conversion efficiency to 4.06% from 3.14%. Kim *et al.* have designed P3HT end-functionalized with hydroxyl, ethyl and perfluoro groups. [203] After confirming the presence of these end groups on P3HT with ^{1}H-NMR and MALDI-MS, they combined

these materials with PCBM and integrated the resulting blend into solar cells to analyze the effect of the end groups on the surface energy of P3HT. It was critical that the resulting end-functionalized P3HT surface energy was compatible with PCBM's surface energy in order to reduce phase separation in the P3HT:PCBM blend. P3HT end functionalized with perfluoro groups yielded almost the same surface energy as PCBM, while other end groups afforded higher surface energies. This effect when translated to solar cell PCE's, resulted in 4.5% for P3HT-CF_3, while others showed lower PCE values. Further, the McCullough group studied P3HT end functionalized with two bromine atoms instead of two bare hydrogens. [204] They observed that the bromine groups acted as charge carrier trapping sites, which decreased the OFET mobility and reduced the solar cell performance through exciton quenching. P3HT was also end functionalized with carboxyl groups to adsorb the polymer on TiO_2 in dye sensitized solar cells. [201,196] Besides P3HT, other polymers such as poly(meta-phenylenes) (PMP) obtained by Suzuki polycondensation, have been studied as well.[205] Schluter and coworkers have suggested the slow addition of an AB type monomer onto a monofunctionalized end capping unit, before letting the polymerization proceed via a chain growth mechanism. This method, allowed them to cap both bromo and boron chain ends with independent end groups as confirmed by MALDI-MS measurements.

In the context of donor-acceptor type polymer synthesis, conventional methods such as Suzuki and Stille coupling methods, based on step growth type polycondensations, have been employed. Apart from concerns about the effects on the molecular weight and repeat unit structure, the nature of end groups has widely been overlooked for these kinds of polymers. Hence their effects on molecular structure and

charge transport have not been evaluated thus far. For the incorporation of end groups, methods have been suggested in Chapter 1 in context with methods for controlling the molecular weight via the Carothers equation in step growth type polymers. Following those, there have been few reports on the synthesis and evaluation of the nature of end groups on the donor-acceptor type polymers obtained by these step growth type polymerizations. Leclerc[151] and Andersson[36] have reported the synthesis of carbazole and fluorene based donor-acceptor type polymers end capped with benzene moieties. However, there has been no attempt to confirm the presence of end groups on these polymers. Their end capping procedure involves the sequential addition of monofunctionalized benzene moieties, bromobenzene and phenylboronic acid, after the polymerization. Recently, Bazan and coworkers have reported on the addition of monofunctionalized thiophene moieties following the Stille polycondensation.[109] They employed XPS to confirm the absence of reactive functional groups such as bromine and tin atoms. They claimed that the absence of these groups was indicative of successful end capping reactions. Soon after this report, the Marks group attempted the same end capping procedure and XPS analysis.[110] They argued that the XPS analysis did not show any significant difference between the spectra obtained for the end capped and non-end capped polymers. Consequently, there is still much speculation over the effectiveness of this analysis method.

In this context, we discuss our efforts regarding end capping reactions for dithienogermole-benzothiadiazole based donor-acceptor polymers via a 1% stoichiometric imbalance approach. End capped dithienogermole-benzothiadiazole, E(DTG-BTD), has been functionalized with toluene end groups. Toluene was chosen to

ease the identification of end groups through taking advantage of the characteristic chemical shift of the toluene methyl protons in the ^{1}H-NMR spectrum. A non-end capped polymer with hydrogen end groups, NE(DTG-BTD), was synthesized as well to act as a model. Differences between the end capped and non-end capped polymers' molecular order were evaluated and correlated with the polymers' charge transport properties. Toluene end groups were confirmed by ^{1}H-NMR and MALDI-MS techniques. Additionally, X-ray analyses were conducted, which illustrated the closer π–π stacking distances for E(DTG-BTD). Bottom gate-bottom contact OFETs showed maximum charge carrier mobilities of 0.6 cm^2/V.s. for E(DTG-BTD), which is almost an order of magnitude higher than the value of 0.077 cm^2/V.s. obtained for NE(DTG-BTD).

5.2 Polymer Synthesis and Characterization

Synthesis schemes are outlined in Figure 5-1, and the end capped DTG-BTD copolymer synthesis is described in Chapter 4. The control polymer, NE(DTG-BTD) was synthesized in the same way: through Stille polycondensation of 1% stoichiometric imbalance of distannylated monomer to the dibromo monomer, but omitting the post-polymerization end-capping reaction. After the polymerizations, reactions were cooled to room temperature and precipitated into methanol. Collected solids were washed with methanol, acetone, hexane and chloroform in a Soxhlet extractor. Precipitation again into methanol afforded both polymers in moderate yields of 68-70 % as black solids. The purity of the polymers was analyzed by elemental analysis. Both polymers yielded purity in agreement with the expected amount of C, H and N in the 0.4% theoretical limit, as shown in Table 5-1.

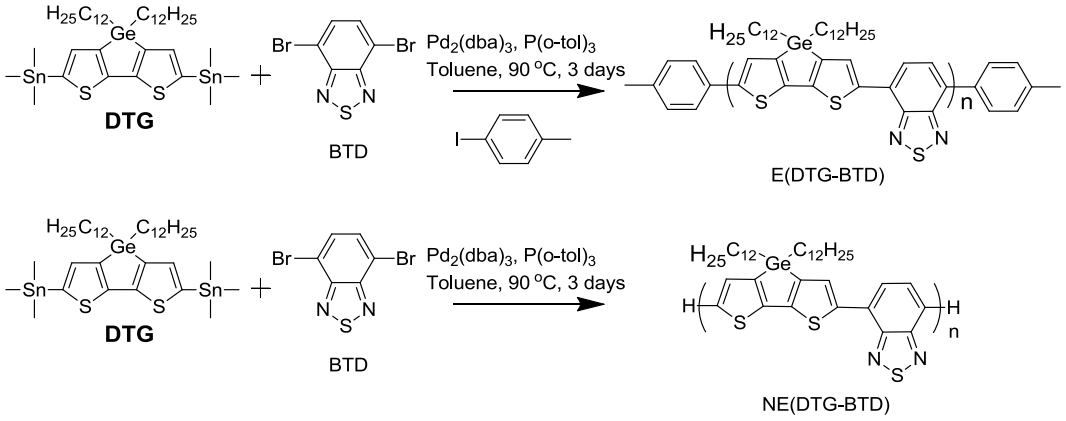

Figure 5-1. Reaction schemes for the synthesis of E(DTG-BTD) and NE(DTG-BTD)

Molecular weights were determined by GPC using two different solvents and temperatures; in THF at 40 ^{o}C and trichlorobenzene (TCB) at 135 ^{o}C, and the results are summarized in Table 5-1. The end capped polymer showed a M_n of 33 kDa with a PDI of 2.43 in THF and a M_n of 12.2 kDa with a PDI of 5.34 in TCB solvents. The non-end capped polymer had a M_n of 28 kDa with a PDI of 2.66 in THF and a M_n of 11 kDa with a PDI of 6.48 in TCB. GPC measurements using TCB as the solvent showed broader molecular weight distributions compared to those using THF as the solvent. The difference of measured molecular weights between the two conditions might have originated from aggregations formed when TCB was used as the solvent for the elution process. Nevertheless, GPC yielded similar molecular weights for both polymers.

Table 5-1. GPC estimated molecular weights in THF and TCB, and elemental analysis of the polymers.

	M_n (kDa) THF	M_w (kDa) THF	PDI	M_n (kDa) TCB	M_w (kDa) TCB	PDI	EA (Calcd/Found) C	H	N
E(DTG-BTD)	33.2	81.0	2.43	12.2	65.1	5.34	64.49/64.64	7.69/8.38	3.96/3.54
NE(DTG-BTD)	28.2	75.0	2.66	11.0	71.5	6.48	64.49/64.16	7.69/8.10	3.96/3.77

Furthermore, the repeat units and the nature of the end groups have been examined by NMR experiments using $C_2D_2Cl_4$ as the solvent at 373 ^{o}K. Both polymers

showed the expected aryl and aliphatic proton chemical shifts, confirming the repeat unit structure. Toluene end groups are characterized by a distinctive chemical shift of the toluene methyl protons near 2.3 ppm in ^{1}H-NMR.The E(DTG-BTD) polymer showed a peak at 2.38 ppm, indicating the presence of toluene methyl protons. This peak was absent in the NE(DTG-BTD) polymer spectrum (as seen in Figure 5-2a). Next, to confirm the presence of toluene molecules as the end groups on the polymer, HSQC and NOESY experiments were carried out. The ^{1}H,^{13}C HSQC 2D NMR spectrum of E(DTG-BTD) displayed a correlation pattern of the proton chemical shift at 2.38 ppm with a carbon chemical shift at 20.6 ppm (Figure 5-2b). This is the characteristic carbon chemical shift for a methyl carbon attached to a benzene molecule. Additionally, through-space correlations between toluene methyl protons and toluene aromatic protons have been analyzed. The ^{1}H, ^{1}H NOESY spectrum displayed a correlation pattern between the 2.38 ppm peak and a peak at 7.22 ppm, which would be expected for benzene aromatic protons. (Figure 5-2c) It is worth noting here that these two correlation patterns were absent in the spectrum of the NE(DTG-BTD) polymer HSQC and NOESY spectra. Furthermore, in the ^{1}H-NMR spectrum of the E(DTG-BTD), the area under the 2.38 ppm peak can be integrated and can be compared to the area under the peak corresponding to methyl protons in the n-dodecyl chain, to estimate the number average molecular weight of the polymer. The integration ratio, and therefore the number of repeat units, was found to be 40. Multiplying the number of repeat units with the repeat unit molecular weight resulted in an M_n of 28 kDa for the E(DTG-BTD) polymer.

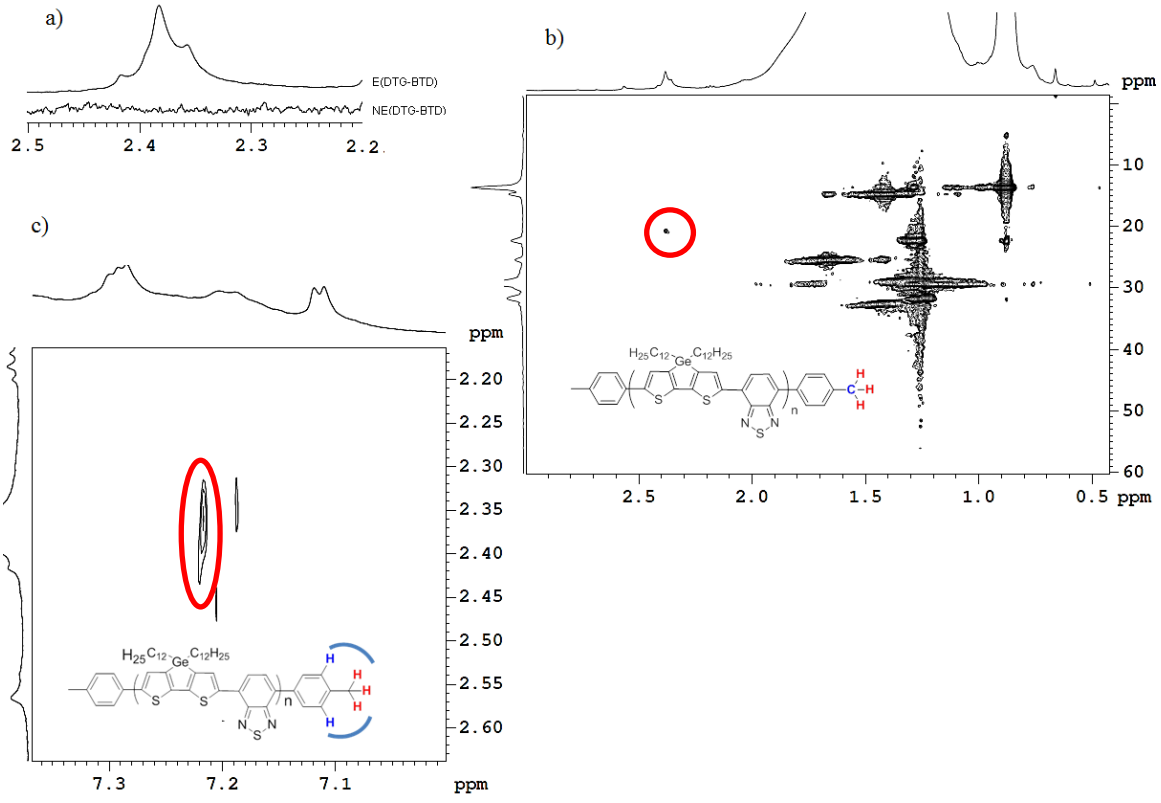

Figure 5-2. NMR characterization of toluene end groups. a) ^{1}H NMR (500 MHz) of E(DTG-BTD) and NE(DTG-BTD) at 373 ^{o}K in $C_2D_2Cl_4$ between 2.2-2.5 ppm. b) ^{1}H-^{13}C 2D HSQC NMR (^{1}H (500 MHz), ^{13}C (125 MHz) of E(DTG-BTD) at 373 ^{o}K in $C_2D_2Cl_4$ c) ^{1}H,^{1}H 2D NOESY (500 MHz) of E(DTG-BTD) at 373 ^{o}K in $C_2D_2Cl_4$

This value is quite close to the number obtained from the GPC analysis in THF as shown in Table 5-1. In this regard, using toluene end groups allows for direct estimation of polymer molecular weights, whereas GPC results need to be calibrated against polystyrene standards. However, it should be taken into account that it is not possible to evaluate the extent of the polymer end capping through these and therefore MALDI-MS data are needed. The MALDI-MS results for E(DTG-BTD) and NE(DTG-BTD) are therefore the focus of the next section. Matrix-assisted laser desorption-ionization time-of-flight (MALDI-TOF) mass spectroscopy was conducted to examine the

repeat units and end groups on the polymers. (Figure 5-3) Firstly, MALDI-TOF mass spectra displayed peaks corresponding to the expected oligomers in the range of n=4 to n=8, while higher molecular weight species were too heavy to be desorbed from the matrix. The oligomer peaks were separated by 708 amu, consistent with the expected mass of the DTG-BTD repeat unit. In Figure 5-3b and Figure 5-3d, expanded regions of the mass spectrum of each polymer are displayed between *m/z* 2700 and *m/z* 3700 in order to evaluate the residual masses of oligomers and to identify the end groups. Polymer structures are represented by illustrations over each peak in the MALDI spectrum. For the polymer E(DTG-BTD), the three largest peaks in the region of n=4 have been assigned as seen in Figure 5-3b. The peak at *m/z* 2830 is consistent with the tetramer with two hydrogen end groups. The highest intensity peak at *m/z* 2922 is due to the tetramer with one toluene and one hydrogen end group. The peak at *m/z* 2966 is attributed to the tetramer with an additional BTD unit end capped with hydrogen. Careful observations reveal the complex nature of the step growth polymerization. Previously, Schluter and Janssen groups performed detailed end groups analysis for Suzuki polycondensation polymers in which they observe neither bromo nor boron end groups.[205,206] According to their suggestions, these groups might have been lost during the Suzuki polymerization by various reasons including cyclization, ligand scrambling, dehalogenation and hydrolytic deboronation. Loss of functional groups such as halogen and tin atoms is also observed for Stille couplings by dehalogenation and destannylation.[207] In this context, possible competing side reactions result in the loss of functional groups as depicted in Figure 5-4. A scenario is illustrated in which a starting AB type oligomer, such as compound 1 in Figure 5-4, can be assumed. It undergoes

successful end capping, forming compound 2, and further monomer addition results in longer polymer chains. Compound 1 can lose a bromine atom to yield compound 4, and then can follow three paths: it can form a dead chain by destannylation (compound 5), undergo another end capping reaction forming compound 6, or through continued addition of the BTD monomer, the polymer chain can grow longer. The oligomer residues at 2830, 2922 and 2966 m/z can be explained by side reactions leading to toluene and hydrogen end groups. Additionally, hydrogen end groups prevent further monomer addition, explaining why toluene end capping is only ever observed at one end of the polymer. Further, the pentamer peak has been assigned at *m/z* 3540 and three other peaks can be observed near it. The peak at *m/z* 3632 is assigned to a pentamer end-capped with a toluene moiety. This is expected as the polymerization has been run for 1% in stoichiometric imbalance of the DTG ditin monomer. The peak at *m/z* 3496 represents a tetramer with an extra DTG unit, end capped with toluene. Consistently, these oligomer residues undergo the aforementioned side reactions causing the loss of functional groups during the reaction. Side reactions are also observed in the mass spectrum of NE(DTG-BTD) polymer. As seen in the expanded mass spectrum in Figure 5-3d, the peaks represent only oligomers end capped with hydrogens. As no end capping reaction was performed for this polymer, it can be said that debromination is active during the polymerization. On the other hand, the oligomers with and additional DTG molecule end capped with hydrogen can indicate the loss of tin groups during the polymerization by destannylation, or after the polymerization during precipitations into methanol.

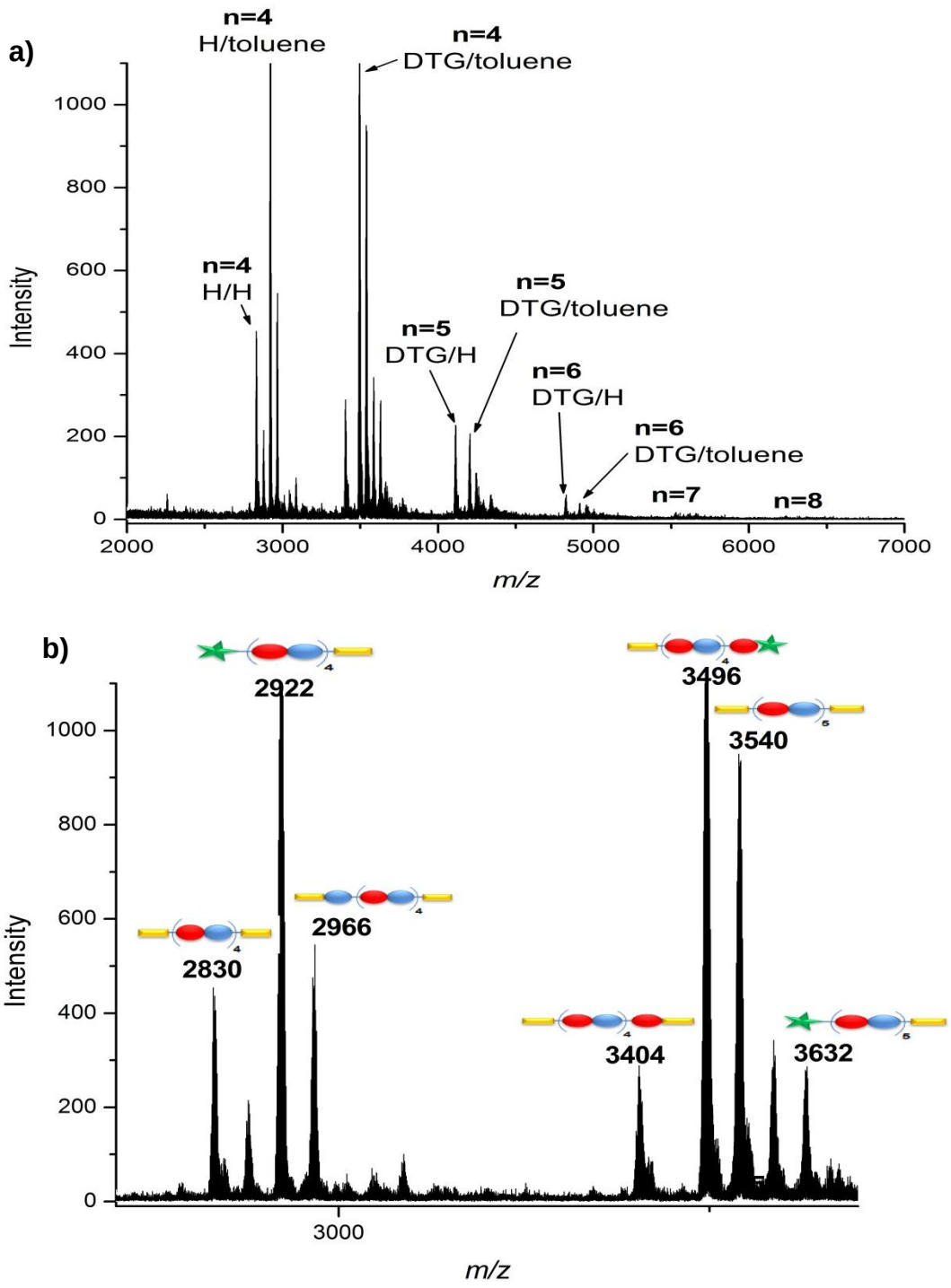

Figure 5-3. MALDI-MS spectra of polymers. a) E(DTG-BTD), b) Expanded region between 2700-3700 m/z for E(DTG-BTD), c) NE(DTG-BTD) and d) expanded region between 2700-3700 m/z for NE(DTG-BTD). The assigned oligomer residues are highlighted by representative cartoons in the legend.

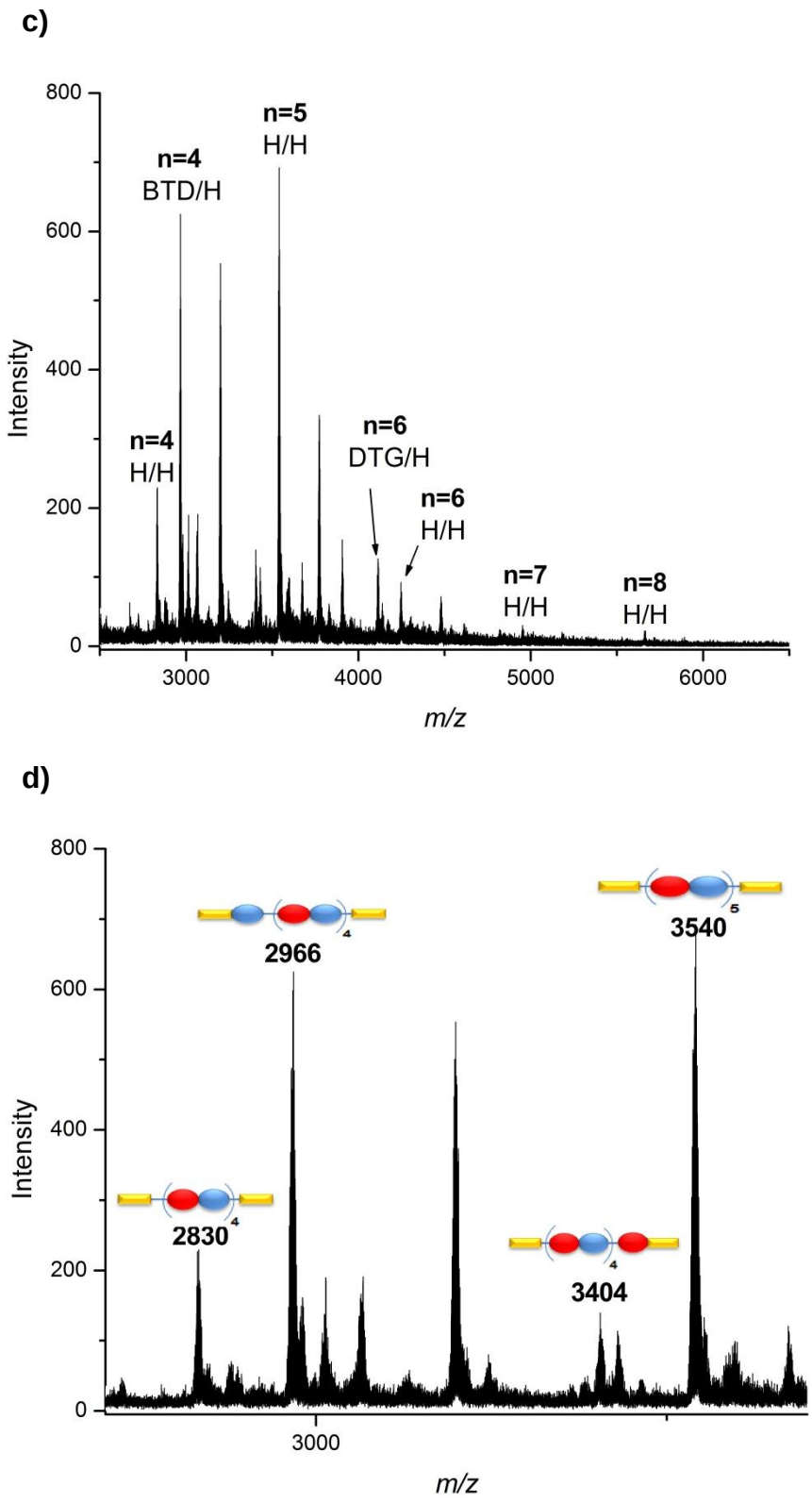

Figure 5-3. continued.

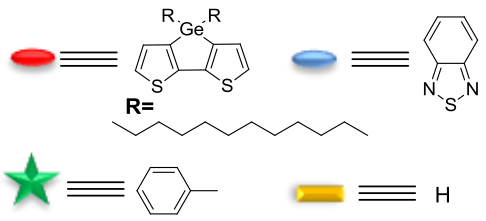

Figure 5-3. continued.

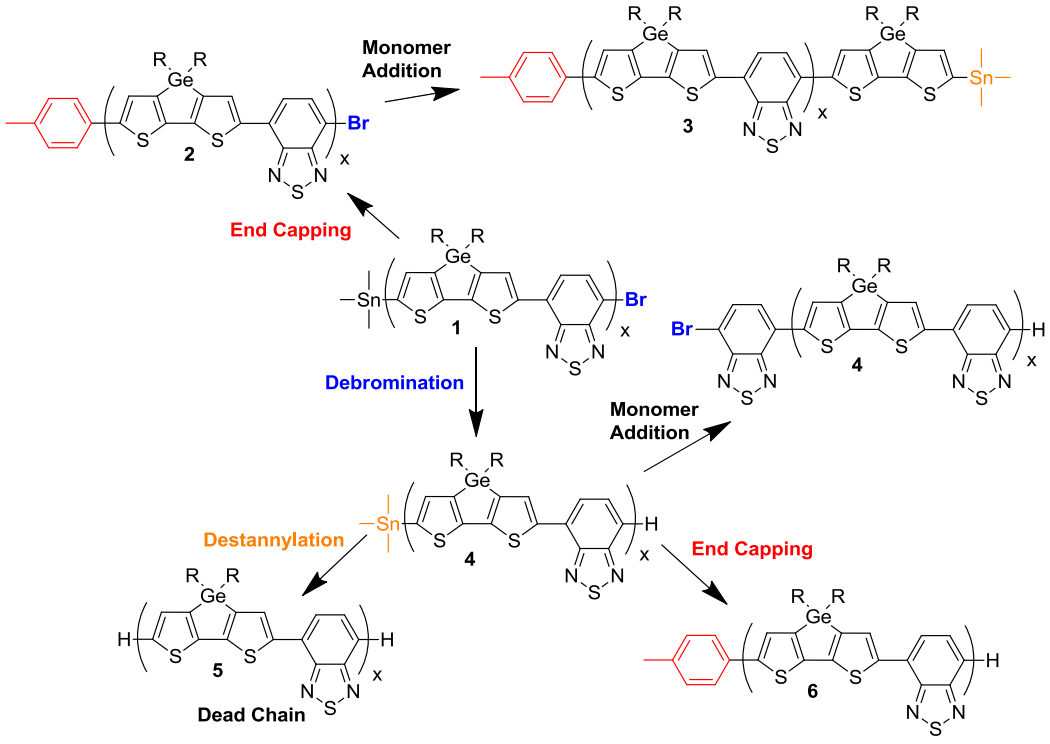

Figure 5-4. Possible scenario showing the loss mechanisms of debromination and destannylation resulting in hydrogen end capped oligomers and successful end cappings with toluene units.

In addition, we investigated the presence of atoms in the repeat unit structure as well as the residual bromine and tin atoms contained in the polymers through XPS analyses. Figure 5-5 shows XPS spectra for the spin cast films of E(DTG-BTD) and NE(DTG-BTD) using a Mg anode as the X-ray source. Both polymers exhibited the orbital energies of atoms such as Ge, N, C, and S present in the composition of the repeat unit. Also, an Al anode was used as an X-ray source for XPS analysis of NE(DTG-BTD), but no significant changes--except the disappearance of high energy

peaks due to Ge auger electrons—were observed. Furthermore, we investigated the presence of Br and Sn atoms in the polymers. The expected Br 3d and Sn $3d_{5/2}$ orbital energies are highlighted by blue and red arrows respectively in Figure 5-5.

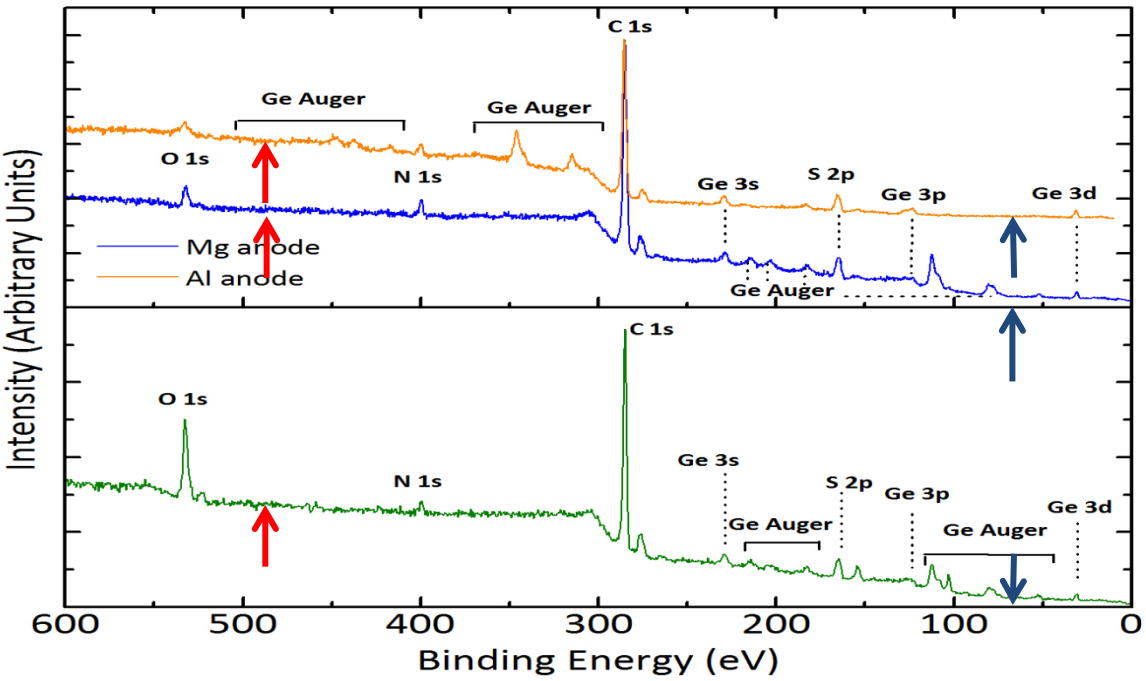

Figure 5-5. XPS spectra of NE(DTG-BTD) with two different X-ray sources of Mg and Al and E(DTG-BTD) with Mg source. The expected Br 3d and Sn $3d^{5/2}$ orbital energies are highlighted as blue and red arrows respectively.

No peak was observed due to the presence of Br or Sn atoms. In general, we found no substantial differences between the spectra of the polymers, and therefore conclude that XPS is not a valuable tool to assess the absence of Sn and Br atoms in these polymers. We performed inductively coupled plasma (ICP) analyses to quantify the amount of Sn residues present in the polymers. This measurement was done in the Geology Department of UF by Dr. George Kamenov. E(DTG-BTD) was found to contain 1979 ppm (0.20 % by weight) Sn 122 isotopes, while NE(DTG-BTD) contained only 1583 ppm (0.16% by weight). The Sn content is comparable in both polymers, therefore

it can be speculated that residual tin atoms are either buried inside the polymer network or they are still bonded to DTG units.

UV-VIS spectroscopy and DPV electrochemical characterization methods were also used to examine the structural differences between E(DTG-BTD) and NE(DTG-BTD). Figure 5-6 shows the absorption profiles of the polymers in dilute toluene solutions and in thin films. Solution absorption spectrum for NE(DTG-BTD) demonstrates dual band absorption maximums at 420 nm and 684 nm, with a trough at 422 nm tailing off to 890 nm. The solution absorption spectrum for E(DTG-BTD) presents with a similar dual absorption profile, but with an additional shoulder around 800 nm due to aggregation. In thin film absorption spectra, both polymers preserve their aforementioned dual band absorption profiles. For E(DTG-BTD) there is a 15 nm red shift in the low energy band maximum as well as a shoulder around 775 nm, which is more pronounced in the thin film spectrum than it was previously in the solution spectrum. This red shifted shoulder is attributed to a vibronic aggregation band indicative of more ordered planar chains.[208,115]

For the electrochemical characterization of the polymers, differential pulse voltammetry has been conducted and the voltammograms are shown in Figure 5-7. Both polymers demonstrate reduction around -1.5 V and oxidation around 0.25 V. The reduction potential onsets were -1.41 V for both polymers. As both polymers contain the BTD acceptor unit, their reduction potentials are at the same level. However, the end capped polymer has an onset of oxidation at 0.18 V whereas the non-end capped polymer has a slightly higher oxidation onset at 0.22 V.

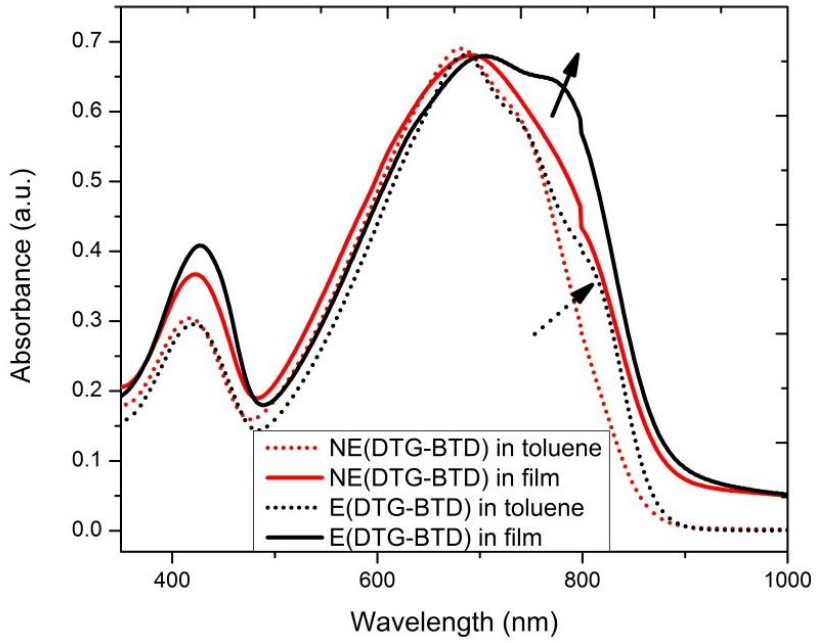

Figure 5-6. Absorption spectra for dilute solutions of E(DTG-BTD) and NE(DTG-BTD) in toluene and for thin film. Arrows highlight the aggregation bands.

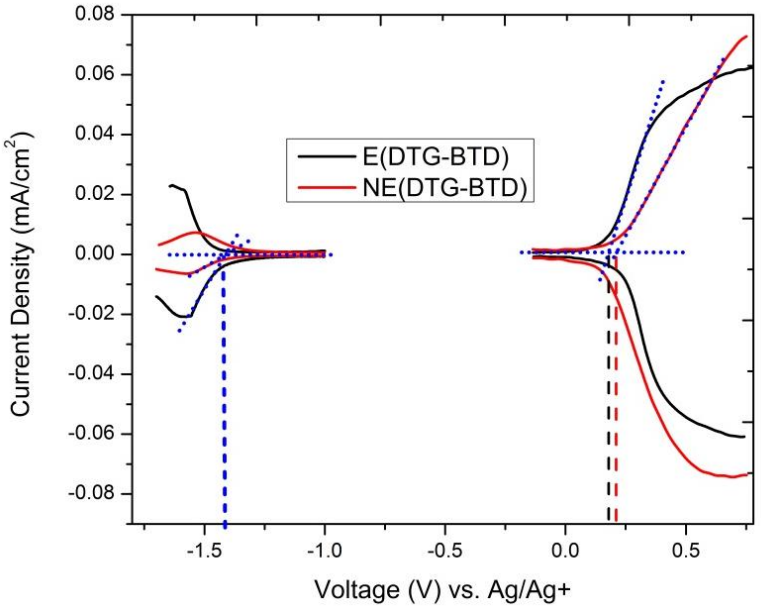

Figure 5-7. Differential Pulse Voltammograms of E(DTG-BTD) (black, solid line) and NE(DTG-BTD) (red, solid line) recorded in 0.1 M $TBAPF_6$/PC electrolyte solution with a scan rate of 50 mV/s vs. Ag/Ag^+ reference electrode.

5.3 OFET Performances

Charge transport measurements were performed through the fabrication and testing of OFET devices based on E(DTG-BTD) and NE(DTG-BTD). OFET devices were built in the bottom contact-bottom gate architecture where the polymer was deposited onto an HMDS surface functionalized substrate, Si/SiO_2. The polymers were deposited using two different methods: drop casting from a 2 mg/mL dichlorobenzene solution, and spin coating from a 10 mg/mL chloroform solution. Then, the samples were annealed at 200 ^oC for 60 minutes. The annealing temperature was chosen as it provided the highest hole mobility, as determined through optimization experiments conducted by Dr. S. Reddy Puniredd. As a note, no thermal decomposition occurs at this temperature, whereas 2% weight loss is observed at 350 ^oC as revealed by TGA measurements. Two different processing methods were used to confirm that charge transport property differences originated from the variations in the chemical structures of the polymers and were not consequences of the processing method. The results of the charge transport behaviors are shown in Figure 5-8 and summarized in Table 5-2. The OFET transfer plots show that holes are the dominant charge carriers in both polymers for both processing methods.

Table 5-2 summarizes the mobility values for the charge carriers. Firstly, it is observed that drop casted samples generate higher mobilities for both polymers compared to spin cast samples. This effect is due to the fact that while drop casting from a low volatile solvent, the polymer has more time for self-assembly. Spin casting results in uniform films; however the polymer has less time to self- assemble itself due to fast evaporation of the volatile solvent.

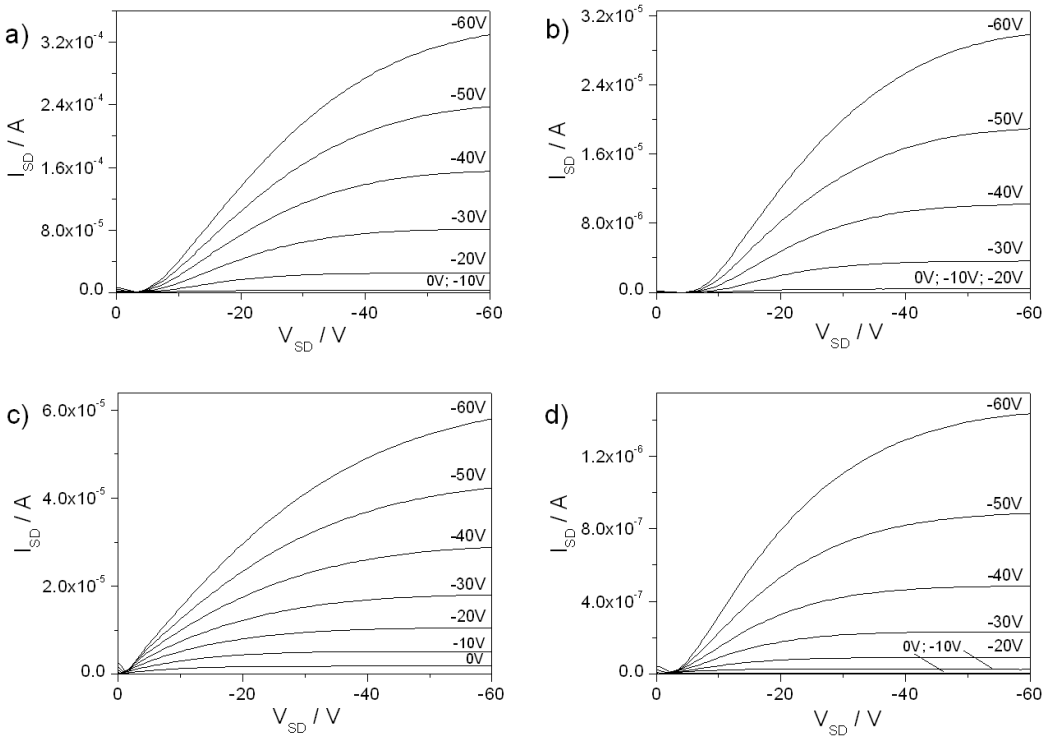

Figure 5-8. Transistor output curves for drop-cast and spin-coated a) and c) E(DTG-BTD), b) and d) NE(DTG-BTD) thin films.

Hence, more than an order of magnitude difference is observed between the observed mobilities for E(DTG-BTD) (0.6 cm^2/V.s. for drop casting *vs.* 0.05 cm^2/V.s. for spin casting) when using the two methods, and an even more pronounced difference is seen for NE(DTG-BTD) (0.07 cm^2/V.s. for drop casting *vs*. 0.002 cm^2/V.s. for spin casting). Next, charge mobilities were compared for E(DTG-BTD) and NE(DTG-BTD). For the drop cast samples, the difference is again almost an order of magnitude higher for E(DTG-BTD) (0.6cm^2/V.s) when compared to the mobilities obtained for NE(DTG-BTD) (0.07 cm^2/V.s.) and a 20 fold increase for E(DTG-BTD) (0.05 cm^2/V.s.) compared to NE(BTG-DTG) (0.002 cm^2/V.s) in the spin cast samples.

Table 5-2. Summary of hole mobilities for E(DTG-BTD) and NE(DTG-BTD) processed from drop casting and spin casting.

	Hole Mobility (cm^2/V.s.)& (on/off ratio)	
	Drop cast	Spin cast
E(DTG-BTD)	0.55 ± 0.05 (9×10^5)	0.043 ± 0.013 (7×10^4)
NE(DTG-BTD)	0.061 ± 0.016 (2×10^5)	0.002 ± 0.0005 (1×10^4)

5.4 X-ray and Morphology Analyses

In order to examine the difference in charge carrier mobilities, the molecular order and surface morphology were investigated using grazing incidence wide-angle X-ray scattering (GIWAXS) and atomic force microscopy (AFM) techniques. As seen in Figure 5-9, the GIWAXS patterns show significant variations in molecular order between E(DTG-BTD) and NE(DTG-BTD) for both spin cast and drop cast samples. In the drop cast film of E(DTG-BTD) a small number of relative isotropic reflections appear in the q_{xy} direction due to the ordered polymer backbones in lamellar structures though the crystalline domains remain randomly oriented with respect to each other and the surface. As no spots or arcs are observed in the q_z direction no long-range alignment appears to be present in the polymer. This is due to the effect of the drop-casting method, which allows for random nucleation and self-assembly processes to occur during crystallization. The schematic organization of the polymer chains is depicted as a cartoon in the inset of Figure 5-9a. π–π stacking distances have been calculated by meridional integration along q_z at $q_{x,y} = 0$ directions to be 0.355 nm for E(DTG-BTD) (Figure 5-10a). For the drop cast NE(DTG-BTD) thin film, no reflections in the q_z and q_{xy} direction were observed indicating low interchain order. This low molecular order can be attributed to poor interactions between conjugated backbones (Figure 5-9b). It is worth noting here that a typical amorphous halo is present in the meridional integration

of the pattern due to the flexible alkyl side chains. Nevertheless, NE(DTG-BTD) polymer chains form lamellar stacks as confirmed by the very weak small-angle scattering intensities indicative of highly disordered polymer chains as is illustrated in the inset of Figure 5-9b. These observations of the drop cast films explain the dramatic decrease in the charge carrier mobility for the NE(DTG-BTD) samples. In the spin cast film, X-ray patterns obtained from both polymers show an evident reflection on the q_z direction, along with a weak arc in the q_{xy}.

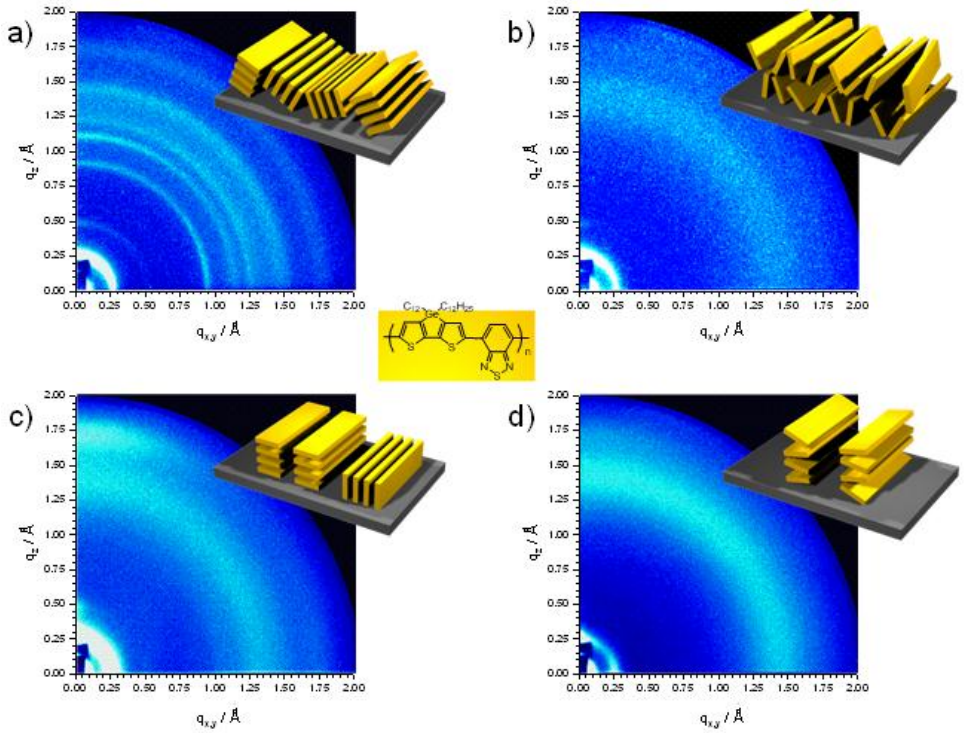

Figure 5-9. GIWAXS characterization of E(DTG-BTD) and NE(DTG-BTD) a) and c) patterns of drop-cast and spin-coated E(DTG-BTD), b)and d) patterns of drop-cast and spin-coated NE(DTG-BTD). Insets schematically illustrate the surface organization of the polymers.

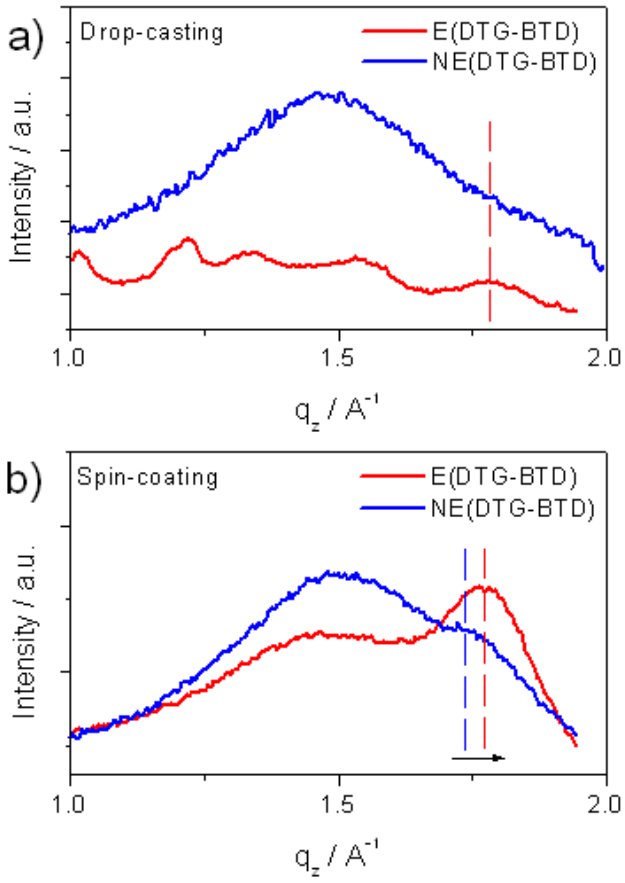

Figure 5-10. GIWAXS integrations of the wide-angle scattering region along qz at qx,y = 0 for E(DTG-BTD) and NE(DTG-BTD) a) after drop-casting and b) spin-coating. The dashed lines mark the position of the π-stacking peak maximum for E(DTG-BTD) (red) and NE(DTG-BTD) (blue). The arrow in b) indicates the shift of the □-stacking distance from 0.360 nm for NE(DTG-BTD) to 0.355 nm for E(DTG-BTD).

However, for E(DTG-BTD) the reflection in the q_z direction is higher in intensity and less diffuse. This reflection results in a π–π stacking distance of 0.355 nm for the E(DTG-BTD) polymer chains preferentially arranged face-on (out of plane) on the substrate.(Figure 5-9c). The very weak scattering intensities in the equatorial plane of the pattern are indicative of a small portion of polymer chains stacking edge-on (in plane) on the substrate. Integration of this reflection results in π–π stacking distance of 0.360 nm for NE(DTG-BTD) which means that there are less interactions between

polymer chains than in the E(DTG-BTD) films. In the spin cast NE(DTG-BTD) film, the aforementioned q_z reflection is more diffuse and weaker in intensity as shown in Figure 5-9d. While the polymer arranges face-on on the substrate the molecular order is much lower compared to E(DTG-BTD). Special thanks should be given to Dr. Wojtek Pisula and Dr. S. Reddy Puniredd for X-ray discussions and GIWAXS data analysis.

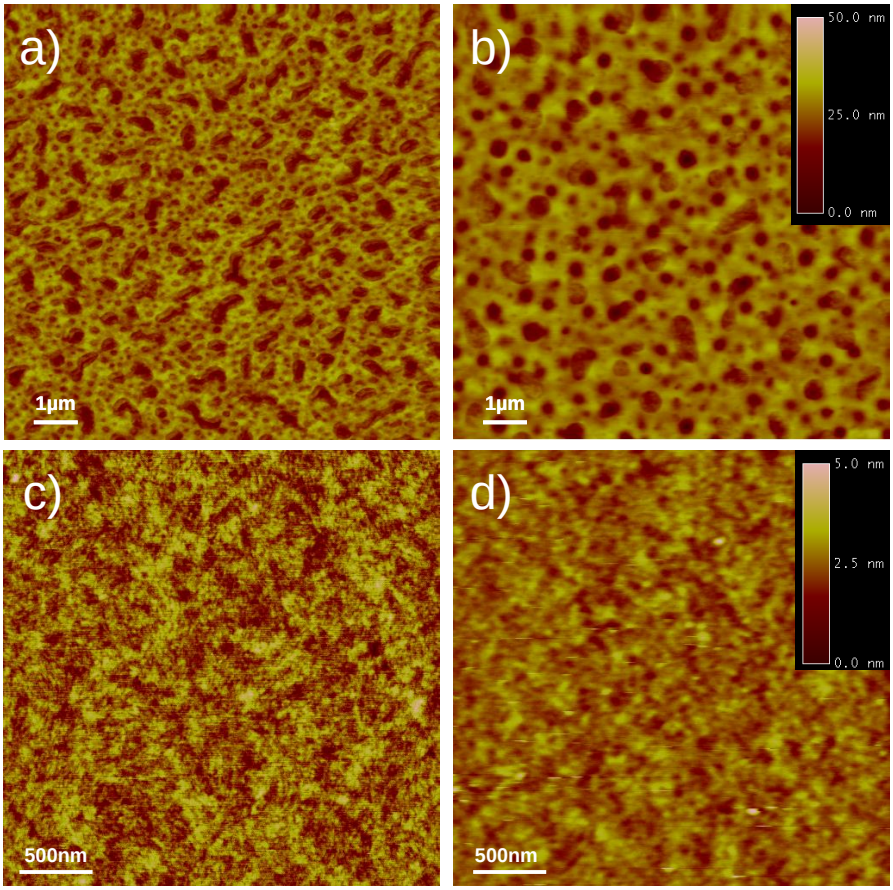

Figure 5-11. Tapping mode AFM height images of drop-cast and spin-coated a) and c) E(DTG-BTD), b) and d) NE(DTG-BTD). Height scale is identical for each processing methods.

Additionally, AFM analyses have been carried out to examine the film microstructure and topography and AFM topographs are shown in Figure 5-11. At first glance, the drop cast E(DTG-BTD) and NE(DTG-BTD) films' topographs show almost identical layered networks. Upon closer inspection, the E(DTG-BTD) microstructure

exhibits a dense, finely structured network whereas this network is much coarser for NE(DTG-BTD). This provides a clue to the origin of the observed improvements in hole mobility. The E(DTG-BTD) polymer, with denser and finer network, can enable for more charge percolation pathways for charge transport. For the spin coated films, E(DTGBTD) exhibits fine, short interconnected fibers, whereas the NE(DTG-BTD) film surface shows a globular topography of small spheres. These results complement the observations obtained from the GIWAXS analyses. E(DTG-BTD) showed more ordered polymer chains with closer interchain interactions for both processing conditions in the GIWAXS analyses. This results in a well interconnected fibrous microstructure via improved self- assembly of the polymer chains, while reduced interchain interactions in NE(DTG-BTD) lead to isotropic globular entities.

5.5 Conclusions and Perspectives

Conjugated polymers are ideal for high performance OFET applications because their charge transport properties can be enhanced through both chemical design and, unlike their inorganic counterparts, through solution processing techniques. Chapter 5 described a method for controlling the molecular order in conjugated polymers, in which toluene end groups were placed after a Stille polycondensation with 1% excess of ditin monomer. Characteristic chemical shifts of methyl protons and carbon on the toluene moiety allowed for the simple identification of these end groups with NMR. This is the first report in the literature that confirms the presence of end groups on donor-acceptor type polymers. Further, we showed the confirmation of toluene end groups with MALDI-MS. The charge transport properties of the end capped DTG-BTD polymers were found to be superior to the properties of its non-end capped analogue. We attribute these

results to the enhanced interchain interactions and higher polymer ordering in thin films, as evidenced by GIWAXS analyses. This is also the first time observation of the effects of end groups on the molecular order of conjugated polymers. We speculate that toluene end groups can bind together the aggregates in the thin film, increasing the connectivity between crystallites. This enables more pathways for charge percolation leading to high charge carrier mobilites.

5.6 Experimental Details

Poly[DONOR-alt-ACCEPTOR)] A 100 mL flame dried Schlenk flask was charged with carefully weighed DONOR (1.01 eq), ACCEPTOR (1 eq), $Pd_2(dba)_3$ (4% eq.) and $P(o\text{-}tol)_3$ (8 % eq.). The mixture was cycled with argon and vacuum three times. After addition of degassed toluene (20 mL), the reaction was heated to 90 ^{o}C for 3 days. This was followed by the addition of 4-iodotoluene (in excess) and the reaction was allowed to run for another 20 hours. The reaction was cooled to room temperature and precipitated into methanol (500 mL). The precipitates were collected in a thimble and the polymer was washed with Soxhlet extraction using methanol, acetone, hexane and chloroform. The chloroform fraction was concentrated to 50 mL and diethylammoniumdiethyldithiocarbamate was added. After stirring for 2 hours under argon, the polymer was precipitated again into methanol (350 mL). The mixture was filtered over a 0.45µm size polypropylene membrane and the solid was dried under vacuum for 2 days to afford the title polymer.

Poly5-5'(4,4-didodecyl-4H-germolo[3,2-b:4,5-b']dithiophene)alt-4,7-(benzo[c][1,2,5]thiadiazole) E(DTG-BTD) The polymer was obtained as 0.240 g (68 %) of a black solid. ^{1}H NMR (500 MHz, $C_2D_2Cl_4$): *δ:* 8.40-7.70 (m, 4H), 2.20-0.60 (m, 50H) Mn= 33,214 g/mol, Mw= 81,013 g/mol, PDI: 2.43 Elemental Analysis for repeat

unit $C_{38}H_{54}GeN_2S_3$: Calcld: C, 64.49; H, 7.69; Ge, 10.26; N, 3.96; S, 13.59 found: C, 64.64; H, 8.38; N, 3.54 Td= 500 ^oC (55 % weight loss), 350 ^oC (2% weight loss)

Poly5-5'(4,4-didodecyl-4H-germolo[3,2-b:4,5-b']dithiophene)*alt*-4,7-(benzo[c][1,2,5]thiadiazole) NE(DTG-BTD) The end capping step in the above protocol has been skipped, but all other processes remained the same. The polymer was obtained as a black solid of 0.247 g. (70 %) ^1H NMR (500 MHz, $C_2D_2Cl_4$): *δ:* 8.40-7.70 (m, 4H), 2.20-0.60 (m, 50H) Mn= 28,150 g/mol, Mw= 74,959 g/mol, PDI: 2.66 Elemental Analysis for repeat unit $C_{38}H_{54}GeN_2S_3$: Calcld: C, 64.49; H, 7.69; Ge, 10.26; N, 3.96; S, 13.59 found: C, 64.16; H, 8.10; N, 3.77

CHAPTER 6
CONCLUSIONS AND PERSPECTIVES

This thesis has focused on controlling molecular organization in conjugated polymers. Polymer chains, with strong intermolecular interactions through delocalized π orbitals, are important for efficient charge transport in high performance organic field effect transistors. Synthetic organic chemistry tools, such as the incorporation of heavy atoms in the repeat unit structure of polymers and addition of proper end capping units to polymer chains, have been introduced in pursuit of higher molecular order and improved charge transport properties in conjugated polymers. Chapter 4 and Chapter 5 describe the structure-property relationships in dithienogermole (DTG) based polymers. In Chapter 4, the synthesis of six DTG and dithienosilole (DTS) based donor-acceptor polymers was carried out using Stille polycondensations with 1% stoichiometric imbalance. Specifically, we diverged from the common stoichiometric balance method for controlling the nature of end groups. DTG based polymers have been targeted due to their long C-Ge bond lengths, which can push solubilizing alkyl chains away from the aromatic units of the polymers. We observed this interaction to study its effect on optical, electronic and physical properties of the DTG polymers, and drew comparisons to properties obtained for DTS based polymers. In general, DTG polymers showed longer wavelength absorptions in the visible spectrum, as well as higher HOMO and lower LUMO energy levels, resulting in lower band gaps. The longer C-Ge bond in DTG was effective in improving intermolecular interactions by pushing the long dodecyl side chains away from the polymers' aromatic units. Closer π interactions allowed efficient charge transport for dithienogermole-benzothiadiazole copolymers, resulting in hole mobilities of 0.6 $cm^2/V.s$ However, DTG based polymers showed poor performances in

solar cell devices. This demonstrates that not all highly ordered materials are well suited for photovoltaic applications, which rely heavily on the morphology of the polymer and fullerene blend.

Chapter 5 demonstrated the successful end capping of dithienogermole-benzothiadiazole copolymer with toluene end groups, as confirmed by ^{1}H NMR and MALDI-MS. The toluene end groups were effective in directing improved stacking of the polymer chains, as shown by UV thin film measurements. The X-ray analyses showed improved molecular organization in an end capped polymer compared to its non-end capped analogue, which led to higher charge transport independent of the processing conditions. These observations are the first examples of studies investigating molecular order as it relates to charge transport properties in end capped donor-acceptor type polymers. Further insight in this research can be suggested in this field of research. Benzene molecules functionalized with methyl ethoxy- ethoxy (MEE) groups in the para position can be substituted instead of toluene end groups. As these MEE side chains can move freely, their molecular ordering is expected to be lower than the toluene functionalized polymers discussed in this thesis. The observation of this effect would support our results by confirming end capping as influential in controlling molecular order. Furthermore, chain growth type polymerizations can be employed for facile incorporation of end groups. The chain growth pathway would also allow the choice of various end group moieties, such as naphthalene and anthracene that are capable of π stacking. This path will also be a useful tool in confirming our speculation that end groups can join together the polymer chain ends.

Chapter 3 discussed the importance of strict synthetic protocols for generating scalable, high quality PGreen polymers. Also, changing the polymer synthesis method from oxidative polymerization to Stille coupling resulted in increased solar cell efficiencies. Additionally, Chapter 3 demonstrated the preparation of a large scale aesthetically pleasing solar cell panels that can achieve a 7.6 Volt output on a sunny Florida day. Discrepancies between the small spin coated and large slot die coated solar cell performances have been investigated and left questions of how to decrease the series resistance by employing materials that have high charge transport properties. Lastly, an alternating polyfluorene copolymer has been synthesized that displays electrochromic, electroluminescent and photovoltaic activity. The lack of absorption in the red and blue regions resulted in a purple colored instead of green colored material.

In conclusion, organic chemistry is and will be at the center of preparing future large area polymer solar cells with power conversion efficiencies exceeding 10% and in the fabrication of organic field effect transistors with >10 cm^2/V.s hole mobilities. In the near future, high performing conjugated polymers will surround the most practical personal and commercial electronic appliances, such as smart windows, sophisticated textiles, clean energy sources and transparent laptops. The field will be driven by advancements in conjugated polymers due to their facile processing with low cost equipment.

LIST OF REFERENCES

1. Fu, H. S.; Cheng, Y. M.; Chou, P. T.; Chi, Y., *Materials Today* **2011,** 14, (10), 472-479.

2. Kondo, Y.; Tanabe, H.; Kudo, H.; Nakano, K.; Otake, T., *Materials* **2011,** 4, (12).

3. Schmidtke, J., *Optics Express* **2010,** 18, (19), A477-A486.

4. Hoffmann, R., *Angewandte Chemie-International Edition in English* **1987,** 26, (9).

5. Whangbo, M. H.; Hoffmann, R.; Woodward, R. B., Pro*ceedings of the Royal Society of London Series a-Mathematical Physical and Engineering Sciences* **1979,** 366, (1724).

6. Roncali, J., *Macromolecular Rapid Communications* **2007,** 28, (17).

7. Walczak, R. M.; Cowart, J. S., Jr.; Reynolds, J. R., *Journal of Materials Chemistry* **2007,** 17, (3).

8. Ko, S.; Mondal, R.; Risko, C.; Lee, J. K.; Hong, S.; McGehee, M. D.; Bredas, J.-L.; Bao, Z., *Macromolecules* **2010,** 43, (16).

9. Beaujuge, P. M.; Vasilyeva, S. V.; Ellinger, S.; McCarley, T. D.; Reynolds, J. R., *Macromolecules* **2009,** 42, (11).

10. Lu, K.; Sun, X.; Liu, T.; Di, C.; Xi, H.; Yu, G.; Gao, X.; Du, C., *J Polym. Sci.Part A: Polym. Sci.* **2009,** 47.

11. Groenendaal, B. L.; Jonas, F.; Freitag, D.; Pielartzik, H.; Reynolds, J. R., *Advanced Materials* **2000,** 12, (7), 481-494.

12. Lambert, T. L.; Ferraris, J. P., *Journal of the Chemical Society-Chemical Communications* **1991**, (11).

13. Thompson, B. C.; Kim, Y. G.; McCarley, T. D.; Reynolds, J. R., *Journal of the American Chemical Society* **2006,** 128, (39), 12714-12725.

14. Perepichka, I. F.; Levillain, E.; Roncali, J., *Journal of Materials Chemistry* **2004,** 14, (11).

15. Roncali, J.; Garreau, R.; Yassar, A.; Marque, P.; Garnier, F.; Lemaire, M., *Journal of Physical Chemistry* **1987,** 91, (27).

16. Wudl, F.; Kobayashi, M.; Heeger, A. J., *Journal of Organic Chemistry* **1984,** 49, (18).

17. Hong, S. Y.; Marynick, D. S., *Macromolecules* **1992,** 25, (18).

18. Sotzing, G. A.; Lee, K. H., *Macromolecules* **2002,** 35, (19).

19. Havinga, E. E.; Tenhoeve, W.; Wynberg, H., *Polymer Bulletin* **1992,** 29, (1-2).

20. Steckler, T. T.; Zhang, X.; Hwang, J.; Honeyager, R.; Ohira, S.; Zhang, X.-H.; Grant, A.; Ellinger, S.; Odom, S. A.; Sweat, D.; Tanner, D. B.; Rinzler, A. G.; Barlow, S.; Bredas, J.-L.; Kippelen, B.; Marder, S. R.; Reynolds, J. R., *Journal of the American Chemical Society* **2009,** 131, (8).

21. Kono, T.; Kumaki, D.; Nishida, J.-i.; Sakanoue, T.; Kakita, M.; Tada, H.; Tokito, S.; Yamashita, Y., *Chemistry of Materials* **2007,** 19, (6).

22. Ponce Ortiz, R.; Facchetti, A.; Marks, T. J.; Casado, J.; Zgierski, M. Z.; Kozaki, M.; Hernández, V.; LópezNavarrete, J. T., *Adv. Funct. Mater* **2009**, (19).

23. Dhanabalan, A.; van Dongen, J. L. J.; van Duren, J. K. J.; Janssen, H. M.; van Hal, P. A.; Janssen, R. A. J., *Macromolecules* **2001,** 34, (8).

24. Blouin, N.; Michaud, A.; Gendron, D.; Wakim, S.; Blair, E.; Neagu-Plesu, R.; Belletete, M.; Durocher, G.; Tao, Y.; Leclerc, M., *Journal of the American Chemical Society* **2008,** 130, (2).

25. Zhou, E.; Yamakawa, S.; Tajima, K.; Yang, C.; Hashimoto, K., *Chemistry of Materials* **2009,** 21, (17).

26. Chen, H.-Y.; Hou, J.; Hayden, A. E.; Yang, H.; Houk, K. N.; Yang, Y., *Advanced Materials* **2010,** 22, (3).

27. Beaujuge, P. M.; Reynolds, J. R., *Chemical Reviews* **2010,** 110, (1).

28. Groenendaal, L.; Zotti, G.; Aubert, P. H.; Waybright, S. M.; Reynolds, J. R., *Advanced Materials* **2003,** 15, (11).

29. Beaupre, S.; Boudreault, P.-L. T.; Leclerc, M., *Advanced Materials* **2010,** 22, (8).

30. Admassie, S.; Inganas, O.; Mammo, W.; Perzon, E.; Andersson, M. R., *Synthetic Metals* **2006,** 156, (7-8).

31. Dyer, A. L.; Thompson, E. J.; Reynolds, J. R., *Acs Applied Materials & Interfaces* **2011,** 3, (6).

32. Amb, C. M.; Kerszulis, J. A.; Thompson, E. J.; Dyer, A. L.; Reynolds, J. R., *Polymer Chemistry* **2011,** 2, (4).

33. Shi, P.; Amb, C. M.; Knott, E. P.; Thompson, E. J.; Liu, D. Y.; Mei, J.; Dyer, A. L.; Reynolds, J. R., *Advanced Materials* **2010,** 22, (44).

34. Muehlbacher, D.; Scharber, M.; Morana, M.; Zhu, Z.; Waller, D.; Gaudiana, R.; Brabec, C., *Advanced Materials* **2006,** 18, (21).

35. Lu, G.; Usta, H.; Risko, C.; Wang, L.; Facchetti, A.; Ratner, M. A.; Marks, T. J., *Journal of the American Chemical Society* **2008,** 130, (24).

36. Inganas, O.; Zhang, F. L.; Andersson, M. R., *Accounts of Chemical Research* **2009,** 42, (11), 1731-1739.

37. Beaujuge, P. M.; Amb, C. M.; Reynolds, J. R., *Accounts of Chemical Research* **2010,** 43, (11).

38. Wang, C.; Dong, H.; Hu, W.; Liu, Y.; Zhu, D.,. *Chemical Reviews* **2012,** 112, (4).

39. Bredas, J. L.; Calbert, J. P.; da Silva, D. A.; Cornil, J., Organic semiconductors: *Proceedings of the National Academy of Sciences of the United States of America* **2002,** 99, (9).

40. da Silva, D. A.; Kim, E. G.; Bredas, J. L.,. *Advanced Materials* **2005,** 17, (8).

41. Hutchison, G. R.; Ratner, M. A.; Marks, T. J., *Journal of the American Chemical Society* **2005,** 127, (7).

42. Bromley, S. T.; Mas-Torrent, M.; Hadley, P.; Rovira, C., *Journal of the American Chemical Society* **2004,** 126, (21).

43. Cornil, J.; Bredas, J.-L.; Zaumseil, J.; Sirringhaus, H., *Advanced Materials* **2007,** 19, (14).

44. Bredas, J. L.; Beljonne, D.; Coropceanu, V.; Cornil, J., *Chemical Reviews* **2004,** 104, (11).

45. Street, R. A.; Northrup, J. E.; Salleo, A., *Physical Review B* **2005,** 71, (16).

46. Garnier, F.; Yassar, A.; Hajlaoui, R.; Horowitz, G.; Deloffre, F.; Servet, B.; Ries, S.; Alnot, P., *Journal of the American Chemical Society* **1993,** 115, (19).

47. Meng, H.; Sun, F. P.; Goldfinger, M. B.; Jaycox, G. D.; Li, Z. G.; Marshall, W. J.; Blackman, G. S., *Journal of the American Chemical Society* **2005,** 127, (8).

48. Locklin, J.; Li, D. W.; Mannsfeld, S. C. B.; Borkent, E. J.; Meng, H.; Advincula, R.; Bao, Z., *Chemistry of Materials* **2005,** 17, (13).

49. Xiao, S. X.; Myers, M.; Miao, Q.; Sanaur, S.; Pang, K. L.; Steigerwald, M. L.; Nuckolls, C., *Angewandte Chemie-International Edition* **2005,** 44, (45).

50. Moon, H.; Zeis, R.; Borkent, E. J.; Besnard, C.; Lovinger, A. J.; Siegrist, T.; Kloc, C.; Bao, Z. N., *Journal of the American Chemical Society* **2004,** 126, (47).

51. Sarma, J.; Desiraju, G. R., *Accounts of Chemical Research* **1986,** 19, (7).

52. Takimiya, K.; Kunugi, Y.; Konda, Y.; Niihara, N.; Otsubo, T., *Journal of the American Chemical Society* **2004,** 126, (16).

53. Chen, T. A.; Rieke, R. D., *Journal of the American Chemical Society* **1992,** 114, (25).

54. McCullough, R. D.; Lowe, R. D.; Jayaraman, M.; Anderson, D. L., *Journal of Organic Chemistry* **1993,** 58, (4), 904-912.

55. McCullough, R. D.; Tristramnagle, S.; Williams, S. P.; Lowe, R. D.; Jayaraman, M., *Journal of the American Chemical Society* **1993,** 115, (11).

56. Loewe, R. S.; Khersonsky, S. M.; McCullough, R. D., *Advanced Materials* **1999,** 11, (3).

57. Loewe, R. S.; Ewbank, P. C.; Liu, J. S.; Zhai, L.; McCullough, R. D., *Macromolecules* **2001,** 34, (13).

58. Babel, A.; Jenekhe, S. A., *Synthetic Metals* **2005,** 148, (2).

59. Bao, Z.; Locklin, J., *Organic Field-Effect Transistors*. CRC Press: Boca Raton, FL, 2007.

60. Wang, G. M.; Swensen, J.; Moses, D.; Heeger, A. J., *Journal of Applied Physics* **2003,** 93, (10).

61. Bao, Z. N.; Lovinger, A. J., *Chemistry of Materials* **1999,** 11, (9).

62. Sirringhaus, H.; Tessler, N.; Friend, R. H., *Science* **1998,** 280, (5370).

63. Chang, J. F.; Sun, B. Q.; Breiby, D. W.; Nielsen, M. M.; Solling, T. I.; Giles, M.; McCulloch, I.; Sirringhaus, H., *Chemistry of Materials* **2004,** 16, (23).

64. Kline, R. J.; McGehee, M. D.; Kadnikova, E. N.; Liu, J. S.; Frechet, J. M. J.,. *Advanced Materials* **2003,** 15, (18).

65. Tsao, H. N.; Cho, D.; Andreasen, J. W.; Rouhanipour, A.; Breiby, D. W.; Pisula, W.; Muellen, K., *Advanced Materials* **2009,** 21, (2).

66. Niemi, V. M.; Knuuttila, P.; Osterholm, J. E.; Korvola, J., *Polymer* **1992,** 33, (7).

67. Kossmehl, G., *Makromolekulare Chemie-Macromolecular Symposia* **1986,** 4.

68. Jikei, M.; Katoh, J.; Sato, N.; Yamamoto, K.; Nishide, H.; Tsuchida, E., S. *Bulletin of the Chemical Society of Japan* **1992,** 65, (8).

69. Myers, R. E., *Journal of Electronic Materials* **1986,** 15, (2).

70. Ogawa, K.; Stafford, J. A.; Rothstein, S. D.; Tallman, D. E.; Rasmussen, S. C.,. *Synthetic Metals* **2005,** 152, (1-3).

71. Ma, C.; Xu, Y.; Zhang, C.; Xu, Y.; Xiang, W.; Mi, O., *Journal of Electroanalytical Chemistry* **2009,** 634, (1).

72. McCarley, T. D.; Noble, C. O.; DuBois, C. J.; McCarley, R. L., *Macromolecules* **2001,** 34, (23).

73. Andersson, M. R.; Selse, D.; Berggren, M.; Jarvinen, H.; Hjertberg, T.; Inganas, O.; Wennerstrom, O.; Osterholm, J. E., *Macromolecules* **1994,** 27, (22).

74. Vangeneugden, D. L.; Vanderzande, D. J. M.; Salbeck, J.; van Hal, P. A.; Janssen, R. A. J.; Hummelen, J. C.; Brabec, C. J.; Shaheen, S. E.; Sariciftci, N. S., *Journal of Physical Chemistry B* **2001,** 105, (45).

75. Abdou, M. S. A.; Lu, X. T.; Xie, Z. W.; Orfino, F.; Deen, M. J.; Holdcroft, S., *Chemistry of Materials* **1995,** 7, (4).

76. Cai, T.; Zhoub, Y.; Wanga, E.; Hellström, S.; Zhang, F.; Xu, X.; Inganäs, O.; Andersson, M. R., *Sol. En. Mat. Sol. Cells* **2010**, (94).

77. Cheng, Y. J.; Luh, T. Y., *Journal of Organometallic Chemistry* **2004,** 689, (24).

78. Bao, Z. N.; Chan, W. K.; Yu, L. P., *Journal of the American Chemical Society* **1995,** 117, (50).

79. Carsten, B.; He, F.; Son, H. J.; Xu, T.; Yu, L., *Chemical Reviews* **2011,** 111, (3).

80. Ziegler, C. B.; Heck, R. F., *Journal of Organic Chemistry* **1978,** 43, (15).

81. Herrmann, W. A.; Brossmer, C.; Ofele, K.; Reisinger, C. P.; Priermeier, T.; Beller, M.; Fischer, H., *Angewandte Chemie-International Edition in English* **1995,** 34, (17).

82. Grushin, V. V., *Chemistry-a European Journal* **2002,** 8, (5).

83. Kosugi, M.; Shimizu, Y.; Migita, T., *Chemistry Letters* **1977**, (12).

84. Milstein, D.; Stille, J. K., *Journal of the American Chemical Society* **1978,** 100, (11).

85. Azizian, H.; Eaborn, C.; Pidcock, A., *Journal of Organometallic Chemistry* **1981,** 215, (1).

86. Benaglia, M.; Toyota, S.; Woods, C. R.; Siegel, J. S., *Tetrahedron Letters* **1997,** 38, (27).

87. Murata, M.; Oyama, T.; Watanabe, S.; Masuda, Y., *Synthetic Communications* **2002,** 32, (16).

88. Miyaura, N.; Suzuki, A., *Chemical Reviews* **1995,** 95, (7).

89. Suzuki, A., *Journal of Organometallic Chemistry* **1999,** 576, (1-2).

90. Suzuki, A. B., H. C., Suzuki Coupling, Organic Syntheses via Boranes. In Aldrich Chemical Company: Milwaukee, WI, 2003 Vol. 3.

91. Kimbrough, R. D., *Environmental Health Perspectives* **1976,** 14, (APR).

92. Giroux, A.; Han, Y. X.; Prasit, P., *Tetrahedron Letters* **1997,** 38, (22).

93. Tse, M. K.; Cho, J. Y.; Smith, M. R., *Organic Letters* **2001,** 3, (18).

94. Ishiyama, T.; Takagi, J.; Ishida, K.; Miyaura, N.; Anastasi, N. R.; Hartwig, J. F., *Journal of the American Chemical Society* **2002,** 124, (3).

95. Sakamoto, J.; Rehahn, M.; Wegner, G.; Schluter, A. D., *Macromolecular Rapid Communications* **2009,** 30, (9-10), 653-687.

96. Treacher, K.; Stosel, P.; Spreitzer, H.; Becker, A.; Falcou, H. 2005.

97. Wang, E.; Hou, L.; Wang, Z.; Hellstrom, S.; Mammo, W.; Zhang, F.; Inganas, O.; Andersson, M. R., *Organic Letters* **2010,** 12, (20).

98. Guo, X.; Kim, F. S.; Jenekhe, S. A.; Watson, M. D., *Journal of the American Chemical Society* **2009,** 131, (21).

99. Mei, J.; Kim, D. H.; Ayzner, A. L.; Toney, M. F.; Bao, Z., *Journal of the American Chemical Society* **2011,** 133, (50).

100. Yokoyama, A.; Suzuki, H.; Kubota, Y.; Ohuchi, K.; Higashimura, H.; Yokozawa, T., *Journal of the American Chemical Society* **2007,** 129, (23).

101. Facchetti, A.; Vaccaro, L.; Marrocchi, A., *Angewandte Chemie-International Edition* **2012,** 51, (15).

102. Rudenko, A. E.; Wiley, C. A.; Stone, S. M.; Tannaci, J. F.; Thompson, B. C., *Journal of Polymer Science Part A: Polymer Chemistry*. **2012**; Vol. 50, p 3691.

103. Berrouard, P.; Najari, A.; Pron, A.; Gendron, D.; Morin, P.-O.; Pouliot, J.-R.; Veilleux, J.; Leclerc, M., *Angewandte Chemie-International Edition* **2012,** 51, (9).

104. Sevignon, M.; Papillon, J.; Schulz, E.; Lemaire, M., *Tetrahedron Letters* **1999,** 40, (32).

105. Wang, Q.; Takita, R.; Kikuzaki, Y.; Ozawa, F., *Journal of the American Chemical Society* **2010,** 132, (33).

106. Odian, G., *Principles of Polymerization*. John Wiley and Sons: 2004.

107. Amb, C. M.; Chen, S.; Graham, K. R.; Subbiah, J.; Small, C. E.; So, F.; Reynolds, J. R., *Journal of the American Chemical Society* **2011,** 133, (26), 10062-10065.

108. Blouin, N.; Michaud, A.; Leclerc, M., *Advanced Materials* **2007,** 19, (17).

109. Park, J. K.; Jo, J.; Seo, J. H.; Moon, J. S.; Park, Y. D.; Lee, K.; Heeger, A. J.; Bazan, G. C., *Advanced Materials* **2011,** 23, (21).

110. Guo, X.; Ponce Ortiz, R.; Zheng, Y.; Kim, M.-G.; Zhang, S.; Hu, Y.; Lu, G.; Facchetti, A.; Marks, T. J., *Journal of the American Chemical Society* **2011,** 133, (34).

111. Schubert, D. W.; Dunkel, T., *Materials Research Innovations* **2003,** 7, (5).

112. DeLongchamp, D. M.; Vogel, B. M.; Jung, Y.; Gurau, M. C.; Richter, C. A.; Kirillov, O. A.; Obrzut, J.; Fischer, D. A.; Sambasivan, S.; Richter, L. J.; Lin, E. K., *Chemistry of Materials* **2005,** 17, (23).

113. Tsao, H. N.; Muellen, K., *Chemical Society Reviews* **2010,** 39, (7).

114. Degarmo, E. P.; Black, J. T.; Kohser, R. A., *Materials and Processes in Manufacturing*. 9th edition ed.; Wiley: 2003.

115. Mortimer, R. J.; Graham, K. R.; Grenier, C. R. G.; Reynolds, J. R., *Acs Applied Materials & Interfaces* **2009,** 1, (10).

116. Girotto, C.; Rand, B. P.; Genoe, J.; Heremans, P., *Solar Energy Materials and Solar Cells* **2009,** 93, (4).

117. Steirer, K. X.; Reese, M. O.; Rupert, B. L.; Kopidakis, N.; Olson, D. C.; Collins, R. T.; Ginley, D. S., *Solar Energy Materials and Solar Cells* **2009,** 93, (4).

118. Chen, L. M.; Hong, Z. R.; Kwan, W. L.; Lu, C. H.; Lai, Y. F.; Lei, B.; Liu, C. P.; Yang, Y., *Acs Nano* **2010,** 4, (8), 4744-4752.

119. Krebs, F. C.; Gevorgyan, S. A.; Alstrup, J., *Journal of Materials Chemistry* **2009,** 19, (30).

120. Sondergaard, R.; Hosel, M.; Angmo, D.; Larsen-Olsen, T. T.; Krebs, F. C., *Materials Today* **2012,** 15, (1-2).

121. Garnier, F.; Hajlaoui, R.; Yassar, A.; Srivastava, P., *Science* **1994,** 265, (5179).

122. Shaheen, S. E.; Radspinner, R.; Peyghambarian, N.; Jabbour, G. E., *Applied Physics Letters* **2001,** 79, (18).

123. Holdcroft, S., *Advanced Materials* **2001,** 13, (23).

124. Bao, Z. N.; Rogers, J. A.; Katz, H. E., *Journal of Materials Chemistry* **1999,** 9, (9).

125. Krebs, F. C.; Jorgensen, M.; Norrman, K.; Hagemann, O.; Alstrup, J.; Nielsen, T. D.; Fyenbo, J.; Larsen, K.; Kristensen, J., *Solar Energy Materials and Solar Cells* **2009,** 93, (4).

126. Steiger, J.; Heun, S.; Tallant, N., *Journal of Imaging Science and Technology* **2003,** 47, (6).

127. Yoshioka, Y.; Jabbour, G. E., *Synthetic Metals* **2006,** 156, (11-13).

128. de Gans, B. J.; Duineveld, P. C.; Schubert, U. S., *Advanced Materials* **2004,** 16, (3).

129. Hoth, C. N.; Choulis, S. A.; Schilinsky, P.; Brabec, C. J., *Advanced Materials* **2007,** 19, (22), 3973.

130. Wengeler, L.; Schmidt-Hansberg, B.; Peters, K.; Scharfer, P.; Schabel, W., *Chemical Engineering and Processing* **2011,** 50, (5-6).

131. Blankenburg, L.; Schultheis, K.; Schache, H.; Sensfuss, S.; Schroedner, M., *Solar Energy Materials and Solar Cells* **2009,** 93, (4).

132. Thrane, L.; Jorgensen, T. M.; Jorgensen, M.; Krebs, F. C., *Solar Energy Materials and Solar Cells* **2012,** 97.

133. Manceau, M.; Angmo, D.; Jorgensen, M.; Krebs, F. C., *Organic Electronics* **2011,** 12, (4).

134. Sondergaard, R.; Manceau, M.; Jorgensen, M.; Krebs, F. C., *Advanced Energy Materials* **2012,** 2, (4).

135. Espinosa, N.; Garcia-Valverde, R.; Urbina, A.; Krebs, F. C., *Solar Energy Materials and Solar Cells* **2011,** 95, (5).

136. Sirringhaus, H., *Nature* **2009,** 457, (7230).

137. Ong, B. S.; Wu, Y. L.; Liu, P.; Gardner, S., *Journal of the American Chemical Society* **2004,** 126, (11).

138. McCulloch, I.; Heeney, M.; Bailey, C.; Genevicius, K.; Macdonald, I.; Shkunov, M.; Sparrowe, D.; Tierney, S.; Wagner, R.; Zhang, W. M.; Chabinyc, M. L.; Kline, R. J.; McGehee, M. D.; Toney, M. F., *Nature Materials* **2006,** 5, (4).

139. Li, Y.; Sonar, P.; Singh, S. P.; Soh, M. S.; van Meurs, M.; Tan, J., *Journal of the American Chemical Society* **2011,** 133, (7).

140. Babel, A.; Jenekhe, S. A., *Advanced Materials* **2002,** 14, (5).

141. Babel, A.; Jenekhe, S. A., *Journal of the American Chemical Society* **2003,** 125, (45).

142. Yan, H.; Chen, Z.; Zheng, Y.; Newman, C.; Quinn, J. R.; Dotz, F.; Kastler, M.; Facchetti, A., *Nature* **2009,** 457, (7230).

143. Liu, Y.; Wan, X.; Wang, F.; Zhou, J.; Long, G.; Tian, J.; You, J.; Yang, Y.; Chen, Y., *Advanced Energy Materials* **2011,** 1, (5).

144. Sun, Y.; Welch, G. C.; Leong, W. L.; Takacs, C. J.; Bazan, G. C.; Heeger, A. J., *Nature Materials* **2012,** 11, (1).

145. Yu, G.; Gao, J.; Hummelen, J. C.; Wudl, F.; Heeger, A. J., *Science* **1995,** 270, (5243).

146. Zhao, G. J.; He, Y. J.; Li, Y. F., *Advanced Materials* **2010,** 22, (39), 4355.

147. Li, G.; Shrotriya, V.; Huang, J. S.; Yao, Y.; Moriarty, T.; Emery, K.; Yang, Y., *Nature Materials* **2005,** 4, (11).

148. Ma, W. L.; Yang, C. Y.; Gong, X.; Lee, K.; Heeger, A. J., *Advanced Functional Materials* **2005,** 15, (10).

149. Park, S. H.; Roy, A.; Beaupre, S.; Cho, S.; Coates, N.; Moon, J. S.; Moses, D.; Leclerc, M.; Lee, K.; Heeger, A. J., *Nature Photonics* **2009,** 3, (5).

150. Liang, Y. Y.; Wu, Y.; Feng, D. Q.; Tsai, S. T.; Son, H. J.; Li, G.; Yu, L. P., *Journal of the American Chemical Society* **2009,** 131, (1), 56.

151. Liang, Y.; Feng, D.; Wu, Y.; Tsai, S.-T.; Li, G.; Ray, C.; Yu, L., *Journal of the American Chemical Society* **2009,** 131, (22).

152. Zou, Y.; Najari, A.; Berrouard, P.; Beaupre, S.; Aich, B. R.; Tao, Y.; Leclerc, M., A *Journal of the American Chemical Society* **2010,** 132, (15).

153. Troshin, P. A.; Susarova, D. K.; Moskvin, Y. L.; Kuznetsov, I. E.; Ponomarenko, S. A.; Myshkovskaya, E. N.; Zakharcheva, K. A.; Balakai, A. A.; Babenko, S. D.; Razumov, V. F., *Advanced Functional Materials* **2010,** 20, (24), 4351-4357.

154. Saeki, A.; Tsuji, M.; Seki, S., *Advanced Energy Materials* **2011,** 1, (4), 661-669.

155. Urien, M.; Wantz, G.; Cloutet, E.; Hirsch, L.; Tardy, P.; Vignau, L.; Cramail, H.; Parniex, J. P., *Organic Electronics* **2007,** 8, (6), 727-734.

156. Bjorklund, N.; Lill, J. O.; Rajander, J.; Osterbacka, R.; Tierney, S.; Heeney, M.; McCulloch, I.; Colle, M., *Organic Electronics* **2009,** 10, (2), 215-221.

157. Nielsen, K. T.; Bechgaard, K.; Krebs, F. C., *Macromolecules* **2005,** 38, (3), 658-659.

158. Thompson, C. B. Variable Bandgap Poly(3,4-alkylenedioxythiophene)-Based Polymers for Photovoltaic and Electrochromic Applications. University of Florida Gainesville, FL,, 2005.

159. Cardona, C. M.; Li, W.; Kaifer, A. E.; Stockdale, D.; Bazan, G. C., *Advanced Materials* **2011,** 23, (20), 2367-2371.

160. Pisula, W.; Tomovic, Z.; Simpson, C.; Kastler, M.; Pakula, T.; Mullen, K., *Chemistry of Materials* **2005,** 17, (17), 4296-4303.

161. Fuoss, P. H.; Brennan, S., *Annual Review of Materials Science* **1990,** 20, 365-390.

162. DeLongchamp, D. M.; Kline, R. J.; Fischer, D. A.; Richter, L. J.; Toney, M. F., *Advanced Materials* **2011,** 23, (3), 319-337.

163. Small, C. E.; Chen, S.; Subbiah, J.; Amb, C. M.; Tsang, S. W.; Lai, T. H.; Reynolds, J. R.; So, F., *Nature Photonics* **2012,** 6, (2), 115-120.

164. Scharber, M. C.; Wuhlbacher, D.; Koppe, M.; Denk, P.; Waldauf, C.; Heeger, A. J.; Brabec, C. L., *Advanced Materials* **2006,** 18, (6), 789-+.

165. Bundgaard, E.; Krebs, F. C., *Solar Energy Materials and Solar Cells* **2007,** 91, (11), 954-985.

166. Beaujuge, P. M. Spectral Engineering in π-Conjugated Organic Polymers. University of Florida, Gainesville, Fl, 2009.

167. Beaujuge, P. M.; Subbiah, J.; Choudhury, K. R.; Ellinger, S.; McCarley, T. D.; So, F.; Reynolds, J. R., *Chemistry of Materials* **2010,** 22, (6), 2093-2106.

168. Subbiah, J.; Beaujuge, P. M.; Choudhury, K. R.; Ellinger, S.; Reynolds, J. R.; So, F., *Acs Applied Materials & Interfaces* **2009,** 1, (6), 1154-1158.

169. Voorhies, J. D.; Schurdak, E. J., *Anal. Chem.* **1962**, (34), 939.

170. Amb, C. M.; Craig, M. R.; Koldemir, U.; Subbiah, J.; Choudhury, K. R.; Gevorgyan, S. A.; Jorgensen, M.; Krebs, F. C.; So, F.; Reynolds, J. R., *Acs Applied Materials & Interfaces* **2012,** 4, (3), 1847-1853.

171. Campoy-Quiles, M.; Ferenczi, T.; Agostinelli, T.; Etchegoin, P. G.; Kim, Y.; Anthopoulos, T. D.; Stavrinou, P. N.; Bradley, D. D. C.; Nelson, J., *Nature Materials* **2008,** 7, (2), 158-164.

172. Subbiah, J.; Amb, C. M.; Reynolds, J. R.; So, F., *Solar Energy Materials and Solar Cells* **2012,** 97, 97-101.

173. Koldemir, U.; Graham, K. R.; Salazar, D. H.; McCarley, T. D.; Reynolds, J. R., *Journal of Materials Chemistry* **2011,** 21, (18), 6480-6482.

174. Kilbinger, A. F. M.; Feast, W. J., *Journal of Materials Chemistry* **2000,** 10, (8), 1777-1784.

175. Peet, J.; Kim, J. Y.; Coates, N. E.; Ma, W. L.; Moses, D.; Heeger, A. J.; Bazan, G. C., *Nature Materials* **2007,** 6, (7).

176. Morana, M.; Wegscheider, M.; Bonanni, A.; Kopidakis, N.; Shaheen, S.; Scharber, M.; Zhu, Z.; Waller, D.; Gaudiana, R.; Brabec, C., *Advanced Functional Materials* **2008,** 18, (12).

177. Zhang, M.; Tsao, H. N.; Pisula, W.; Yang, C.; Mishra, A. K.; Muellen, K., *Journal of the American Chemical Society* **2007,** 129, (12).

178. Bijleveld, J. C.; Shahid, M.; Gilot, J.; Wienk, M. M.; Janssen, R. A. J., *Advanced Functional Materials* **2009,** 19, (20), 3262-3270.

179. Usta, H.; Lu, G.; Facchetti, A.; Marks, T. J., *Journal of the American Chemical Society* **2006,** 128, (28), 9034-9035.

180. Beaujuge, P. M.; Pisula, W.; Tsao, H. N.; Ellinger, S.; Mullen, K.; Reynolds, J. R., *Journal of the American Chemical Society* **2009,** 131, (22), 7514-+.

181. Chu, T. Y.; Lu, J. P.; Beaupre, S.; Zhang, Y. G.; Pouliot, J. R.; Wakim, S.; Zhou, J. Y.; Leclerc, M.; Li, Z.; Ding, J. F.; Tao, Y., *Journal of the American Chemical Society* **2011,** 133, (12), 4250-4253.

182. Zhang, Z.-G.; Min, J.; Zhang, S.; Zhang, J.; Zhang, M.; Li, Y., *Chemical Communications* **2011,** 47, (33).

183. Subramaniyan, S.; Xin, H.; Kim, F. S.; Shoaee, S.; Durrant, J. R.; Jenekhe, S. A., *Advanced Energy Materials* **2011,** 1, (5).

184. Scharber, M. C.; Koppe, M.; Gao, J.; Cordella, F.; Loi, M. A.; Denk, P.; Morana, M.; Egelhaaf, H. J.; Forberich, K.; Dennler, G.; Gaudiana, R.; Waller, D.; Zhu, Z. G.; Shi, X. B.; Brabec, C. J., *Advanced Materials* **2010,** 22, (3), 367.

185. Gendron, D.; Morin, P.-O.; Berrouard, P.; Allard, N.; Aich, B. R.; Garon, C. N.; Tao, Y.; Leclerc, M., *Macromolecules* **2011,** 44, (18).

186. Ohshita, J.; Hwang, Y. M.; Mizumo, T.; Yoshida, H.; Ooyama, Y.; Harima, Y.; Kunugi, Y., *Organometallics* **2011,** 30, (12), 3233-3236.

187. Hwang, Y. M.; Ohshita, J.; Harima, Y.; Mizumo, T.; Ooyama, Y.; Morihara, Y.; Izawa, T.; Sugioka, T.; Fujita, A., *Polymer* **2011,** 52, (18), 3912-3916.

188. Fei, Z. P.; Kim, Y.; Smith, J.; Domingo, E. B.; Stingelin, N.; McLachlan, M. A.; Song, K.; Anthopoulos, T. D.; Heeney, M., *Macromolecules* **2012,** 45, (2), 735-742.

189. Kim, J. S.; Fei, Z. P.; James, D. T.; Heeney, M., *Journal of Materials Chemistry* **2012,** 22, (19), 9975-9982.

190. Hou, J. H.; Park, M. H.; Zhang, S. Q.; Yao, Y.; Chen, L. M.; Li, J. H.; Yang, Y., *Macromolecules* **2008,** 41, (16), 6012-6018.

191. Mancilha, F. S.; DaSilveira Neto, B. A.; Lopes, A. S.; Moreira, P. F., Jr.; Quina, F. H.; Goncalves, R. S.; Dupont, J., *European Journal of Organic Chemistry* **2006**, (21).
192. Nielsen, C. B.; Bjornholm, T., *Organic Letters* **2004,** 6, (19).

193. Chen, J.; Shi, M.-M.; Hu, X.-L.; Wang, M.; Chen, H.-Z., *Polymer* **2010,** 51, (13).
194. Ahmed Aisa, A. M.; EnKe, S.; Richter, H., *Journal of Organometallic Chemistry* **1999**, (575), 126-132.

195. Coffin, R. C.; Peet, J.; Rogers, J.; Bazan, G. C., *Nature Chemistry* **2009,** 1, (8), 657-661.

196. Kruger, R. A.; Gordon, T. J.; Baumgartner, T.; Sutherland, T. C., *Acs Applied Materials & Interfaces* **2011,** 3, (6), 2031-2041.

197. Boudouris, B. W.; Molins, F.; Blank, D. A.; Frisbie, C. D.; Hillmyer, M. A., *Macromolecules* **2009,** 42, (12), 4118-4126.

198. Moon, H. C.; Anthonysamy, A.; Lee, Y.; Kim, J. K., Facile Synthesis of Well- *Macromolecules* **2010,** 43, (4), 1747-1752.

199. Chen, Y. H.; Huang, P. T.; Lin, K. C.; Huang, Y. J.; Chen, C. T., *Organic Electronics* **2012,** 13, (2), 283-289.

200. Lohwasser, R. H.; Thelakkat, M., *Macromolecules* **2010,** 43, (18), 7611-7616.
201. Lohwasser, R. H.; Bandara, J.; Thelakkat, M., *Journal of Materials Chemistry* **2009,** 19, (24), 4126-4130.

202. Jeffries-El, M.; Sauve, G.; McCullough, R. D., *Macromolecules* **2005,** 38, (25), 10346-10352.

203. Kim, J. S.; Lee, Y.; Lee, J. H.; Park, J. H.; Kim, J. K.; Cho, K., *Advanced Materials* **2010,** 22, (12), 1355-+.

204. Kim, Y.; Cook, S.; Kirkpatrick, J.; Nelson, J.; Durrant, J. R.; Bradley, D. D. C.; Giles, M.; Heeney, M.; Hamilton, R.; McCulloch, I., *Journal of Physical Chemistry C* **2007,** 111, (23), 8137-8141.

205. Hohl, B.; Bertschi, L.; Zhang, X. Y.; Schluter, A. D.; Sakamoto, J., *Macromolecules* **2012,** 45, (13), 5418-5426.

206. Jayakannan, M.; van Dongen, J. L. J.; Janssen, R. A. J., *Macromolecules* **2001,** 34, (16), 5386-5393.

207. Groenendaal, L.; Peerlings, H. W. I.; Havinga, E. E.; Vekemans, J.; Meijer, E. W., *Synthetic Metals* **1995,** 69, (1-3).

208. Lee, M. J.; Gupta, D.; Zhao, N.; Heeney, M.; McCulloch, I.; Sirringhaus, H., *Advanced Functional Materials* **2011,** 21, (5), 932-940.

BIOGRAPHICAL SKETCH

Unsal Koldemir is a native Turkish born in Denizli, Turkey in 1982. He graduated from Denizli Anatolian High School where he spent seven years studying math and science courses in English. He was in the top 1% in the national university exam taken by approximately 1.5 million high school graduates. He chose Bilkent University Chemistry Department – the highest ranked Chemistry Department in Turkey- and received full scholarship during studies. He gained his B.S in Chemistry in 2005 and M.S in Chemistry in 2007. His interest in organic chemistry –and chemistry- started in 2004 when he met Dr. Fikret Koc during a paid summer internship in Prof. Peter Eilbracht's research group in Dortmund University. After joining Prof. Reynolds research group in 2007, he was exposed to research on the synthesis of green colored solar cell polymers as well as high performance field effect transistor materials employing donor-acceptor type polymers. He earned his Ph.D in organic and polymer chemistry from the University of Florida in the autumn of 2012. He will work as a post-doctoral researcher in Prof. Alan Sellinger's research group on the synthesis of new acceptor molecules for organic photovoltaics.